

Quarterly Research Review No. 11

1 October through 31 December 1964

GPO PRICE \$ _____

OTS PRICE(S) \$ _____

Hard copy (HC) 5.00

Microfiche (MF) 1.00

Prepared by
Electron Devices Laboratory
Solid-State Electronics Laboratory
Systems Theory Laboratory
Radioscience Laboratory

of the

FACILITY FORM 608	N65-24992	_____
	<small>(ACCESSION NUMBER)</small>	<small>(THRU)</small>
	<u>172</u>	<u>1</u>
	<small>(PAGES)</small>	<small>(CODE)</small>
	<u>CD 63088</u>	<u>10</u>
	<small>(NASA CR OR TMX OR AD NUMBER)</small>	<small>(CATEGORY)</small>

STANFORD ELECTRONICS LABORATORIES

STANFORD UNIVERSITY • STANFORD, CALIFORNIA



CASE FILE COPY

DDC AVAILABILITY NOTICE

Qualified requesters may obtain copies of this report from DDC.
Foreign announcement and dissemination of this report by DDC
is limited.

QUARTERLY RESEARCH REVIEW NO. 11
1 October through 31 December 1964

Prepared by
ELECTRON DEVICES LABORATORY

under

Air Force Contract AF33(657)-11144, QSR No. 7
Air Force Contract AF04(695)-536
Air Force Contract AF33(615)-1504
Air Force Office of Scientific Research Grant No. 323-63
Army Contract DA 36-039 AMC-00094(E), QSR No. 8
Signal Corps Contract DA 36-039 SC-90839, QSR No. 10
Atomic Energy Commission Contract AT(04-3)326 PA No. 8, QSR No. 11
National Aeronautics and Space Administration Grant No. 299-63
Tri-Service Contract Nonr-225(24)

SOLID-STATE ELECTRONICS LABORATORY

under

Air Force Contract AF33(657)-11586, QSR No. 16
Office of Ordnance Research Grant DA 31-124 ARO-D-155
Center for Materials Research Contract SD-87-003, QSR No. 11
National Science Foundation Grant NsF GP 1033
National Aeronautics and Space Administration Grant NsG 555
Office of Naval Research Contract Nonr-225(31)
Tri-Service Contract Nonr-225(24)
Office of Naval Research Contract Nonr-225(44)

and

SYSTEMS THEORY AND RADIOSCIENCE LABORATORIES

under

Tri-Service Contract Nonr-225(24)
Jointly supported by the U. S. Army Signal Corps, the
U.S. Air Force, and the U.S. Navy (Office of Naval Research)
Air Force Contract AF33(657)-11586
Army Contract DA 04(200) AMC-57(Z)

W. R. Rambo, Director

STANFORD ELECTRONICS LABORATORIES
Stanford University Stanford, California

FOREWORD

This report contains a review of unclassified research activities of the Stanford Electronics Laboratories. This report covers the three-month period ending December 31, 1964. Because of contractual specifications the research activities of the Systems Techniques Laboratory and portions of the Radioscience Laboratory are not included in this report but are reported separately.

PERSONNEL OF THE ELECTRON DEVICES LABORATORY

(1 October through 31 December 1964)

DIRECTOR - D. A. Dunn

FACULTY, SENIOR RESEARCH ASSOCIATES, AND RESEARCH ASSOCIATES

W. W. Anderson	D. A. Dunn	R. P. Lagerstrom
P. Burger	S. E. Harris	D. Pigache
O. Buneman	H. Heffner	A. E. Siegman
H. Derfler	R. Hockney	K. Thomassen

RESEARCH ASSISTANTS AND FELLOWS

J. Allen	T. C. Lee	T. Paoli
W. A. Bares	L. Linson	E. J. Powers
J. Bjorkholm	W. Lowenstern	S. Puri
I. C. Chang	O. McDuff	S. Razi
G. Francois	C. M. McIntyre	G. Reiter
A. S. Halsted	J. Markiewicz	T. C. Simonen
H. Hayami	W. Nichparenko	J. E. Simpson
W. Hemphill	J. O'Brien	H. Sonnenberg
J. Hosea	M. Omura	J. Tellefsen
R. Kerr	L. M. Osterink	J. L. Uebbing

PUBLICATIONS AND REPORTS

(1 October through 31 December 1964)

PAPERS PRESENTED AT MEETINGS

American Physical Society, Plasma Physics Division, Nov. 4-7, 1964,
New York.

E. Powers, "Evidence of Anomalous Diffusion Across a Magnetic Field in an RF Discharge." AT(04-3)326 PA 8.

P. Burger, "A Relaxation Type of Oscillation in Ion-Electron Systems." NsG 299-63.

O. Buneman, "Effective Transport Coefficients at Low and High Collision Frequencies." AF-AFOSR 323-63.

PAPERS PRESENTED AT MEETINGS (Cont'd)

American Physical Society, Plasma Physics Division, Nov. 4-7, 1964, New York (Cont'd).

D. Pigache and G. Reiter, "Experimental Indication of Plasma Confinement in a Toroidal Reflex Discharge Using a Bumpy Magnetic Field Configuration." AT(04-3)326 PA 8.

D. A. Dunn, W. Nichparenko, and J. E. Simpson, "Oscillations and Radial Instabilities in a Beam-Generated Plasma."

American Physical Society, 1964 Winter Meeting in the West, Berkeley, 22 December 1964.

A. E. Siegman, "Unstable Optical Resonators for Laser Applications." SC-90839.

PAPERS AND ARTICLES ACCEPTED FOR PUBLICATION

D. A. Dunn, V. Hamza, and J. A. Jolly, "Computer Designs for Beam Pentodes," IEEE Trans. on Electron Devices.

A. E. Siegman and V. Evtuhov, "A Twisted-Mode Technique for Obtaining Axially Uniform Energy Density in a Laser Cavity," Appl. Optics, 4, January 1965. SC-90839.

A. E. Siegman, "Unstable Optical Resonators for Laser Applications," Proc. IEEE, 53, to be published. AF 144, SC-90839

ARTICLES PUBLISHED

H. Derfler, "Nonexistence of Quiescent Plasma States in Ion Propulsion," Phys. Fluids, 7, 1625-1637 (October 1964). NSG 299-63.

A. E. Siegman, "The Laser: An Astounding Beam of Light," Stanford Today, Autumn 1964. No contract.

T. C. Lee and W. W. Anderson, "Edge Emission Involving Manganese Impurities in GaAs at 4.2 °K," Solid State Communications, 2, pp. 265-268, (October 1964). AFOSR 62-286, SC-90839.

I. C. Chang and W. W. Anderson, "Paramagnetic Resonance of Er³⁺ in Calcium and Strontium Oxide," Phys. Letts., 112, (November 15, 1964). Nonr-225(24).

S. E. Harris, E. O. Ammann, and I. C. Chang, "Optical Network Synthesis Using Birefringent Crystals. I. Synthesis of Lossless Networks of Equal-Length Crystals," J.O.S.A., 54, 1267-1279 (October 1964). AF-536.

S. E. Harris and Russell Targ, "FM Oscillation of the He-Ne Laser," Applied Physics Letters, 5, p. 202 (November 15, 1964). AF-144.

S. E. Harris and O. P. McDuff, "FM Laser Oscillation--Theory," Applied Physics Letters, 5, p. 205 (November 15, 1964).

TECHNICAL REPORTS ISSUED BY EDL

(1 October through 31 December 1964)

Air Force Contract AF33(657)-11144

No. 0576-6: R. J. Morris, "Tuning of CW Lasers over Angstrom Bandwidths: Some Possible Approaches."

Air Force Contract AF04(695)-305

No. 0576-7: S. E. Harris, E. O. Ammann, I. C. Chang, "Optical Network Synthesis Using Birefringent Crystals."

Signal Corps Contract DA 36-039 SC-90839

No. 0592-1: A. E. Siegman, "A Proposed 'Twisted-Mode' Technique for Obtaining Single-Axial-Mode Oscillation in a Ruby Laser."

PERSONNEL OF THE SOLID-STATE ELECTRONICS LABORATORY

(1 October through 31 December 1964)

DIRECTOR - J. B. Angell

FACULTY, SENIOR RESEARCH ASSOCIATES, AND RESEARCH ASSOCIATES

J. W. Allen	M. M. McWhorter	R. L. Pritchard
J. B. Angell	J. L. Moll - sabbatical	W. Shockley
J. G. Gibbons	M. Nagata	W. E. Spicer
R. H. Kingston	G. L. Pearson	R. L. White
J. G. Linvill		

RESEARCH ASSISTANTS AND FELLOWS

C. Allen	J. W. Hill	R. Powell
A. Blodgett	P. Hodges	H. Ruegg
M. G. Buehler	W. Kleinfelder	B. Schechtman
Y. S. Chen	J. Koike	J. Shay
C. Y. Duh	R. Koyama	K. Shih
R. Eden	W. Krolikowski	K. Sorenson
J. Eggenburger	D. Landis	E. Tammaru
E. W. Fraser	D. Loescher	R. Woodbury
P. Gary	C. Norris	A. Yu

PUBLICATIONS AND REPORTS

(1 October through 31 December 1964)

PAPERS PRESENTED AT MEETINGS

American Physical Society, Chicago, Illinois, October 23-24, 1964.

W. E. Spicer, "Photoemission Studies of Band Structure - Recent Results." (Invited paper).

C. N. Berglund and W. E. Spicer, "Auger Transitions in Photoemission from Ag."

N. B. Kindig and W. E. Spicer, "d-Band of Cd and CdS - Photoemission Studies."

PAPERS PRESENTED AT MEETINGS (Cont'd)

American Physical Society, Berkeley, California, December 21-23, 1964.

A. J. Blodgett, Jr., and W. E. Spicer, "Experimental Determination of the Density of States in Ni and Fe."

W. E. Spicer and A. J. Blodgett, Jr., "Ferromagnetism and the Density of States in Ni and Fe."

W. F. Krolikowski and W. E. Spicer, "The Energy Band Structure of CuBr."

J. L. Shay and W. E. Spicer, "Band Structure of CdSe."

Second Symposium on Protection Against Radiation in Space, Sponsored by AEC, NASA, and USAF, Gatlinburg, Tennessee, October 12-14, 1964.

W. E. Spicer, "Radiation Effects in Optical Materials." (Invited Paper).

Electrical Engineering Colloquium at New York University, November 10, 1964.

J. B. Angell, "The Impact of Microelectronics on the Future of Computers." Contract AF33(657)-11586.

San Francisco Chap. of IEEE Group on Bio-Medical Engineering, Stanford California, October 20, 1964.

J. G. Linvill, "Research on an Opto-Electronic Reading Aid for the Blind." Nonr-225(44).

PAPERS AND ARTICLES ACCEPTED FOR PUBLICATION

J. G. Linvill, J. B. Angell, and R. L. Pritchard, "Microelectronics vs Electrical Engineering Education," to be published in the special microelectronics issue of the IEEE Proceedings. (December 1964 issue - not out as of January 5, 1965).

ARTICLES PUBLISHED

C. N. Berglund and W. E. Spicer, "Photoemission Studies of Cu and Ag: Theory," Phys. Rev., A136, Nov. 16, 1964, p. 1030.

C. N. Berglund and W. E. Spicer, "Photoemission Studies of Cu and Ag: Experimental," Phys. Rev., A136, Nov. 16, 1964, p. 1044.

C. N. Berglund and W. E. Spicer, "Measurement of Photoemission Electron Energy Distribution by an ac Method," Review of Scientific Instruments, 35, Dec 1964, p. 1665.

H. C. Casey, Jr., and G. L. Pearson, "Rare Earths in Covalent Semiconductors: the Thulium-Gallium Arsenide System," J. Appl. Phys., 35, 3401 (1964).

ARTICLES PUBLISHED (Cont 'd)

M. G. Buehler, W. Shockley, and G. L. Pearson, "Hall Measurements Using Corbino-Like Current Sources in Thin Circular Disks," Appl. Phys. Letters, 5, 228 (1964).

TECHNICAL REPORTS ISSUED BY SSL

(1 October through 31 December 1964)

Office of Naval Research Contract Nonr-225(24)

No. 5064-3: Bevan Peigfeng Wu, "A Study of Red Photoluminescence of Gallium Phosphide Crystals."

No. 5207-1: Juri Vilms, "Quantum Efficiency and Radiative Lifetime in p-Type GaAs."

Office of Naval Research Contract Nonr-225(44)

No. 4816-2: John Knud Knox-Seith, "Improving the Reliability of Digital Systems by Redundancy and Restoring Organs."

PERSONNEL OF SYSTEMS THEORY LABORATORY

(1 October through 31 December 1964)

DIRECTOR - G. F. Franklin (on sabbatical)

ACTING DIRECTOR - R. W. Newcomb

FACULTY AND RESEARCH ASSOCIATES

N. M. Abramson

T. Cover

W. Harman

M. Hoff

T. Kailath

D. Luenberger

P. Mantey

R. Mattson

R. W. Newcomb

R. Smallwood

D. Tuttle

B. Widrow

RESEARCH ASSISTANTS AND FELLOWS

B. Anderson

K. Belser

D. Blumenthal

T. Bullock

C. Burrus

N. Carlson

J. Chang

D. Cogswell

W. Davis

U. Dennis

C. Dorny

R. Dressler

J. En

M. Ferguson

T. Fong

E. Fraser

S. Fralick

N. Gaarder

R. Geesey

G. Gerson

F. Glanz

G. Gucker

M. Gyi

P. Haley

T. Humphrey

C. Isberg

E. Jones

P. Kennedy

A. Kramer

G. Lack

B. McCullough

G. Masters

J. Matheson

L. Meier

B. Miller

A. Nichols

J. Omura

Y. Patt

D. Peterson

J. Rosing

C. Shafer

P. Skov

J. Smith

I. Sobel

D. Specht

L. Talbert

P. Wong

PUBLICATIONS AND REPORTS
(1 October through 31 December 1964)

PAPERS PRESENTED AT MEETINGS

National Electronics Convention, Chicago, Illinois.

N. Abramson, "A Theory of Adaptive Systems."

PAPERS AND ARTICLES ACCEPTED FOR PUBLICATION

N. Abramson, "Information Theory and Real Information," Proceedings of the Polytechnic Institute of Brooklyn Symposium on Systems Theory.

ARTICLES PUBLISHED

N. Abramson, "The Technological Time Constant," IEEE Student Journal, Nov 1964, (reprinted from Proc. IEEE, Sept 1964).

PERSONNEL OF RADIOSCIENCE LABORATORY

(1 October through 31 December 1964)

Only a small number of the personnel have contributed to this manuscript; therefore, only the contributors are listed below.

DIRECTOR - O. G. Villard, Jr.

FACULTY, SENIOR RESEARCH ASSOCIATES, AND RESEARCH ASSOCIATES

L. A. Manning

A. M. Peterson

V. R. Eshleman

RESEARCH ASSISTANTS

D. C. Brown

R. Nowak

D. D. J. Fang

PUBLICATIONS AND REPORTS

(1 October through 31 December 1964)

ARTICLES PUBLISHED

L. A. Manning, "Theoretical Heights and Durations of Echoes from Large Meteors," Radio Science, Journal of Research HBS/URSI, 68D, No. 10, October 1964.

L. A. Manning, "Experimental Determination of Meteoric Line Densities and Attachment Rates," Radio Science, Journal of Research HBS/URSI, 68D, No. 10, October 1964.

TECHNICAL REPORTS ISSUED BY RSL

(1 October through 31 December 1964)

Air Force Contract AF19(604)-7436

No. 8: H. T. Howard, "An Antenna Array for Radar Astronomy Studies in the 20 to 55 Mc Range."

Final: H. T. Howard, B. B. Lusignan, V. R. Eshleman, "Radar Astronomy and Propagation Research."

Air Force Office of Scientific Research Grant AFOSR 62-370

No. 3412-6: Neil Mather Brice, "Discrete Emissions from the Upper Atmosphere."

Office of Naval Research Contract Nonr-225(64)

No. 95: Theodore M. Watt, "Phase Height Oscillations in the Ionosphere."

S-20: R. L. Mester and G. H. Barry, "Technical Report No. S-20." (Report SECRET, Title Unclassified.)

No. 96: L. A. Roben, "Wide Sweep No. 1." (Report SECRET, Title Unclassified.)

No. 97: T. A. Potemra and G. H. Barry, "Ground Detection of Infra-sonic Waves Generated at High Altitudes." (Report SECRET, Title Unclassified.)

National Aeronautics and Space Administration Grant NsG 30-60

No. 7: Theodore M. Watt, "Phase Height Oscillations in the Ionosphere."

National Aeronautics and Space Administration Grant NsG-377

No. 3: H. T. Howard, "An Antenna Array for Radar Astronomy Studies in the 20 to 55 Mc Range."

SR 4: Von R. Eshleman, "Radar Astronomy of Solar System Plasmas."

National Science Foundation Grant NSF-G-17217

No. 3408-2: Ward J. Helms and John P. Turtle, "A Cooperative Report on the Correlation Among Auroral, Magnetic, and ELF Phenomena at Byrd Station, Antarctica."

Contract IA 9039

Final: R. B. Fenwick, "Operational Use of Backscatter Sounding in Broadcasting."

I. ELECTRON DEVICES LABORATORY

Leader	*Subject Area	Project	Contract	Title	Page
Anderson	QE	0173	AFOSR 323-63	Optical spectra of ions in semiconductors	I-1
		0174	Nonr(24)	Microwave spectra of transition-group ions in semiconductor lattices	I-1
		0178	SC-839	Optical maser materials	I-1
Buneman	P	0251	AFOSR 323-63	An I-F plasma experiment	I-6
		0253	AT-326	Anomalous cross-field diffusion	I-6
		0254	NsG 63	Plasma thermionic diodes	I-13
		0255	Nonr(24)	Computer model of a 2-dimensional plasma	I-16
		0256	AT-326	Current flow in plasmas	I-17
		0309	AF 144	Neutralized charged particle streams	I-19
Dunn	P	0311	Nonr(24)	Pinch effects in plasma beams	I-23
		0312	AF 144	Amplification in beam-generated plasmas	I-23
		0313	AMC-094(E)	Computer experiments on beam-generated plasmas	I-26
		0321	AMC-094(E)	Electron beam focusing in ionized gases	I-30
		0322	AF 144	Noise generation in plasmas	I-32
		0323	Nonr(24)	High power microwave transmission in multimode cylindrical waveguide	I-38
Heffner	QE	0414	Nonr(24)	Emission of electrons in solids	I-40
		0415	Nonr(24)	Utilization of optical masers	I-40
Siegman	QE	0558	AMC-094(E)	Investigation of noise in electron guns	I-42
		0572	AFOSR 323-63	Infrared and submillimeter maser studies	I-42
Harris		0576	AF 144	Microwave light modulation methods	I-46
Siegman	QE	0577	AMC-094(E)	Microwave phototubes and light demodulators	I-49
		0581	AF 536	Infrared modulation by free carrier absorption	I-50
Harris		0582	AF 536	Optical phase- and frequency-modulation techniques	I-52
Siegman		0592	SC-839	Laser photomixing studies	I-53

* Subject area codes: P, Plasmas; QE, Quantum Electronics; SS, Solid-State; ST, System Theory; ET, Electron Tubes; RS, Radioscience. When a double reference is given (SS-ST), the work is such that portions of it may appear in each of the laboratories listed.

Contents (Cont 'd)

I. ELECTRON DEVICES LABORATORY (Cont 'd)

Leader	*Subject Area	Project	Contract	Title	Page
Derfler	P	0816	AF 1504	Study of transient phenomena in low pressure gas discharge plasmas	I-56
		0832	AMC-094(E)	RF behavior of plasma diodes	I-65
		0833	NSG 63	DC states of plasma diodes	I-73
Lagerstrom	P	0908	AF 144	Ion and plasma beam sources	I-77

II. SOLID-STATE ELECTRONICS LABORATORY

Angell	SS	4651	AF 586	Physical principles of magnetic adaptive components	II-1
		4657	AF 586	Self-repairing circuit techniques	II-2
Gibbons		4715	Nonr(24)	Transient performance of transistor switches under high level injection	II-5
Linvill		4813	Nonr(44)	Application of solid-state phenomena to microsystems	II-5
		4818	Nonr(31)	Applications of electro-optical phenomena in solids	II-6
		4819	Nonr(44)	Tactical Communication	II-6
		4820	Nonr(31)	Light detection and amplification in semiconductors	II-8
Moll		5002	NsF 1033	High-field transport problem	II-11
		5059	AF 586	Hot electrons in thin metal films	II-12
Pearson		5101	D-155	Diffusion of impurities in III-V compound semiconductor	II-12
		5103	D-155	Anomalous diffusion in compound semiconductors	II-19
		5107	Nonr(24)	Properties of GaAs p-n junctions	II-19
		5108	NSG 555	A study on GaAs _x P _{1-x}	II-19
		5109	NSG 555	Epitaxial growth of III-V semiconductor compounds	II-30
		5110	D-155	The effects of gamma radiation on silicon semiconductor devices	II-34

Contents (Cont 'd)

II. SOLID-STATE ELECTRONICS LABORATORY (Cont 'd)

Leader	*Subject Area	Project	Contract	Title	Page
Pearson	SS	5111	Nonr(24)	Diffusion of impurities in compound semiconductors under partial pressure of one constituent	II-40
Pearson-Moll		5112	NSG 555	Epitaxial growth of GaP	II-48
Spicer		5207	Nonr(24)	Radiative lifetime measurement in GaAs	II-49
Widrow		6758	Nonr(24)	Analysis and synthesis of some adaptive networks	II-49

III. SYSTEMS THEORY LABORATORY

Abramson	ST	6103	Nonr(24)	Pattern recognition and machine learning	III-1
		6105	Nonr(24)	Information theory	III-2
Epley		6203	Nonr(24)	State-logic relations for sequential networks	III-4
		6206	Nonr(24)	Multi-tape sequential machines	III-4
Huffman		6209	Nonr(24)	Logical design of fast circuits	III-5
Franklin		6301	Nonr(24)	Development of simulation facility	III-5
Luenberger		6452	Nonr(24)	Modeling of linear systems	III-5
Grace		6557	Nonr(24)	Theory and design of nonlinear reactance subharmonic generations	III-7
Tuttle		6657	Nonr(24)	Studies of the describing-function method of nonlinear network analysis	III-8
Widrow		6755	AMC-57(Z)	Digital adalines	III-9
		6762	Nonr(24)	Model-referenced adaptive control systems	III-10
		6763	Nonr(24)	Adaptive computer diagnosis of electrocardiograms	III-11
		6764	AMC-57(Z)	Optical input to computers	III-12
		6766	AMC-57(Z)	Conduction effects suitable for adaptive devices	III-12
		6767	AMC-57(Z)	Two-layer adaptation studies	III-12

Contents (Cont 'd)

III. SYSTEMS THEORY LABORATORY (Cont 'd)

Leader	*Subject Area	Project	Contract	Title	Page
Widrow	ST	6772 6773	AF 586 AMC-57(Z)	Pattern recognizing control systems Convergent automatic synthesis procedures for sequential sampled-data networks with feedback	III-13 III-13
Mattson	ST	6950 6952	Nonr(24) Nonr(24)	Threshold logic elements and adaptive systems A study of adaptive input-coding techniques	III-14 III-14
Kailath		7050	Nonr(24)	Communication theory	III-16
IV. RADIOSCIENCE LABORATORY					
Manning	RS	3550	Nonr(24)	Meteor echo properties	IV-1
Peterson		3606	Nonr(24)	Ionospheric winds and irregularities in electron density in the ionosphere	IV-1

ILLUSTRATIONS

<u>Figure</u>	<u>Page</u>
1. Yellow emission lines of ${}^4F_{4/2} \rightarrow {}^6H_{13/2}$ transition in ZnS:Dy at 77 °K	I-2
2. Emission of ZnS:Tb at 77 °K and 4.2 °K	I-3
3. Comparison of emission spectra from three different ZnS:Tb crystals	I-4
4. Plot of E/p as a function of pR and B/p in helium	I-10
5. Comparison of the theoretical and experimental rf electric field required to sustain a constant-current discharge vs magnetic field	I-11
6. Potential fluctuations near the emitter when $\alpha > 1, \eta_2 > 0$	I-13
7. Potential fluctuations near the emitter when $\alpha > 1, \eta_2 < 0$	I-14
8. Potential fluctuations near the emitter when $\alpha < 1, \eta_2 > 0$	I-14
9. Potential fluctuations near the emitter when $\alpha < 1, \eta_2 < 0$	I-14
10a. Collision frequency/plasma frequency = 0.0001, Debye number/wave number = 10.00, drift velocity/thermal velocity = 1.00	I-18
10b. Collision frequency/plasma frequency = 0.0001, Debye number/wave number = 10.00, drift velocity/thermal velocity = 1.40	I-18
10c. Collision frequency/plasma frequency = 0.0100, Debye number/wave number = 10.00, drift velocity/thermal velocity = 1.00	I-18
11. Dynamic display of density variation	I-24
12. Variation of density with current, voltage, and field from a common operating point	I-25
13. Radial variation of potential for different values of α for an electron beam in argon with $r_w/r_c = 3$	I-28
14. Reflex discharge and coaxial probe system	I-34
15. Density and temperature variation in the afterglow	I-35
16. Density and temperature profiles in time	I-36
17. TM_{010} cavity on P.I.G. discharge	I-37
18. The solid lines show the range in kilometers for 1 db of power loss of microwave energy in the TE_{01} mode in circular waveguide as a function of frequency and waveguide diameter	I-39
19. Superposition of filter characteristics on the photo-multiplier characteristic	I-41
20. Equipment for studying the transverse profile of cw laser beams	I-44
21. Curves 1 through 16 give the transverse power density in a laser beam	I-45

<u>Figure</u>	<u>Page</u>
22. Experimental curve at $K_{rel}(E)$ (functional notation) from Nelson and Remeika's paper	I-55
23. Comparison between theory and experiment for laser delay time	I-55
24. Electric field excited by an oscillating dipole sheet as a function of distance	I-61
25. Wave energy excited at a fixed distance from an oscillating dipole sheet as a function of frequency	I-62
26. Effect of collisions on electric field excited by an oscillating dipole sheet as a function of distance	I-62
27. Heating by electron bombardment	I-63
28. Bombarder characteristics	I-64
29. Electron and ion emitter geometry	I-69
30. Electric field amplitudes of the first six resonances for molybdenum emitters spaced 1 cm apart at $T = 2200^\circ K$	I-70
31. Plots of $L/\lambda_o \omega^2/\omega_{po}^2 - 1$ vs $\log L/\lambda_o$ for the first six modes	I-71
32. Ion (γ_p)-, atom (γ_a)-, and particle ($\gamma_a + \gamma_p$)- emission rates in $cm^{-2} sec^{-1}$ vs the fraction θ of the ionic monolayer covering a tungsten surface at $848^\circ K$	I-74
33. Ion (γ_p)-, atom (γ_a)-, and particle ($\gamma_a + \gamma_p$)- emission rates in $cm^{-2} sec^{-1}$ vs the fraction θ of the ionic monolayer covering a tungsten surface at $1800^\circ K$	I-77
34. Code selection nomograph	II-4
35. Negative resistance circuit and V-1 characteristic	II-5
36. The physical measuring set up	II-7
37a. Magnitude of skin impedance	II-7
37b. Phase angle of skin impedance	II-8
38. Estimated propagation delay for three "state-of-the-art" opto-electronic logic building blocks vs power dissipation . .	II-10
39. Illustration of Hall coefficient measurement using a square array of points centered on a thin circular sample	II-13
40. Boundary condition is satisfied along vertical axis by adjusting the currents (dashed lines) from A_1 to image those from A	II-15
41. Hall-effect correction factors using a square array of points centered on a thin circular sample	II-18
42. Appearance of sample No. 20 after growth (all 50X)	II-22

<u>Figure</u>	<u>Page</u>
43. X-ray diffraction pattern of powered sample of Si GaAs $P_x 1-x$ ($a_0 = 5.515 \text{ \AA}$)	II-23
44. Comparison of transmission data near band edge	II-23
45. $\alpha^{1/2}$ vs photon energy at band edge of sample No. 23	II-24
46. Reststrahlen bands	II-25
47. Lattice absorption bands of GaAs $.15P_{.85}$ at 300°K	II-26
48. Lattice absorption bands of GaAs $.325P_{.675}$ at 300°K	II-27
49. Lattice absorption bands of GaAs $.52P_{.48}$ at 300°K	II-27
50. Lattice absorption bands of GaAs $.65P_{.35}$ at 300°K	II-28
51a. Combination bands of the alloyed crystal in the region of $13\mu-14\mu$	II-29
51b. Integrated intensity vs composition	II-29
52. Carrier concentration vs total radiation dose shielded N-type silicon (unijunction transistors)	II-36
53. Carrier concentration vs radiation dose high resistivity N-type silicon	II-37
54. Sketch showing expected variation of damage rate in silicon with thickness of shielding	II-39
55. A schematic diffusion ampoule	II-40
56. Diffusion profile of Zn in GaAs at 900°C for 1.5 hrs with no As added	II-42
57. Diffusion profile of Zn in GaAs at 900°C for 1.5 hrs with excess As added corresponding to P_{As_4} (calculated) = 0.2 atms	II-43
58. Diffusion profile of Zn in GaAs at 900°C for 1.5 hrs with excess As added corresponding to P_{As_4} (calculated) = 0.31 atms	II-43
59. Diffusion profile of Zn in GaAs at 900°C for 1.5 hrs with excess As added corresponding to P_{As_4} (calculated) = 0.42 atms	II-44
60. Diffusion profile of Zn in GaAs at 900°C for 1.5 hrs with excess As added corresponding to P_{As_4} (calculated) = 0.57, 2, 3.75 and 9.6 atms	II-44
61. Variation of ρ_{Si} , x_j , and $\bar{\sigma}$ as function of arsenic pressure for Zn diffusion in GaAs at $T = 900^\circ \text{C}$ and $t = 1.5 \text{ hrs}$ assuming that there is no interaction between As and Zn . . .	II-45
62. Variation of surface zinc concentration as function of arsenic pressure for Zn diffusion in GaAs at $T = 900^\circ \text{C}$ and $t = 1.5 \text{ hrs}$ assuming that there is no interaction be- tween As and Zn	II-46

Figure

Page

63. Diffusion profiles of Zn in GaAs at 900 °C for 1.5 hrs with same amount of excess As added corresponding to P_{AS_4} (calculated) = 0.53 atms II-47

CROSS INDEX

Office of Naval Research Contract Nonr-225(24)

Project	Title	*Subject Area	Leader	Page
ELECTRON DEVICES LABORATORY				
0174	Microwave spectra of transition-group ions in semiconductor lattices	QE	Anderson	I-1
0255	Computer model of a 2-dimensional plasma	P	Buneman	I-16
0311	Pinch effects in plasma beams	P	Dunn	I-23
0323	High power microwave transmission in multimode cylindrical waveguide	P	Dunn	I-38
0414	Emission of electrons in solids	QE	Heffner	I-40
0415	Utilization of optical masers	QE	Heffner	I-40
SOLID-STATE ELECTRONICS LABORATORY				
4715	Transient performance of transistor switches under high level injection	SS	Gibbons	II-5
5107	Properties of GaAs p-n junctions	SS	Pearson	II-19
5111	Diffusion of impurities in compound semiconductors under partial pressure of one constituent	SS	Pearson	II-40
5207	Radiative lifetime measurement in GaAs	SS	Spicer	II-49
6758	Analysis and synthesis of some adaptive networks	SS-ST	Widrow	II-49
SYSTEMS THEORY LABORATORY				
6103	Pattern recognition and machine learning	ST	Abramson	III-1
6105	Information theory	ST	Abramson	III-2
6203	State-logic relations for sequential networks	ST	Epley	III-4
6206	Multi-tape sequential machines	ST	Epley	III-4
6209	Logical design of fast circuits	ST	Huffman	III-5
6301	Development of simulation facility	ST	Franklin	III-5
6452	Modeling of linear systems	ST	Luenberger	III-5
6557	Theory and design of nonlinear reactance subharmonic generations	ST	Grace	III-7
6657	Studies of the describing-function method of nonlinear network analysis	ST	Tuttle	III-8
6762	Model-referenced adaptive control systems	SS-ST	Widrow	III-10
6763	Adaptive computer diagnosis of electrocardiograms	SS-ST	Widrow	III-11

*Subject area codes: P, Plasmas; QE, Quantum Electronics; SS, Solid-State; ST, Systems Theory; ET, Electron Tubes; RS, Radioscience. When a double reference is given (SS-ST), the work is such that portions of it may appear in each of the laboratories listed.

Cross Index (Cont'd)

Office of Naval Research Contract Nonr-225(24) (Cont'd)

Project	Title	*Subject Area	Leader	Page
SYSTEMS THEORY LABORATORY (Cont'd)				
6950	Threshold logic elements and adaptive systems	SS-ST	Mattson	III-14
6952	A study of adaptive input-coding techniques	ST	Mattson	III-14
7050	Communication theory	ST	Kailath	III-16
RADIOSCIENCE LABORATORY				
3550	Meteor echo properties	RS	Manning	IV-1
3606	Ionospheric winds and irregularities in electron density in the ionosphere	RS	Peterson	IV-1

Office of Naval Research Contract Nonr-225(31)

SOLID-STATE ELECTRONICS LABORATORY				
4818	Applications of electro-optical phenomena in solids	SS	Linvill	II-6
4820	Light detection and amplification in semiconductors	SS	Linvill	II-8

Office of Naval Research Contract Nonr-225(44)

SOLID-STATE ELECTRONICS LABORATORY				
4813	Application of solid-state phenomena to microsystems	SS	Linvill	II-5
4819	Tactical Communications	SS	Linvill	II-6

Air Force Contract AF33(657)-11586

SOLID-STATE ELECTRONICS LABORATORY				
4651	Physical principles of magnetic adaptive components	SS	Angell	II-1
4657	Self-repairing circuit techniques	SS	Angell	II-2
5059	Hot electrons in thin metal films	SS	Moll	II-12
SYSTEMS THEORY LABORATORY				
6772	Pattern recognizing control systems	ST	Widrow	III-13

Cross Index (Cont'd)

Air Force Contract AF04(695)-536

Project	Title	*Subject Area	Leader	Page
ELECTRON DEVICES LABORATORY				
0581	Infrared modulation by free carrier absorption	QE	Siegman	I-50
0582	Optical phase- and frequency-modulation techniques	QE	Harris	I-52

National Aeronautics and Space Administration Grant NsG 555

SOLID-STATE ELECTRONICS LABORATORY				
5108	A study on GaAs _x P _{1-x}	SS	Pearson	II-19
5109	Epitaxial growth of III-V semiconductor compounds	SS	Pearson	II-30
5112	Epitaxial growth of GaP	SS	Pearson	II-48

Department of the Army, Army Research Office Contract DA-31-124 ARO-D-155

SOLID-STATE ELECTRONICS LABORATORY				
5101	Diffusion of impurities in III-V compound semiconductors	SS	Pearson	II-12
5103	Anomalous diffusion in compound semiconductors	SS	Pearson	II-19
5110	The effects of gamma radiation on silicon semiconductor devices	SS	Pearson	II-34

National Science Foundation Grant NsF-GP 1033

SOLID-STATE ELECTRONICS LABORATORY				
5002	High-field transport problem	SS	Moll	II-11

Army Contract DA04(200) AMC-57(Z)

SYSTEMS THEORY LABORATORY				
6755	Digital Adalines	ST	Widrow	III-9
6764	Optical inputs to computers	ST	Widrow	III-12
6766	Conduction effects suitable for adaptive devices	ST	Widrow	III-12
6767	Two-layer adaption studies	ST	Widrow	III-12
6773	Convergent automatic synthesis procedures for sequential sampled-data networks with feedback	ST	Widrow	III-13

Cross Index (Cont'd)

Air Force Contract AF33(657)-11144

Project	Title	*Subject Area	Leader	Page
ELECTRON DEVICES LABORATORY				
0309	Neutralized charged particle streams	P	Dunn	I-19
0312	Amplification in beam-generated plasmas	P	Dunn	I-23
0322	Noise generation in plasmas	P	Dunn	I-32
0576	Microwave light modulation methods	QE	Harris	I-46
0908	Ion and plasma beam sources	P	Lagerstrom	I-77

Air Force Contract AF33(615)-1504

ELECTRON DEVICES LABORATORY				
0816	Study of transient phenomena in low pressure gas discharge plasmas	P	Derfler	I-56

Signal Corps Contract DA 36-039 SC-90839

ELECTRON DEVICES LABORATORY				
0178	Optical maser materials	QE	Anderson	I-1
0592	Laser photomixing studies	QE	Siegman	I-53

Army Contract DA 36-039 AMC-00094(E)

ELECTRON DEVICES LABORATORY				
0313	Computer experiments on beam-generated plasmas	P	Dunn	I-26
0321	Electron beam focusing in ionized gases	P	Dunn	I-30
0558	Investigation of noise in electron guns	ET	Siegman	I-42
0577	Microwave phototubes and light demodulators	ET	Siegman	I-49
0832	RF behavior of plasma diodes	P	Derfler	I-65

National Aeronautics and Space Administration Grant NsG 299-63

ELECTRON DEVICES LABORATORY				
0254	Plasma thermionic diodes	P	Buneman	I-13
0833	DC states of plasma diodes	P	Derfler	I-73

Cross Index (Cont'd)

Atomic Energy Commission Contract AT(04-3)326 PA No. 8

<u>Project</u>	<u>Title</u>	<u>*Subject Area</u>	<u>Leader</u>	<u>Page</u>
ELECTRON DEVICES LABORATORY				
0253	Anomalous cross-field diffusion	P	Buneman	I-6
0256	Current flow in plasmas	P	Buneman	I-17

Air Force Office of Scientific Research Grant No. 323-63

ELECTRON DEVICES LABORATORY				
0173	Optical spectra of ions in semi-conductors	QE	Anderson	I-1
0251	An I-F plasma experiment	P	Buneman	I-6
0572	Infrared and submillimeter maser studies	QE	Siegman	I-42

Project 0173: OPTICAL SPECTRA OF IONS IN SEMICONDUCTORS

Air Force Office of Scientific Research Grant 323-63
Project Leader: W. W. Anderson
Staff: T. C. Lee

The object of this project is to investigate various semiconductor lattices as hosts for active optical maser ions. This will involve the incorporation of members of the 3d and 4f transition group ions into semiconductor lattices, an investigation of absorption and emission spectra, and a study of the mechanisms of energy transfer from the host lattice to the active ion.

The final report is in production. This project will be terminated with publication of the final report.

Project 0174: MICROWAVE SPECTRA OF TRANSITION-GROUP IONS IN SEMICONDUCTOR LATTICES

Tri-Service Contract Nonr-225(24)
Project Leader: W. W. Anderson
Staff: I. C. Chang

The object of this project is to study the microwave EPR spectra of selected transition-group ions in semiconductor crystal lattices. The ultimate purpose of this work is to evaluate the potentialities of the class of materials proposed by Bleany [Ref. 1] for microwave masers.

A final report is in production. This project will be terminated with publication of the final report.

Project 0178: OPTICAL MASER MATERIALS

Signal Corps Contract DA 36-039 SC-90839
Project Leader: W. W. Anderson
Staff: S. Razi, W. Hemphill

Work during this quarter was concentrated on determining the number of different sites occupied by Tb^{3+} ions in ZnS. We have also prepared some ZnS:Dy crystals and observed a very strong yellow emission.

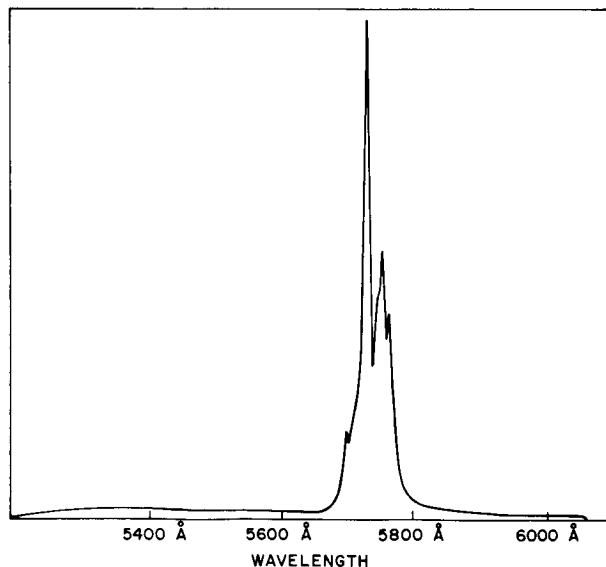
¹B. Bleany, "A New Class of Materials for Bloembergen-Type Masers," Proc. Phys. Soc., 73, London, 937-939 (1959).

For ZnS:Dy, groups of lines, centered at the wavelengths indicated in Table I, were observed and the corresponding term assignments are given. No line near 9300 Å corresponding to the ${}^4F_{9/2} \rightarrow {}^6H_{5/2}$ transition

TABLE 1

Wavelength	Term Assignment	Comments
4800 Å	${}^4F_{9/2} \rightarrow {}^6H_{15/2}$	resonance line
5740 Å	${}^4F_{9/2} \rightarrow {}^6H_{13/2}$	very strong
6600 Å	${}^4F_{9/2} \rightarrow {}^6H_{11/2}$	weak
7460 Å	${}^4F_{9/2} \rightarrow {}^6H_{9/2}$	
8400 Å	${}^4F_{9/2} \rightarrow {}^6H_{7/2}$	weak

was seen. In Fig. 1 we show the strong line group at 5740 Å. The spectrum was taken at 77 °K. At room temperature or at 77 °K, this 5740 Å group is the dominant emission which gives the crystals a bright yellow fluorescence. Short-wavelength uv excitation was used so that the Dy³⁺ ion was acting as the dominant radiative recombination center, even though the Dy³⁺ concentration was about .02 percent by weight.



33015
 FIG. 1. YELLOW EMISSION LINES OF ${}^4F_{9/2} \rightarrow {}^6H_{13/2}$
 TRANSITION IN ZnS:Dy AT 77 °K.

The first step in determining the number of sites occupied by rare-earth ions is a line count as performed for the ${}^4F_{3/2} \rightarrow {}^4I_{9/2}$ transition of ZnS:Nd in the previous QRR. For the ${}^5D_4 \rightarrow {}^7F_5$ transition of ZnS:Tb, the terminal multiplet will split into 7 Stark levels in a crystalline field of C_{3v} symmetry or into 11 levels in a field of lower symmetry. To determine if emission is from more than one excited state, the results of 77 °K and 4.2 °K photoluminescence experiments may be compared as in Fig. 2. The three lines circled in the 77 °K emission disappear at 4.2 °K and are probably from an excited state of the 5D_4 multiplet. All other lines are present in both spectra in approximately the same intensity ratio and may be ascribed to the lowest level of 5D_4 in the various site symmetries. The principal difference is an apparent narrowing of the lines at 4.2 °K and a resultant better resolution. The apparent line shift and narrowing of the strong line near 5450 Å may be due to the fact that there are at least three unresolved lines here separated by 2.3 Å and .65 Å or 7.75 cm^{-1} and 2.2 cm^{-1} as determined by a high resolution trace of this line at 4.2 °K in a different crystal.

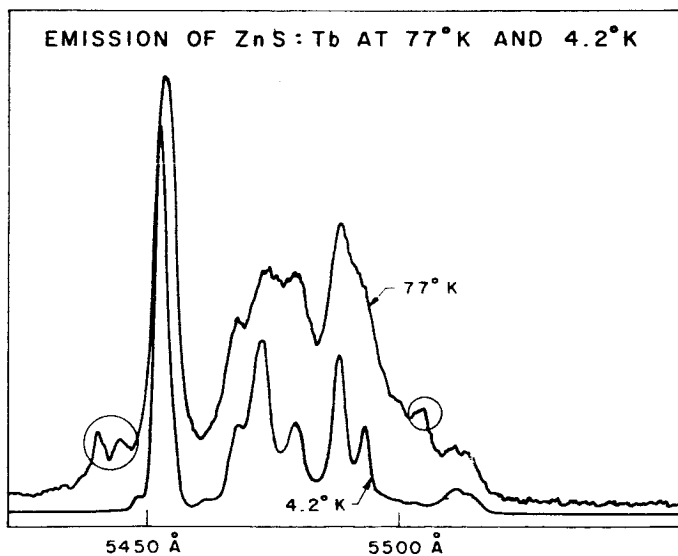
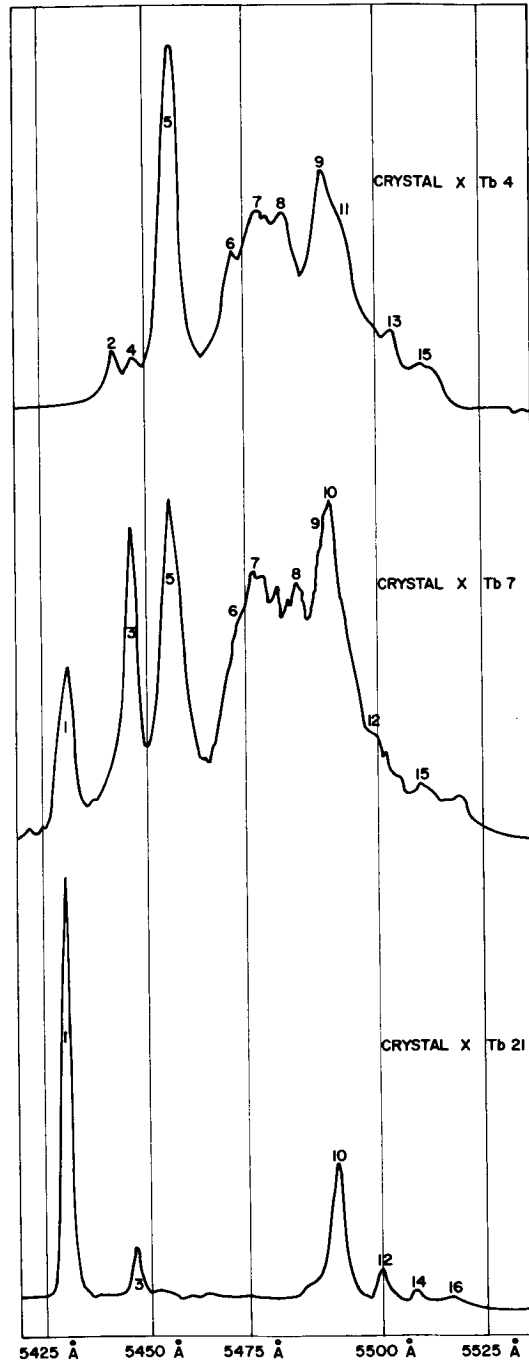


FIG. 2. EMISSION OF ZnS:Tb at 77 °K AND 4.2 °K.

At 4.2 °K we can count 9 lines in Fig. 2 (11 in a higher resolution trace) which may or may not all be due to Tb^{3+} in a common site. In C_{3v}

symmetry, only 5, 6, or 7 transitions would be allowed, depending on whether an A_1 , A_2 or E level was lowest in 5D_4 . Comparing emission from various crystals at 77 °K as in Fig. 3, we can count a minimum of



33016

FIG. 3. COMPARISON OF EMISSION SPECTRA FROM THREE DIFFERENT ZnS:Tb CRYSTALS.

17 lines. Note further that crystals XTb4 and XTb21 have no lines in common, while XTb7 has some lines common to both XTb4 and XTb21. We have numbered corresponding lines for the three crystals. There are thus at least two distinct Tb^{3+} sites. We further note that in crystals with spectra of the type exhibited by XTb21, lines 1 and 3 occur in different intensity ratios as well as the fact that the intensity ratio of these two lines is very different in XTb7 and XTb21. There are thus a minimum of 3 distinct Tb^{3+} sites.

We digress at this point to comment on the spectra of XTb21. Many crystals have been grown which exhibit this type of spectrum. All of the lines are as well resolved and narrow at 77 °K as at 4.2 °K. Other than line No. 3, the relative intensities of the various lines remain the same from crystal to crystal. Line No. 3 can be eliminated by annealing in Zn vapor which leads us to suspect that it is due to a Zn vacancy next to a Tb^{3+} ion. Line No. 1 is narrower ($\Delta \lambda \approx 2.3 \text{ \AA}$) than the other lines. Since this is the shortest wavelength line present, we believe it to be due to a transition from the lowest level of 5D_4 to the lowest level of 7F_5 . Transitions of this type are only strain broadened while the longer wavelength transitions to excited levels of 7F_5 are both strain and lifetime broadened.

If there are a number of Tb^{3+} sites present, we would expect different efficiency of luminescence for different sites depending on the method of excitation. We can observe luminescence under short-wave uv (hole-electron pair production), long-wave uv (direct absorption by Tb^{3+}), ir stimulation (hole liberation and subsequent recombination), and electroluminescence. Preliminary results on crystals of type XTb7 (Fig. 3) show that lines No. 7 and No. 9 are from different sites so that there are now a minimum of 4 distinct Tb^{3+} site symmetries. Comparison of photoluminescence and electroluminescence on the same crystal (again of type XTb7) shows line No. 3 the strongest in electroluminescence with almost no lattice background. The interpretation of these results will be one of the problems for the coming quarter.

Project 0251: AN I-F PLASMA EXPERIMENT

Air Force Office of Scientific Research Grant 323-63
Project Leader: O. Buneman
Staff: J. O. Hosea

The purpose of this project is to perform an experiment, or groups of experiments, that will differentiate between "individual" phenomena in plasmas.

Work on this project has been terminated. Further related work will be carried out under Project 0322 and will be reported under that project number.

Project 0253: ANOMALOUS CROSS-FIELD DIFFUSION

Atomic Energy Commission Contract AT(04-3)326
Project Leader: O. Buneman
Staff: D. Pigache, E. J. Powers, G. Reiter,
J. Hosea

The purpose of this project is the study of diffusion in a cylindrical discharge in a strong axial magnetic field. Measured diffusion rates across the field are higher than the rate proportional to $(1/B^2)$ predicted by binary collision theory. The observed anomalous diffusion rates can only be accounted for by some type of instability, and this project is concerned with a theoretical and experimental study of some of the possible instabilities in such a discharge and their effects on diffusion rates.

A. ANOMALOUS DIFFUSION IN AN RF DISCHARGE

In previous reports we have presented evidence of anomalous diffusion in an rf discharge. In particular, we have mentioned that as the magnetic field is increased from zero the rf voltage and power required to maintain a constant-density discharge initially decrease but start to rise when the magnetic field exceeds a critical value B_c . This rise is attributed to anomalous diffusion and is accompanied by the onset of low-frequency fluctuations. Although the above observations all indicate that anomalous diffusion processes occur in a radio-frequency discharge, it is very difficult to make a direct comparison between them and that predicted by classical diffusion theory. This difficulty is overcome by approaching the problem as discussed below.

In the following we briefly outline the theory of a diffusion-dominated discharge and compare it with the experimental results. A more detailed account of the theory and experiment will be included in a Technical Report which is currently being prepared.

We consider a diffusion-dominated discharge where, for the purposes of discussion, end losses are neglected. Inclusion of end losses would not strongly affect our results provided the length of the tube is sufficiently long compared to the radius. For a steady-state discharge the equation of continuity becomes

$$\nabla \cdot (n\vec{v}) = zn \quad (1)$$

when attachment and volume recombination have been neglected. The electron and ion density, the drift velocity, and the ionization rate per electron are given by n , \vec{v} , and z respectively. Since the discharge is diffusion dominated, $n\vec{v}$ is given by

$$n\vec{v} = -D_{a\perp} \nabla n \quad (2)$$

where $D_{a\perp}$ is the transverse (to the magnetic field) ambipolar diffusion coefficient. It is related to the ambipolar diffusion coefficient D_a in the absence of a magnetic field by the following expression

$$D_{a\perp} = \frac{D_a}{1 + \left(\frac{\omega_e}{\nu_e}\right)\left(\frac{\omega_i}{\nu_i}\right)} \quad (3)$$

where ω_e , ω_i , ν_e , ν_i are the electron cyclotron frequency, the ion cyclotron frequency, the electron-neutral collision frequency, and the ion-neutral collision frequency respectively. Note that $D_{a\perp}$ is proportional to B^{-2} for sufficiently large magnetic field. Substitution of Eq. (2) into Eq. (1) yields

$$D_{a\perp} \nabla^2 n + zn = 0 \quad (4)$$

which says that the rate at which electrons and ions are created per unit volume (zn) equals the rate at which they diffuse out of a unit volume ($-D_{a1} \nabla^2 n$). The solution of Eq. (4) in cylindrical geometry is

$$n(r) = n_0 J_0 \left(\sqrt{\frac{z}{D_a}} r \right) .$$

Application of the boundary condition $n(R) = 0$ yields the following relationship between z and D_{a1}

$$\frac{z}{D_{a1}} = \left(\frac{2.4}{R} \right)^2 \quad (5)$$

where R is the radius of the tube. Dividing both sides by the square of the pressure p , and writing D_{a1} in terms of D_a gives

$$\left(\frac{z}{p} \right) \left(\frac{1}{D_a p} \right) = \left(\frac{1}{pR \sqrt{1 + \frac{\omega_e}{v_e} \frac{\omega_i}{v_i}}} \right)^2 . \quad (6)$$

For a given gas and electron velocity distribution z/p is a unique function of the electron temperature T_e . $D_a p$ is also a function of T_e . Therefore, Eq. (6) may be solved to give T_e as a function of pR and $(\omega_e/v_e) (\omega_i/v_i)$

$$T_e = f_1 \left(pR \sqrt{1 + \frac{\omega_e}{v_e} \frac{\omega_i}{v_i}} \right) . \quad (7)$$

The electron temperature T_e may be related to the applied axial rf electric field through the principle of energy balance, which states that in the steady-state situation the rate of energy delivered to an electron by the rf electric field equals the rate of energy lost per electron. That is,

$$\text{Re} [-e \vec{E} \cdot \vec{v}^*] = \left(\frac{3}{2} kT_e \right) \kappa(T_e) v_e \quad (8)$$

where $-e$ is the charge on an electron, \vec{E} is the effective value of the applied rf electric field, \vec{v}^* is the complex conjugate of the electron's rf drift velocity, $\kappa(T_e)$ is the total fractional loss of energy suffered by an electron upon colliding with a neutral gas particle, and $3/2 kT_e$ is the average thermal energy of an electron. $\kappa(T_e)$ takes into account that an electron loses its energy in elastic, exciting, and ionizing collisions. It also takes into account the fact that the electrons lost to the wall are "hot", whereas the electrons created to take their place are "cold" and must be heated to a temperature T_e by the rf electric field. By using the data given by Lehnert [Ref. 1] for $\kappa(T_e)$, we are able to solve Eq. (8) for E/p as a function of T_e

$$E/p = f_2 (T_e) . \quad (9)$$

By combining Eqs. (7) and (9) we express E/p in terms of pR and $(\omega_e/\nu_e) (\omega_i/\nu_i)$

$$E/p = f_3 \left(pR \sqrt{1 + \frac{\omega_e}{\nu_e} \frac{\omega_i}{\nu_i}} \right) . \quad (10)$$

For H_e^+ ions

$$\frac{\omega_e}{\nu_e} \frac{\omega_i}{\nu_i} = \mu_e \mu_i B^2 \cong 0.6 \left[\frac{B(\text{kG})}{p(\text{mmHg})} \right]^2 \quad (11)$$

where the data for the electron mobility μ_e is taken from Brown [Ref. 2] and for the ion mobility μ_i from Biondi and Chanin [Ref. 3]. Eqs. (10)

¹B. Lehnert, Proceedings of the Second International Conference on the Peaceful Uses of Atomic Energy, Geneva, 1958. (United Nations, Geneva, 1958), Vol. 32, p. 349.

²S. C. Brown, Basic Data of Plasma Physics, (Technology Press and John Wiley and Sons, New York, 1959).

³M. R. Biondi and L. M. Chanin, Phys. Rev., 94, 910 (1954).

and (11) relate the variation of E/p to pR and B/p . We recall that B/p and pR were the two similarity parameters used to plot the dc and rf critical field data for comparison purposes in previous QRR's.

The functional dependence of E/p on pR and B/p is shown in Fig. 4 for helium. Note that it is a universal curve good for all combinations of p , R , and B as long as the initial assumptions upon which the theory is based hold true. It predicts for a fixed p and R that the rf electric field required to sustain a steady-state discharge should decrease monotonically as we increase B . In summary then, according to the classical theory, the effect of applying an axial magnetic field is to decrease $D_{a\perp}$, z , T_e , and E monotonically.

In Fig. 5 we present a typical experimental result. The two top curves are plots of the theoretical and experimental rf electric fields

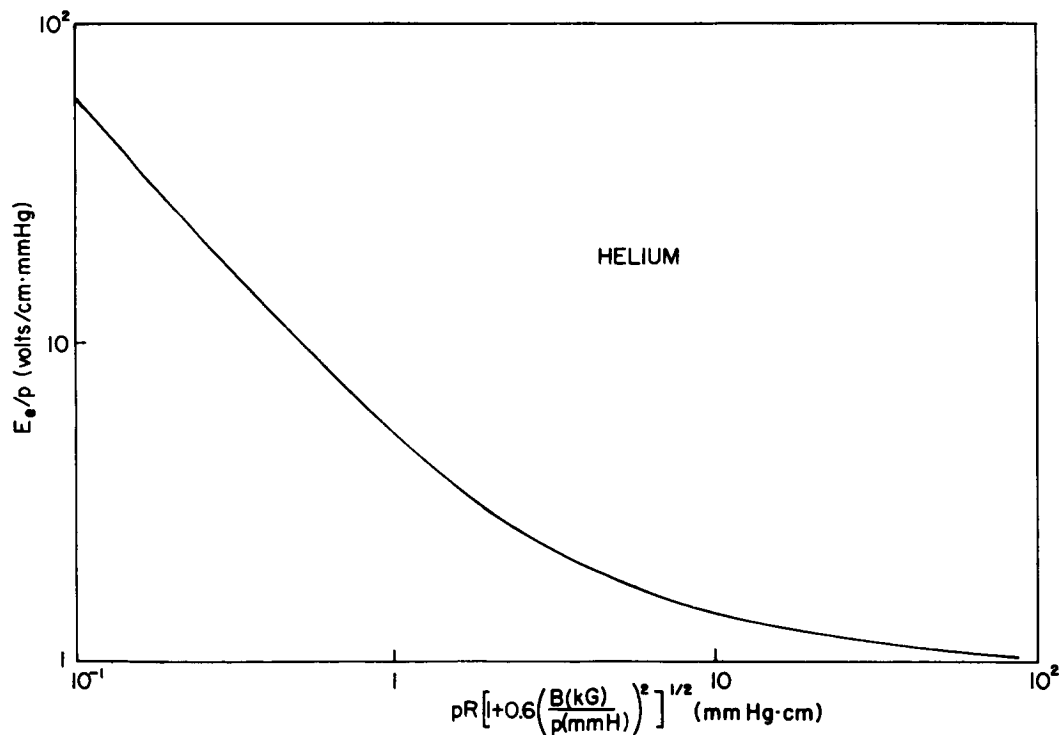
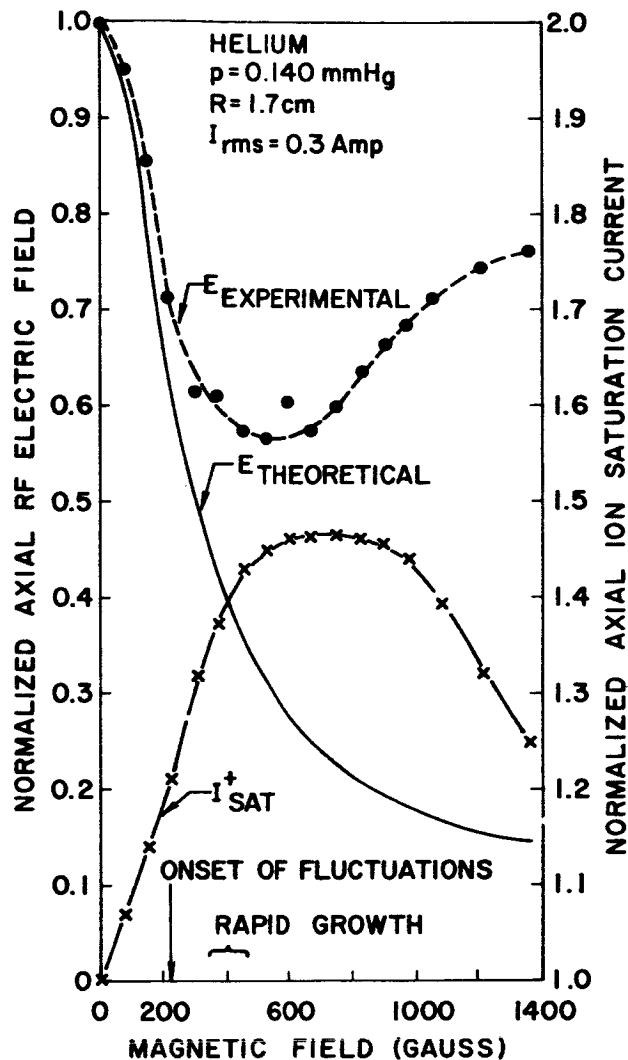


FIG. 4. PLOT OF E/p AS A FUNCTION OF pR AND B/p IN HELIUM.



32396

FIG. 5. COMPARISON OF THE THEORETICAL AND EXPERIMENTAL RF ELECTRIC FIELD REQUIRED TO SUSTAIN A CONSTANT-CURRENT DISCHARGE VS MAGNETIC FIELD. Variation of the ion saturation current to a probe located on the axis of the discharge vs magnetic field.

required to sustain a constant-current discharge. They are both normalized to unity at $B = 0$. The theoretical curve is based upon Fig. 4 which was computed assuming classical diffusion theory. We see that the measured field decreases in fairly good agreement with the theoretical curve, but only up to a field of approximately a few hundred gauss. Above this field the experimental rf electric field diverges from that predicted by classical

diffusion theory and eventually rises. It is this divergence and rise which we interpret in terms of anomalous diffusion. The rising portion of the rf electric-field curve indicates that the ionization rate is increasing. Since in the steady-state discharge production equals loss, this rise in the production (or ionization) rate implies an increase in the loss (or diffusion) rate which is in contradiction with classical diffusion theory. We note also that the transition to anomalous diffusion is accompanied by the onset of low frequency fluctuations. These fluctuations have been described in previous QRR's.

In the lower curve we have plotted the ion saturation current as measured by a double probe located on the axis of the tube midway between the two rf electrodes. It is normalized to unity at zero magnetic field. We see that increasing the magnetic field causes the ion density (which is roughly proportional to the ion saturation current) to rise, level off, and then to decrease. This fall off in density is another indication that the magnetic field is no longer containing the plasma as well as it did at lower values of magnetic field.

Thus for the first time we are able to compare the experimentally determined behavior of a parameter, in this case the rf electric field, with that predicted by classical diffusion theory. Comparison of the two confirms our interpretation of the earlier results, namely that anomalous diffusion occurs in radio-frequency discharges.

B. BAGEL II

It has been found during the last quarter that some misalignment of the magnetic coils still exists at both ends of the straight section opposite to the cathode anode structure. Four radially moveable Langmuir probes have been added in this straight section--at both ends and in the middle. One probe is vertical, three others are horizontal. These probes permit us to check if the plasma is well centered in the tube. Although this misalignment existed, a preliminary study of the decay time in the afterglow was made. It seems that the main cause of loss during the first 200 μ s is classical diffusion across the magnetic field and volume recombination thereafter. This experiment will continue when the plasma is more perfectly centered in the tube.

Project 0254: PLASMA THERMIONIC DIODES

National Aeronautics and Space Administration
Grant NsG 299-63

Project Leader: O. Buneman

Staff: P. Burger, M. F. O'Neal

The purpose of this project is to study the randomization of electron energies in thermionic diodes by computer methods.

We summarized the results obtained for the low-pressure (collisionless) one-dimensional thermionic converter.

When the separation between the emitter and collector plates is larger than ten electron Debye lengths, the operation of the diode is determined essentially by two parameters:

1. The ratio of charge densities near the emitter called $\alpha = J_{si} m_i / J_{se} m_e$, where J_{si} , J_{se} are the saturation currents of the ions and electrons respectively and m_i , m_e are their respective masses.
2. The applied potential, which has the normalized form $\eta_2 = eV_2/kT$ where V_2 is the applied potential in volts, and T is the emitter temperature.

Depending whether η_2 is positive or negative and α is larger or smaller than unity we define four operating regions. The stable or unstable behavior of the diode can be demonstrated by plotting the potential as function of time at some point in the diode. This corresponds to an ideal probe inserted into the diode space. We plot the potential for the four regions on Figs. 6-9 at a point which is approximately ten

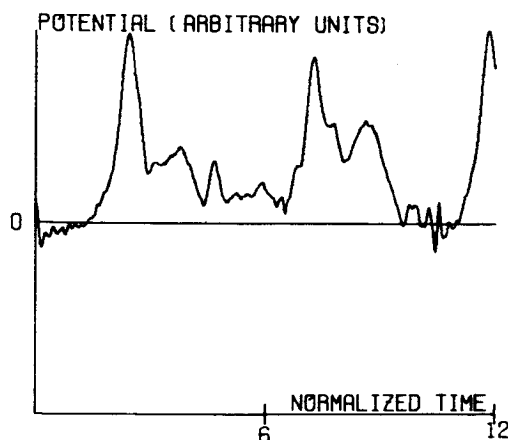


FIG. 6. POTENTIAL FLUCTUATIONS NEAR THE EMITTER WHEN $\alpha > 1$, $\eta_2 > 0$.

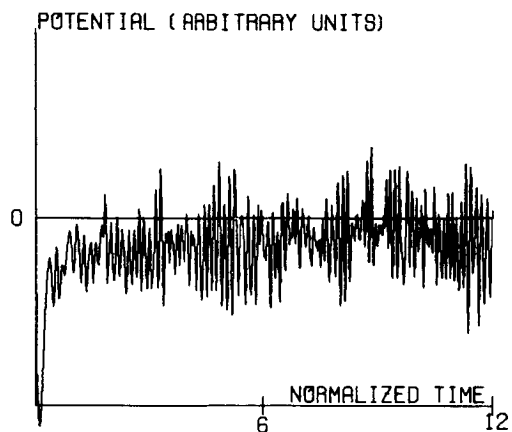


FIG. 7. POTENTIAL FLUCTUATIONS NEAR THE EMITTER WHEN $\alpha > 1, \eta_2 < 0$.

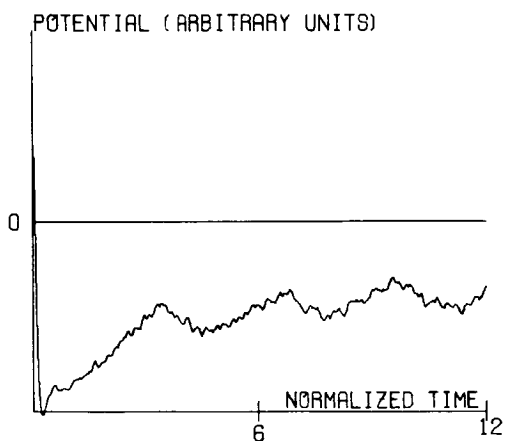


FIG. 8. POTENTIAL FLUCTUATIONS NEAR THE EMITTER WHEN $\alpha < 1, \eta_2 > 0$.

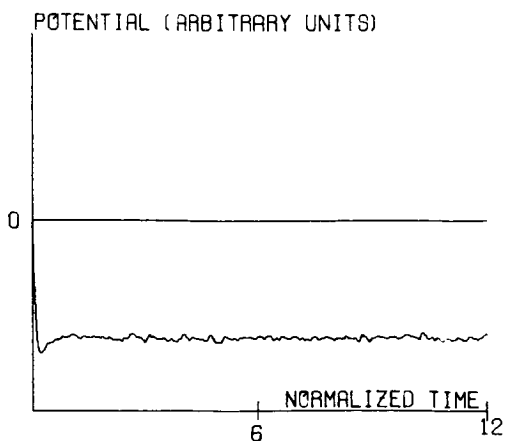


FIG. 9. POTENTIAL FLUCTUATIONS NEAR THE EMITTER WHEN $\alpha < 1, \eta_2 < 0$.

electron Debye lengths from the emitter. We expect the fluctuations to be the largest here, because this point is in the general neighborhood where a potential minimum (for the electron-rich case) or a potential maximum (for the ion-rich case) is formed. The simulated converter is fifty electron Debye lengths long. On these figures time is normalized to the average electron transit time and since the ratio of ion to electron mass is 64, the average ion transit time is eight times the average electron transit time. The scale of the potential axis is in arbitrary units because the actual value of the potential depends on the applied potential and we are interested here only in the general behavior of the diode. This behavior depends only on whether the potential is positive or negative and not on its actual value.

In the first region ($\eta_2 > 0, \alpha > 1$) the converter exhibits large-amplitude, low-frequency oscillations (see Fig. 6). The frequency of these oscillations is approximately equal to one over the average ion transit time, and thus can be easily detected in cesium diodes which operate in this region. We have studied these oscillations in detail and reported results in earlier QRR's. The diode operating in the second region, ($\alpha > 1, \eta_2 < 0$) exhibits high-frequency oscillations (see Fig. 7). It is difficult to observe these fluctuations in a cesium diode because their frequency is of the order of the electron plasma frequency near the emitter, i.e., thousands of megacycles and the amplitudes are small (typically a tenth of a volt). Nevertheless the computer simulation technique shows that the diode will be noisy in this region.

If the converter operates in the third region ($\eta_2 > 0, \alpha < 1$) a true potential minimum is formed near the emitter which limits the electron current flowing in the diode below its saturation value (see Fig. 8). The fluctuations become small--though there is a trace of collective oscillations with ion frequency--and apparently the operation of the diode is stabilized. The stabilization is increased by applying negative voltage to the collector (see Fig. 9). In this region ($\eta_2 < 0, \alpha < 1$) the fluctuations are due only to shot-noise effects and are of negligible amplitude. These calculations indicate that an extremely quiet and stable plasma is created in a cesium diode when it operates in the electron-rich region with a negative bias on the collector. The results are summarized in Table 1 on the following page.

TABLE 1. THE STABLE AND UNSTABLE REGIONS OF THE CONVERTER.

	$\eta_2 > 0$	$\eta_2 < 0$
ION RICH	UNSTABLE (LOW FREQUENCY)	UNSTABLE (HIGH FREQUENCY)
ELECTRON RICH	STABLE	STABLE

We are considering the expansion of the computer simulation procedure at the present. We will introduce surface effects at the emitter (changing work functions for ions, electrons as functions of cesium coverage), elastic collisions for ions and electrons with neutrals and volume ionization processes. These additions to the existing computer simulation technique will enable us to simulate the operation of a real thermionic converter much better than with the collisionless technique.

Project 0255: COMPUTER MODEL OF A 2-DIMENSIONAL PLASMA

Tri-Service Contract Nonr-225(24)*
 Project Leader: O. Buneman
 Staff: R. Hockney

The object of this project is programming simple 2-dimensional plasma problems into an IBM 7090, ions and electrons being simulated by rods of positive and negative charge which trace out their orbits in fully self-consistent fields.

* This work conducted at the Stanford Computation Center and partially supported by NSF Grant NSF-GP 948.

It has been decided to convert the computer simulation to one which can deal with the problem of anomalous diffusion. The required modifications are:

1. Inclusion of a constant magnetic field perpendicular to the region.
2. Injection of plasma particles with a Maxwellian velocity distribution from one boundary.

The first modification has been completed and tested by observing the proper E and B drifts of particles in crossed E and B fields. The calculation of the inverse error function required in (2) has been done and the injection of particles is presently being tested.

Mr. Bruce Beron has joined the project and is writing a very flexible "display" program for use with this simulation. We will be able to display a great variety of plasma parameters, e.g., Temp. currents, voltages from the whole or part of the plasma by adjusting input parameters to the display program.

Project 0256: CURRENT FLOW IN PLASMAS

Atomic Energy Commission Contract AT(04-3)326 PA No. 8

Project Leader: O. Buneman

Staff: G. Reiter

The purpose of this investigation is the study of the effects of binary collisions on the electron-ion two-stream instability.

In the last quarterly report, a dispersion relation was obtained for longitudinal oscillation of a uniform plasma with a dc electric field applied. Numerical computations showed that the calculated steady-state distribution was stable for drift velocities up to 1.4 times the thermal velocities. A peculiarity of the equilibrium distribution used was the limitation on the maximum value of q_e/a_{ee} imposed by the condition that $a_{ei}^2 > 0$. This arises from the neglect of the nonelastic processes maintaining the steady state, such as brehmstrahlung. Treating these phenomenologically, we find that a_{ie} and a_{ei} can be specified to be equal to a_{ee} , a_{ii} , for much larger ranges of q_e/a_{ee} . When this is done, the resulting steady-state distribution becomes unstable for $q_{ee}/a_{ee} \approx 1.2$, and $K_D/K > 10$. If the collision frequency is increased, retaining the values of the other parameters, the distribution becomes stable once more.

These results may be seen from the Nyquist diagrams below (Fig. 10 a, b, c). The irregularity of parts of the curve is due to the restricted number of points calculated but does not affect the accuracy of the results.

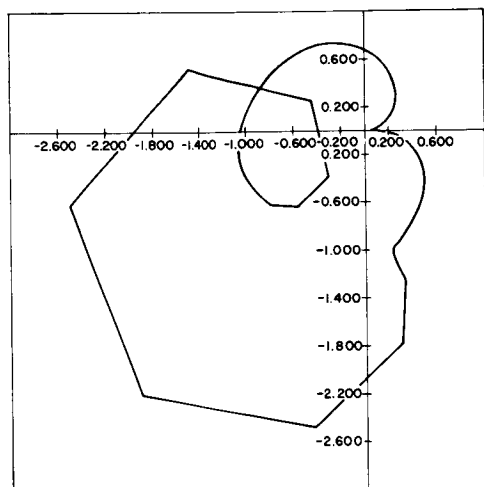


FIG. 10a. COLLISION FREQUENCY/PLASMA FREQUENCY = 0.0001, DEBYE NUMBER/WAVE NUMBER = 10.00, DRIFT VELOCITY/THERMAL VELOCITY = 1.00.

33017

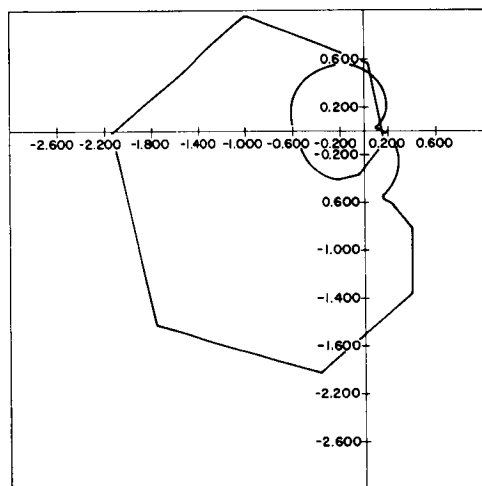


FIG. 10b. COLLISION FREQUENCY/PLASMA FREQUENCY = 0.0001, DEBYE NUMBER/WAVE NUMBER = 10.00, DRIFT VELOCITY/THERMAL VELOCITY = 1.40.

33018

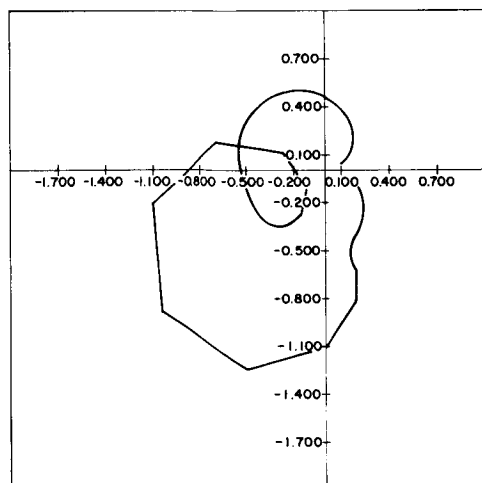


FIG. 10c. COLLISION FREQUENCY/PLASMA FREQUENCY = 0.0100, DEBYE NUMBER/WAVE NUMBER = 10.00, DRIFT VELOCITY/THERMAL VELOCITY = 1.00.

33019
SEL-64-133

Project 0309: NEUTRALIZED CHARGED PARTICLE STREAMS

Air Force Contract AF33(657)-11144

Project Leader: D. A. Dunn

Staff: P. Burger

The purpose of this project is the study of neutralized streams of electrons or ions in a field-free space.

In the last QRR the equations of motion were derived for the Eulerian description of a plasma. In this description the plasma consists of cold streams and the following equations describe the motion of any one stream of particles.

$$\frac{\partial \rho_{\pm}}{\partial t} + \frac{\partial(\rho_{\pm} v_{\pm})}{\partial x} = 0 \quad (1)$$

$$\frac{\partial(\rho_{\pm} v_{\pm})}{\partial t} + \frac{\partial(\rho_{\pm} v_{\pm}^2)}{\partial x} - \left(\frac{q}{m}\right) E(x, t) \rho_{\pm} = 0 \quad (2)$$

The subscripts + or - designate that part of the stream which travels in the positive or negative x direction, respectively; ρ and v are the respective average charge density and velocity of the stream and E is the electric field. The electric field is determined from Poisson's equation:

$$\frac{\partial E}{\partial x} = \frac{\sum_i (\rho_+ + \rho_-)}{\epsilon_0} \quad (3)$$

where the sum includes all the streams that make up the plasma. Equation (3) can be integrated if the boundary condition is given. The boundary condition used here is:

$$\int_0^d E dx = V_{\text{appl}} \quad (4)$$

where "d" is the diode length and V_{appl} is the applied potential across the diode.

In order to solve Eqs. (1), (2), (3) and (4) simultaneously a finite-difference method is needed. It is not a trivial procedure to translate differential equations into difference equations and obtain a good approximation to the original equations, and care must be taken at this point. The differential operators $(\partial/\partial t)$ and $(\partial/\partial x)$ have to be replaced by difference operators (Δ_t/h) , (Δ_x/p) where h and p are the finite intervals in time and space which give the coarse graining of the model. The solution of these equations is considered as an initial-value problem in time. It is assumed that the state of the diode is known at time t . By the given equations the changes in the diodes state are calculated for a time interval $\Delta t = h$ and thus its state is determined for the time $(t + h)$. The parameters are recalculated periodically and the operation of the diode is followed in time. The differential operator in time is replaced by a forward difference operator. This means that the term $\left(\frac{\partial f(x,t)}{\partial t}\right)$ is replaced by the formula $\left(\frac{f(x,t+h) - f(x,t)}{h}\right)$ in all equations.

The differential operator in space cannot be replaced so simply. It is assumed first that the diode space is divided into "N" equal cells, so $p = d/N$. The values $\rho(x_n, t)$ and $v(x_n, t)$ are the average charge densities and velocities of a particular stream in these cells. The solution has to be derived separately for the stream traveling in the positive direction and for the part that travels in the negative direction.

Let us consider first the part that travels in the positive x direction (ρ_+, v_+) . The first term in Eq. (1) is replaced by the expression $\frac{\rho_+(x_n, t+h) - \rho_+(x_n, t)}{h}$ according to our earlier discussion. This equation expresses the conservation of charge and it gives the value of $\rho_+(x_n, t+h)$ as a function of $\rho_+(x_n, t)$ and it also depends on the value of the second term. Since this equation expresses the conservation of charge in cell "n", the charge in this cell at time $t+h$ is given by the charge which was there at time t $(\rho(x_n, t))$, the amount of charge which left the cell during one time step $(\text{given approximately by } \rho(x_n, t) \cdot v(x_n, t))$ and the charge which entered from a neighboring cell. Since this part of the stream travels in the positive x direction, the charge that entered into cell "n" had to enter from the cell "n-1", i.e., from the cell which lies in the direction of decreasing x . Consequently,

the backward difference operator has to be used for the spatial operator when this part of the stream is considered. This changes Eq. (1) to the form

$$\frac{\rho_+(x_n, t + h) - \rho_+(x_n, t)}{h} + \frac{\rho_+(x_n, t) v_+(x_n, t) - \rho_+(x_{n-1}, t) v_+(x_{n-1}, t)}{p} = 0 \quad (5)$$

Eq. (5) can be rearranged giving:

$$\rho_+(x_n, t + h) = \rho_+(x_n, t) - \frac{h}{p} \left[\rho_+(x_n, t) v_+(x_n, t) - \rho_+(x_{n-1}, t) v_+(x_{n-1}, t) \right] \quad (6)$$

Eq. (2) can now also be written in difference-equation form for the functions ρ_+ , v_+ using again a forward difference operator to replace the time derivative and a backward difference operator to replace the derivative in space. The resulting equation can be brought into the following form:

$$\rho_+(x_n, t + h) v_+(x_n, t + h) = \rho_+(x_n, t) v_+(x_n, t) - \frac{h}{p} \left[\rho_+(x_n, t) v_+^2(x_n, t) - \rho_+(x_{n-1}, t) v_+^2(x_{n-1}, t) \right] + \frac{q}{m} h \rho_+(x_n, t) E(x_n, t) \quad (7)$$

The values of $\rho_+(x_n, t + h)$ are calculated from Eq. (6) and then Eq. (7) gives the average velocities $v_+(x_n, t + h)$. Hence, if the quantities v_+ , ρ_+ , and the electric field $E(x_n, t)$ are known at time t , the values of q_+ , v_+ can be calculated for time $(t + h)$ with the help of Eqs. (6) and (7). Thus we have obtained our goal and the motion of the stream can be followed in time with a step-by-step procedure. It is assumed here that the parameters h and p are chosen so small that by decreasing their values further no significant change is obtained in the final results. Furthermore, there is a maximum value for the ratio p/h for which the equations are valid. Since the charge at cell x_n at time $t + h$ depends only upon the values of charge and velocity of the stream

at time = t in the cells located at x_n and x_{n-1} , during one time interval $\Delta t = h$ no charge could arrive in this cell from a distance further away than $\Delta x = p$. This means that the velocity of the stream at any point should not exceed the value (p/h) and hence, we have the condition:

$$p/h > \text{MAX}[v_+] \quad (8)$$

Equation (8) states that for every given p (given number of cells) there is a maximum h (time step) for which the calculations are meaningful. In practice we choose p and start the calculations with a particular h until the velocity in the diode exceeds p/h . If this occurs, the calculations are restarted with a smaller value of h .

When the motion of the negatively traveling stream is calculated, similar arguments show that the forward difference operator has to be used to replace the spatial differential operator. The equations of motion become:

$$\rho_-(x_n, t+h) - \rho_-(x_n, t) - \frac{h}{p} \left[\rho_-(x_{n+1}, t) v_-(x_{n+1}, t) - \rho_-(x_n, t) v_-(x_n, t) \right] \quad (9)$$

and

$$\rho_-(x_n, t+h) v_-(x_n, t+h) = \rho_-(x_n, t) v_-(x_n, t) - \frac{h}{p} \left[\rho_-(x_{n+1}, t) v_-^2(x_{n+1}, t) - \rho_-(x_n, t) v_-^2(x_n, t) \right] + \frac{q}{m} h \rho_-(x_n, t) E(x_n, t) \quad (10)$$

The motions of the streams can therefore be calculated by the outlined procedure; only the electric field is to be determined. Upon writing Eq. (3) in a difference-equation form we arrive at the following equation

$$E(x_n, t) = -E_o + \frac{p}{\epsilon_o} \sum_{k=1}^n \rho_T(x_k, t) \left(1 - \frac{1}{2} \delta_{k,n}\right) \quad (11)$$

where $\delta_{k,n}$ is the Kroenecker delta, i.e., $\delta_{k,n} = 1$ for $k = n$, 0 otherwise, and $\rho_T(x_n, t)$ is the total average charge density in cell "n", at time t . Applying the boundary condition Eq. (4), E_0 is determined as follows.

$$E_0 = -\frac{V_{\text{appl}}}{d} + \frac{\rho}{\epsilon_0 N} \sum_{n=1}^N \sum_{k=1}^n \rho_+(x_n, t) \left(1 - \frac{1}{2} \delta_{k,n}\right) \quad (12)$$

where N is the number of cells in the diode space.

The derived equations are now programmed into a digital computer and calculations with the stream model will begin shortly.

Project 0311: PINCH EFFECTS IN PLASMA BEAMS

Tri-Service Contract Nonr-225(24)
 Project Leader: D. A. Dunn
 Staff: J. W. Christie

The purpose of this project is the study of transients and instabilities in beam-generated plasmas.

The final report is in preparation.

Project 0312: AMPLIFICATION IN BEAM-GENERATED PLASMAS

Air Force Contract AF33(657)-11144
 Project Leader: D. A. Dunn
 Staff: J. E. Simpson, W. Nichparenko

The purpose of this project is the study of the amplification of waves on an electron beam resulting from the passage of the beam through a plasma produced by the beam itself.

EXPERIMENTAL RESULTS

A new larger diameter interaction chamber was installed on the experiment. With this new tube the beam-generated plasma is formed inside a glass cylinder 0.860" I.D. as compared to 0.260" I.D. in the previous experiments. The total length remains at 20 inches.

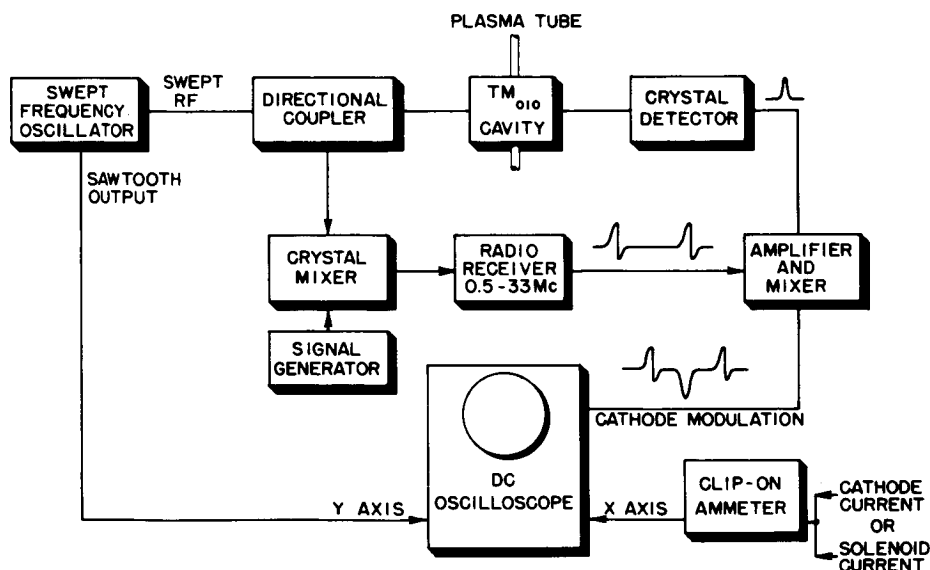
With the new tube, the total-glow regime is again observed. At low beam currents the plasma is formed within the 2 mm diameter of the beam.

At increased currents the plasma suddenly springs to a larger diameter forming the total-glow state. While this discharge had filled the .260" I.D. tubes, it is observed to be about a half inch in diameter in the larger tube, decaying in intensity at larger radii. At gas pressures of 1 micron in argon, the total-glow diameter is larger than at 10 microns. In addition, at high pressures, the discharge tends to show several steps in diameter as the beam current is increased.

The beam current required to establish total glow in the tubes of the two diameters was compared for a number of conditions of pressure, voltage and magnetic field. In the 1 micron pressure range with argon, the large-diameter tube took less current in most cases. At higher pressures, where the transition is not well defined, no clear comparison was possible.

Measurements of gain between two cavities outside the .260" tube were made as a function of the spacing between the cavities. At 1000 Mc an increase in signal from -10 db minimum to a 4 db maximum gain occurred over a 7 cm distance, with a superimposed standing wave of 5 db peak-to-peak. At 1500 Mc the signal decreased by 4 db over the same distance.

Using the apparatus indicated in Fig. 11 the variation of plasma density with beam current, beam voltage, and magnetic field was studied



32681

FIG. 11. DYNAMIC DISPLAY OF DENSITY VARIATION.

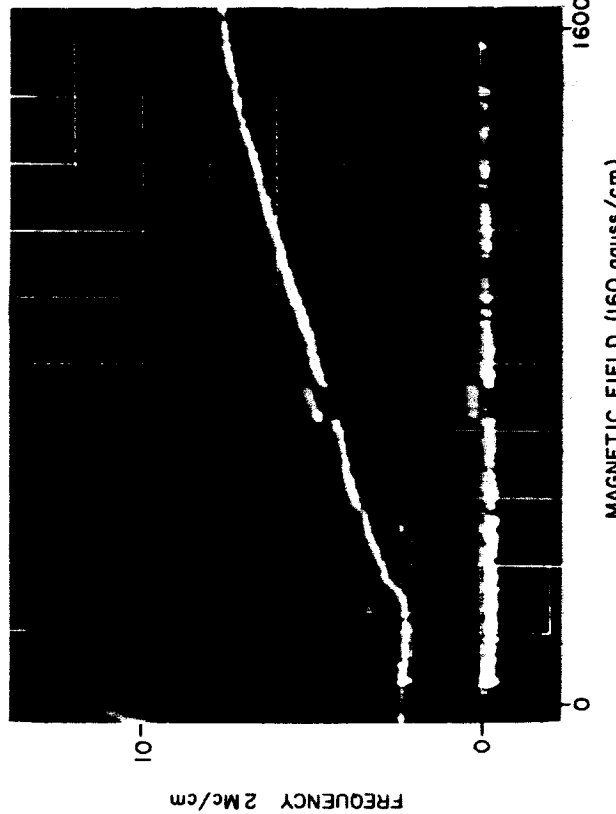
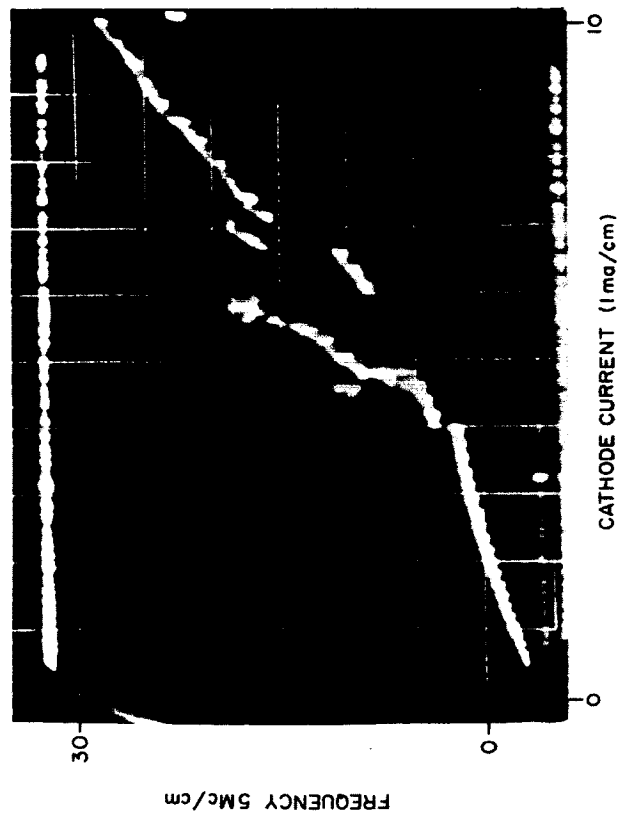
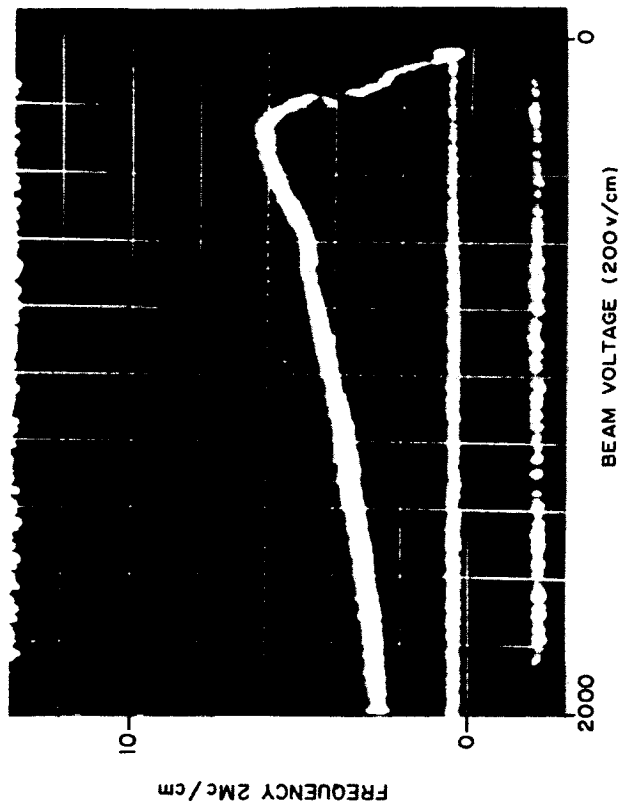


FIG. 12. VARIATION OF DENSITY WITH CURRENT, VOLTAGE, AND FIELD FROM A COMMON OPERATING POINT.

in the .260" diameter tube. In this display the cavity resonance appears as a spot on the oscilloscope with its height proportional to the frequency. Markers separated by twice the tuned frequency of the radio receiver are used to calibrate the vertical scale, while the horizontal scale represents the independent variable. The resonant frequency of the cavity varies in proportion to the total number of electrons in the cross-section. When the plasma occupies only the beam diameter, this number is proportional to the beam density which is given by the relation $n = 3.6 \times 10^{10}$ per cm^3 Mc. The simultaneous display of the cavity frequency and the markers permits errors due to drift and power line transients to be identified as in the case of the step in Fig. 12c.

Density varies linearly with beam current, until the onset of total glow, occurring in Fig. 12a at 4.5 ma. Variation with beam voltage in the low-current regime illustrated in Fig. 12b reveals the change in ionizing cross-section as a function of beam voltage.

In Fig. 12c the density is shown to be proportional to magnetic field. This dependence on field indicates the importance of radial drainage of the argon plasma. The work of Dunn and Self [Ref. 1], assuming purely longitudinal flow, predicts a much higher density independent of B. In helium at 5 microns, the density is nearly independent of B and within a factor of 2 of the Dunn and Self prediction. Since radial flow requires collisions, a reduction in pressure should make longitudinal flow more important. At 0.2 microns in argon this effect was observed. The density is proportional to B up to 1000 gauss and then remains constant.

Project 0313: COMPUTER EXPERIMENTS ON BEAM-GENERATED PLASMAS

Signal Corps Contract DA 36-039 AMC-00094(E)

Project Leader: D. A. Dunn

Staff: A. S. Halsted

The purpose of this project is the study of a beam-generated plasma using a computer model in which transverse motion of beam and plasma

¹D. A. Dunn and S. A. Self, "Static Theory of Density and Potential Distribution in a Beam-Generated Plasma," TR No. 0311-1, July 1963, Stanford Electronics Laboratories, Stanford University, Stanford, Calif.

particles are allowed. Plasma oscillation and beam focusing effects are being studied on the computer.

A. STATIC THEORY OF A BEAM-GENERATED PLASMA

The work on the static theory of plasma generation in cylindrical geometry has been completed and is summarized in a paper "Static Theory of Density and Potential Distribution of a Cylindrical Plasma Column," [Ref. 1] by A. S. Halsted. The abstract of this paper is presented below.

"The equilibrium conditions existing in a low-pressure plasma column are considered assuming radial drainage of ions to the wall. Exact solutions for the plasma density and potential distribution valid throughout the plasma and sheath are presented for both the beam-generated plasma and glow discharge. For a beam-generated plasma, knowledge of either the plasma electron temperature or the axial electron density is normally sufficient to determine a unique set of equilibrium conditions. When the beam partially fills the space, a low-potential sheath forms at the edge of the beam which is separated by a region of slowly varying potential from a second, higher-potential sheath at the wall. The plasma density at the beam edge is less than half of the value on the axis. The radial electric field acting on the beam is found to account for ion-focusing of electron beams."

In the previous QRR, the equations of the static theory in cylindrical geometry were obtained and the solutions for a beam-generated plasma with the beam filling the space were presented. As an illustration of the type of solution obtained when the beam only partially fills the space, consider the case of an electron beam of radius r_c moving axially through a tube of radius r_w in argon gas with $r_w/r_c = 3$. The radial variation of the normalized potential $\eta = (eV/kT_e)$ is shown in Fig. 13 for different values of the dimensionless parameter α , where α is approximately equal to the ratio of Debye length of the plasma to the beam radius, and may be calculated for a given experiment if the plasma electron temperature, the axial electron density, or the Debye length is known. For a

¹Submitted to the Journal of Applied Physics.

different type of gas, the general shape of the potential profile is the same except for a change in the height of the sheath at the wall.

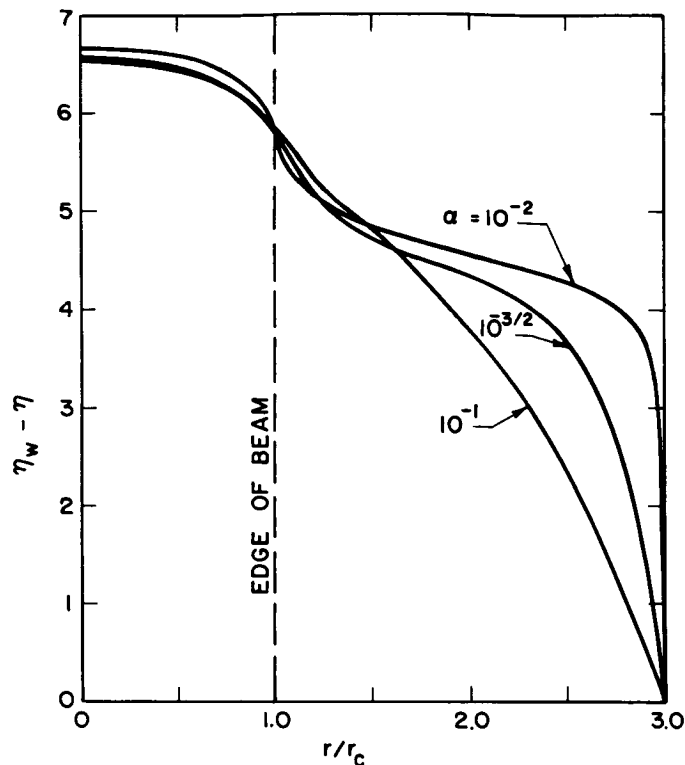


FIG. 13. RADIAL VARIATION OF POTENTIAL FOR DIFFERENT VALUES OF α FOR AN ELECTRON BEAM IN ARGON WITH $r_w/r_c = 3$.

The potential in the region of the beam is observed to vary only slightly with α and to have a total drop of about (kT_e/e) volts from the axis to the edge of the beam. The fact that the space-charge forces which would normally cause the beam to spread radially in the absence of the plasma have been replaced by a radial confining force is of particular interest to us, and is discussed in the following section.

B. GAS FOCUSING OF ELECTRON BEAMS IN A BEAM-GENERATED PLASMA

Up to this point we have been concerned with the dc state of the plasma created by an electron beam of fixed density and position. We

wish now to consider what happens to the beam if we allow it to move radially under the influence of the space-charge fields in the space.

The static theory predicts that:

1. If the beam current and voltage and the gas pressure are high enough to generate a plasma in the space,
2. If the ions and electrons drain radially to the walls, and
3. If the electron beam flows along the axis of the tube and is not scattered by collisions or rf processes,

then the electron beam will be confined near the axis of the tube. We have found that a number of experiments satisfying the above conditions were conducted in the 1930's, and "gas" or "ion" focusing of electron beams was clearly observed. The following experimental observations are pertinent to our study:

1. Beams of constant cross section and up to one meter in length were observed at 100 - 600 volts.
2. "Knotted" beams, i.e., beams with periodic focus points, were observed. Such a beam shape requires an approximately parabolic potential well in the region of the beam (see Fig. 13).
3. The measured variation in radial potential agrees with that predicted by the static theory [Ref. 2].
4. The dependence of the focusing fields on the pressure and type of gas is as predicted by the theory [Ref. 3].

Encouraged by these results, ion focusing of electron beams is now being studied to provide further experimental verification of the static theory, and the static theory is being applied to understand the results of our own beam-focusing experiments. The experimental work on ion focusing is being conducted under Project 0321.

²W. Rollwag, ZS f. Phys., 89, 395 (1934).

³E. F. Richter, Phys. ZS, 34, 457 (1933).

Project 0321: ELECTRON BEAM FOCUSING IN IONIZED GASES

Army Contract DA 36-039 AMC-00094(E)

Project Leader: D. A. Dunn

Staff: R. P. Lagerstrom, A. S. Halsted

Studies of the potential distribution in a beam-generated plasma [Ref. 1] have indicated that a potential distribution is produced in the vicinity of the beam that is self-focusing, i.e., beam electrons will be returned toward the axis if they start to leave the beam. Low-convergence-angle, kilovolt beams have been reported in previous QRR's to spread appreciably slower in gas at 10^{-5} to 10^{-3} mm Hg than in high vacuum (10^{-6} mm Hg or less). Marked concentration of the beam persisted along the beam as far as 6 times the cathode-anode spacing, but the beam was apparently always spreading--first slowly and finally rapidly--after an initial concentration in the anode region.

New parts have been fabricated this quarter which make the experimental apparatus similar to that used in experiments in the 1930's in which focused beams (knotted beams) and beams of constant diameter (filament beams) were observed at 100-600 volts. These early experiments and additional studies on ion-focusing are discussed under Project 0313. The changes to the apparatus and some preliminary test results are discussed below.

A. CHANGES IN THE APPARATUS

A stand has been placed inside the 18-inch-diameter bell jar which allows open-ended glass, mesh, or metal tubes of diameters up to 2 1/2" to be mounted coaxially surrounding the beam. We expect that this decrease of the radial distance from the beam to the wall will increase the plasma density in the region of the beam, reduce the end effects in the space, and cause the drift of the ions to be more nearly radial. These changes will bring the experiment more into line with the model assumed in deriving the static theory [Ref. 2].

¹D. A. Dunn and S. A. Self, Jour. of Appl. Phys., 35, 113 (1964).

²Project 0313, herein.

A small, circular "ion trap" aperture has been mounted down-stream from the anode aperture. External voltages may be applied through glass-coated leads to the ion trap and to the mesh or metal tubes.

In the gun region of the tube, the cathode-heater spacing has been increased to yield a higher V/I bombarder characteristic. The external shaft and gear arrangement, which allows the anode to cathode spacing to be varied while the tube is in operation, has been rebuilt to give more dependable operation. Several hollow, conical caps, such as were employed by experimenters in the 1930's, have been fabricated, and these may be placed over the anode to reduce the beam diameter.

B. PRELIMINARY TEST RESULTS

All of the results which are discussed below were obtained from measurements on a fan-shaped beam with an ellipsoidal cross section. Major and minor diameters were 1" and 1/4" respectively at a height of 10" above the anode. This undesirable initial condition may have been due to contamination of a part of the cathode surface and the cathode is being replaced. Since the beam had a considerable transverse velocity component in the wide dimension, different phenomena could be observed when the beam was viewed from the wide or the narrow side.

The most interesting behavior was observed when the beam was surrounded by an 8-inch long, 1-inch diameter glass tube with a wire mesh fitted snugly inside the tube. By varying the potential on the mesh, the potential along an 8-inch length of the beam could be controlled. At low gas pressures (10^{-5} mm Hg), the wide dimension of the beam just filled the tube at the top.

At pressures above 10^{-4} mm Hg, the narrow beam (i.e., the beam as viewed along the wide diameter) remained approximately 1/8" wide throughout the length of mesh as long as the mesh wall was held ≤ -50 volts with respect to the anode. The "wide" section of the beam, for the same wall potential, contracted so as to clear the mesh by about 1/8" at the top of the tube. At wall potentials of ≥ -10 volts, the beam spread at the normal rate it would in the absence of the mesh.

At a pressure of 3×10^{-3} mm Hg, the expansion of the wide section of the beam could be halted by making the wall voltage approximately -100 volts. The beam then spread to a width of 1/2" in the mesh tube before contracting to 1/4" at the top of the mesh tube. The beam remained filamentary in the narrow plane.

The total current to the walls was zero when the mesh was held at -20 volts. Alternatively, if the mesh were allowed to float, it would assume a measured potential of -20 volts.

The above behavior was noted at a beam voltage of 1000 volts. Similar effects were noted down to 300 volts.

Our explanation of this behavior is as follows: When the mesh voltage is reduced to less than -20 volts, the plasma electron current to the walls is reduced. The axial potential in the tube will be required to drop a small amount so that a potential rise at the ends of the tube may form to draw out the plasma electron current which no longer reaches the wall. The ions continue to be drawn to the mesh walls, and are stopped from flowing out the end of the tube by the potential which is aiding the electron flow. Consequently, we obtain a predominantly radial flow of the ions to the wall when the mesh is held more negative than -20 volts.

The static theory [Ref. 2] is based upon the assumption that the ion flow to the walls is radial, so that when this condition is satisfied we would expect to observe the focusing effect predicted by the theory. Experimentally, this is indeed the case. The strength of the focusing fields increase with the plasma density and temperature, so that as we go to high pressures, the focusing force increases until we are finally able to confine the electrons which had an initial transverse velocity in the fan beam.

Project 0322: NOISE GENERATION IN PLASMAS

Air Force Contract AF33(657)-11144

Project Leaders: O. Buneman and D. A. Dunn

Staff: K. Thomassen and J. Hosea

The purpose of this project is the study of mechanisms of noise generation in plasmas and methods of coupling noise out of plasmas.

The last two reports have been concerned with the mechanism for noise generation in a Voltage Tunable Magnetron. This work has been published

in a letter to the Proceedings of the Institute of Electrical and Electronics Engineers and we have now shifted our attention to the study of noise in plasmas.

We intend to begin our investigations of noise using a P.I.G. discharge, a plasma source which has been used here in other studies and whose properties are therefore reasonably well understood. Our studies will follow two different lines; we will look at the noise due to instabilities associated with "anomalous diffusion" and that due to the instabilities and nonlinear effects associated with "anomalous resistance."

A. ANOMALOUS DIFFUSION

A crucial question in controlled fusion research is whether the diffusion of plasma across a magnetic field is solely a collisional process or whether more complicated effects contribute. Since collisional diffusion gives a lower limit to the actual diffusion rate it is important to know what are the causes for the anomalous effects which have been seen in various experiments. Reviews of the theories and experiments on this subject have been given by Hoh [Ref. 1], Lehnert [Ref. 2], and Boeschoten [Ref. 3].

It seems that no single effect or instability can explain the many experiments in which "anomalous" diffusion is found. While the mechanism responsible in the dc glow discharge was quite well explained by Kadomtsev and Nedospasov [Ref. 4] there have been other experiments in hot and cold cathode P.I.G. discharges (which are quite different), rf discharges, and high-current high-pressure arc discharges, etc., which have not yet been satisfactorily explained. In all experiments, however, there appears to

¹F. C. Hoh, Rev. Mod. Phys., 34, 267 (1962).

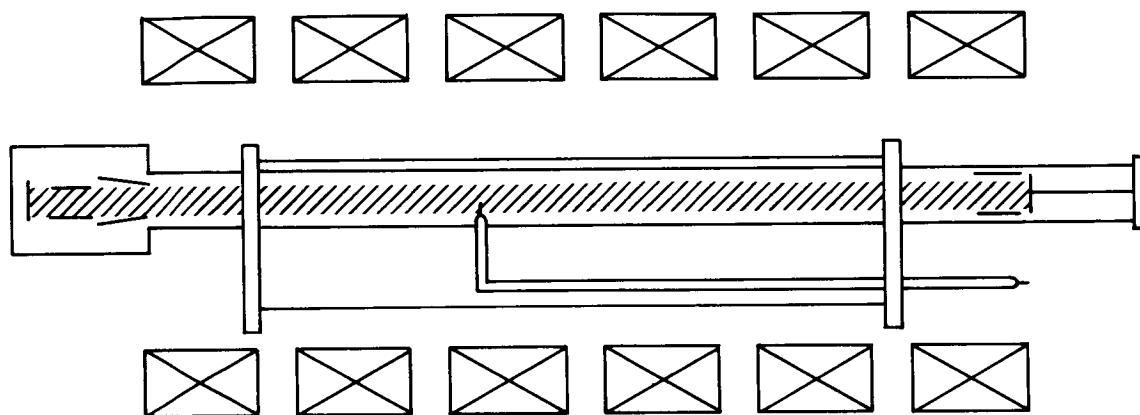
²B. Lehnert, "International Conference on High Magnetic Fields," Nov 1961, M.I.T.

³F. Boeschoten, J. Nucl. Energy, Part C6, 339 (1964).

⁴B. B. Kadomtsev and A. V. Nedospasov, J. Nucl. Energy, Part C1, 230, (1960).

be a simultaneous onset of noise when the critical field is reached (the field at which the anomalous behavior is first exhibited). The character of this noise is different in the cold-cathode P.I.G. discharge, the rf discharge, and the hot-cathode P.I.G. discharge which we intend to study.

Since the role of micro-instabilities in anomalous diffusion may be very important we will begin by attempting to measure the frequencies and longitudinal wavelengths of the noise in the discharge. To do so, a moveable coaxial probe has been constructed as shown in Fig. 14. The box at the left contains a cylindrical hollow cathode (hot), a focusing anode

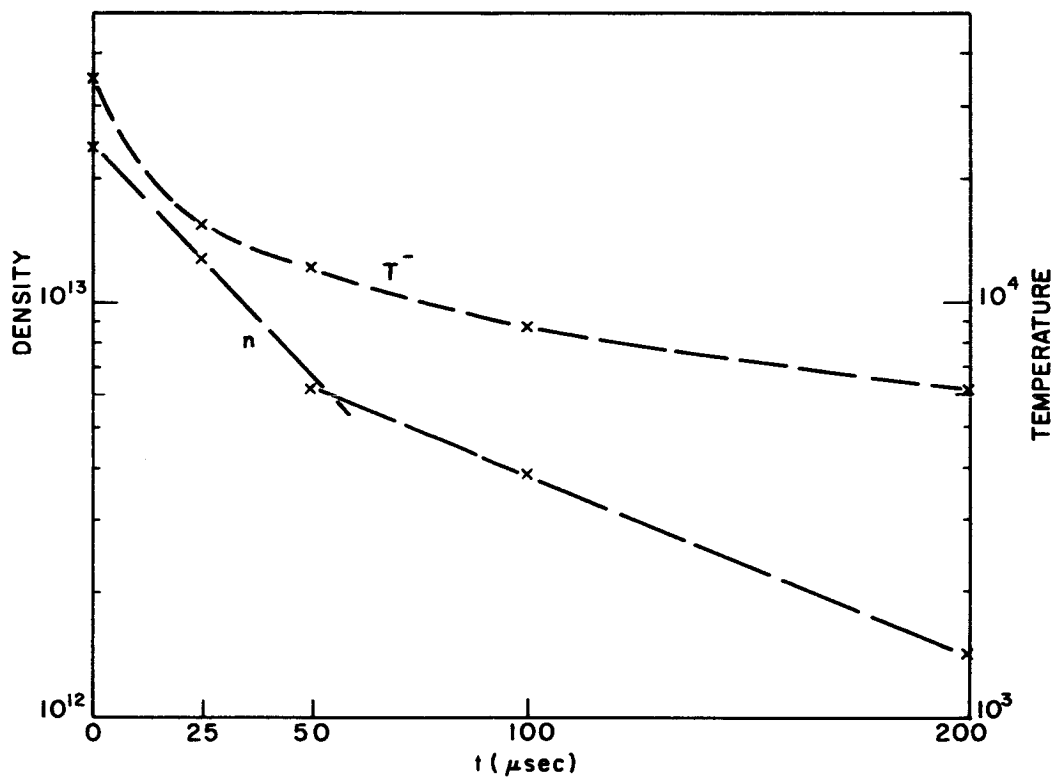


32661

FIG. 14. REFLEX DISCHARGE AND COAXIAL PROBE SYSTEM.

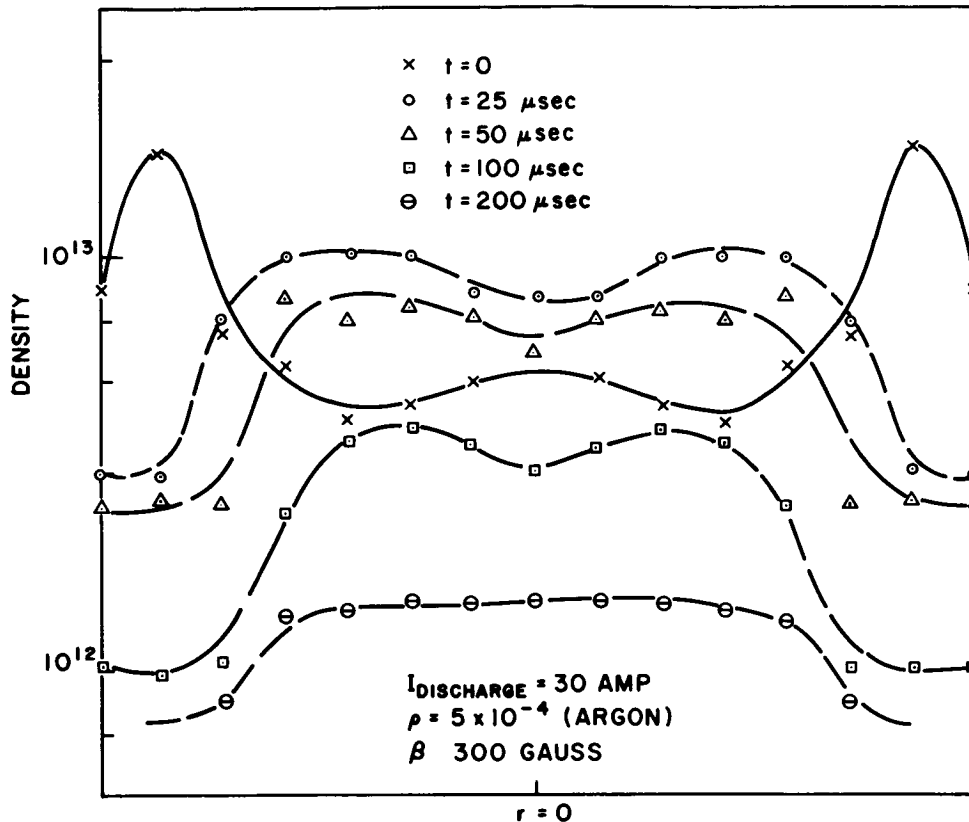
whose diameter gives the size of the plasma, and a reflecting plate at cathode potential. The discharge is about 2 feet long and 1 inch in diameter and is terminated in a cylindrical hollow anode and reflecting plate which serves as a cold cathode. It is immersed in a magnetic field of up to 1300 gauss. The moveable probe system is contained in a 4" diameter glass cylinder which surrounds the discharge tube (but is not concentric with it). By using appropriate flanges the chamber can be made vacuum tight. The probe penetrates the flange through a standard double-Wilson seal and then makes a right angle bend and enters the plasma through an 18 inch longitudinal slit in the smaller diameter (1-3/4") tube, allowing one to determine the variation of noise (giving the wavelength along nearly the entire length of the system).

The measurements of noise are just now beginning as our first measurements were directed toward determining the discharge parameters. For example, the density and electron temperature were measured as a function of radius using a moveable Langmuir probe. Since the discharge was pulsed we also measured the change in these profiles with time. Figure 15 shows a typical plot of density and temperature vs time taken next to the edge of an argon plasma with a discharge current of 30 amp (during the pulse) and with 300 gauss magnetic field. Figure 16 shows the variation of density with radius (the temperature is nearly constant in radius) for various times in the after glow. The discharge is initially hollow due to the hollow cylindrical cathode but rapidly fills in.



32662

FIG. 15. DENSITY AND TEMPERATURE VARIATION IN THE AFTERGLOW.



32663

FIG. 16. DENSITY AND TEMPERATURE PROFILES IN TIME.

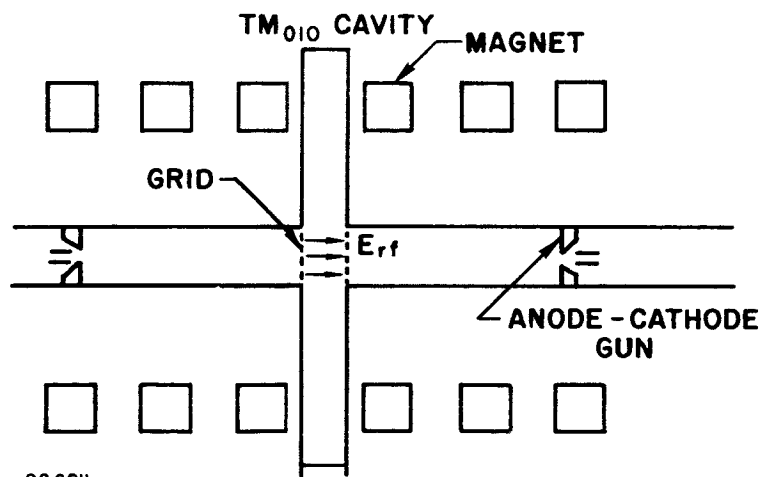
B. ANOMALOUS RESISTIVITY

A plasma composed of two or more populations of charged particles, in which at least one of the components differs in drift velocity from the rest, is capable of supporting "drift instabilities" under certain conditions. These instabilities were studied by E. A. Jackson [Ref. 5] for a plasma made up of two Maxwellian components. The conditions for growth of fluctuations with periodicity λ were found to depend upon the relative drift velocity (u) between components and on the temperature of each population (λ was measured in the direction of the drift). Briefly, for a fixed λ , growth occurs between upper and lower limits of u determined by the temperatures of the two streams.

⁵E. Atlee Jackson, "Drift Instabilities in a Maxwellian Plasma," Phys. of Fluids, Vol. 3, No. 5 (1960).

O. Buneman [Ref. 6] has shown that the drift instabilities can consume the energy of the drift in a few tens of plasma periods. Small fluctuations in the plasma (existing prior to the drift) are amplified by the drift instability mechanism to a high level producing noise and bunching of electrons. Drift energy is transformed into random energy of the electrons and ions through collective collisions (collisions between bunches of electrons and ions) causing an increase in the effective temperature of the plasma. The resulting resistivity of the plasma is much greater than that attributable to individual electron-ion collisions and is denoted as anomalous resistivity. Anomalous resistivity has been measured [Ref. 7] by loading a reentrant cavity with a hydrogen plasma and monitoring the reflection coefficient looking into the cavity vs power applied to the cavity. Qualitative results indicate that a resistive mechanism does exist.

We are continuing the previous experimental work with emphasis now placed on the noise produced by the drift instability and the coupling of this noise out of the plasma. The experimental apparatus consisting of a P.I.G. discharge and microwave cavity is shown in Fig. 17. The plasma is pulsed and investigations are made during the afterglow. A drift is imparted to the electrons during the quiescent afterglow by the axial E field of the TM_{010} cavity, and instabilities and noise ensue.



32664
FIG. 17. TM_{010} CAVITY ON P.I.G. DISCHARGE.

⁶O. Buneman, "Dissipation of Currents in Ionized Media," Phys. Rev., 115, No. 3 (1959).

⁷K. Thomassen, J. Appl. Phys., to be published, January 1965.

NEW PROJECT

Project 0323: HIGH POWER MICROWAVE TRANSMISSION IN MULTIMODE
CYLINDRICAL WAVEGUIDE

Tri-Service Contract Nonr-225(24)

Project Leaders: D. A. Dunn and W. K. Linvill

Staff: W. Lowenstern

This project is a theoretical evaluation of the use of a cylindrical waveguide operating in the TE_{01} mode as a means for transmitting large blocks of power of the order of 1 GW over long distances.

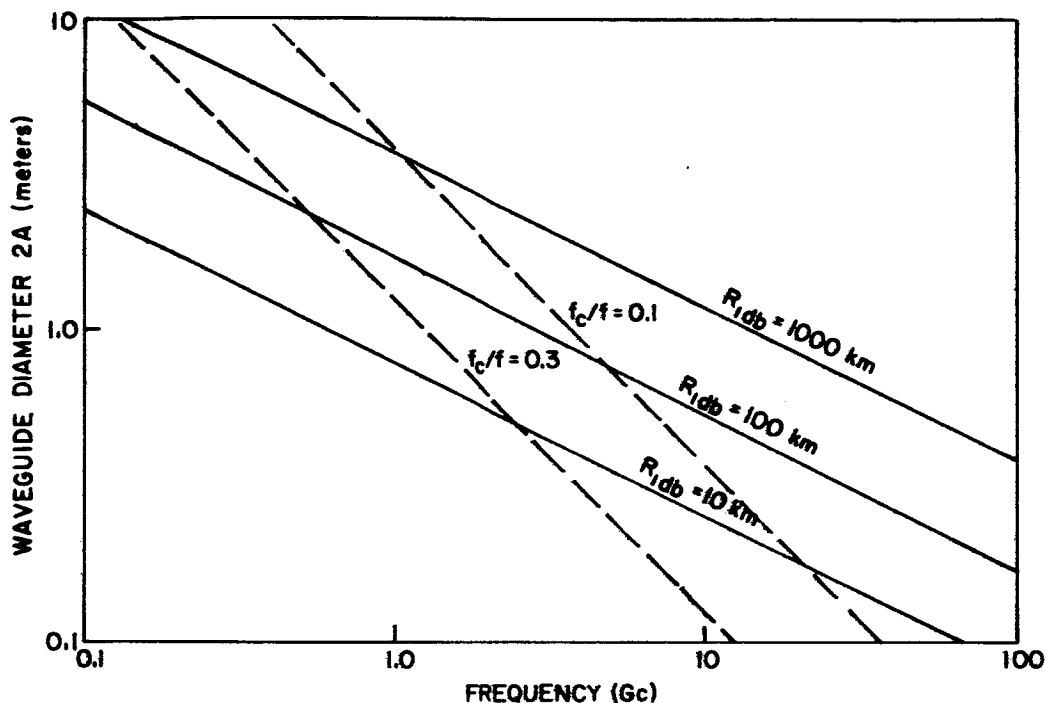
There has been what is apparently a major effort in the Soviet Union in recent years devoted to high power electronics under the direction of P.L. Kapitsa [Ref. 1], including waveguide transmission of microwave power. Recently there has been considerable interest in this country in the transmission of large blocks of microwave power [Ref. 2]. In much of this work the problem of waveguide transmission is examined briefly and it is found that ordinary dominant mode guide has excessive loss and that multi-mode TE_{01} mode guide can have a sufficiently low loss to be interesting as indicated in Fig. 18. In addition, it has been pointed out that the problem of rf breakdown is negligible in a guide with sufficiently low copper loss and that there are no corona losses, insulation breakdowns, or atmospheric effects in a closed waveguide. All of which sounds very favorable.

The problem turns out to be one of mode conversion from the desired TE_{01} mode to other modes such as the TE_{12} mode which have high loss rates. The TE_{01} copper loss is then not the entire loss. This mode conversion problem has been examined in detail in a communications context at Bell Telephone Laboratories and reduced to one of mechanical tolerances. It is the purpose of this project to make a preliminary analysis of this problem of mode conversion in a power transmission context and to make some estimates of the cost of a waveguide transmission system, including the tradeoff between the costs of smaller tolerances and the costs of increased power loss. To make a system comparison with a conventional 60

¹P. L. Kapitsa, "High Power Microwave Electronics," Macmillan, N.Y. (1964).

²E. C. Okress, et al., IEEE Spectrum, 1, 76, Oct 1964.

cycle system or a dc system it will be necessary to include terminal equipment costs and losses. At present such equipment does not exist, but some reasonable extrapolations of existing devices can be made.



32754

FIG. 18. THE SOLID LINES SHOW THE RANGE IN KILOMETERS FOR 1 DB OF POWER LOSS OF MICROWAVE ENERGY IN THE TE_{01} MODE IN CIRCULAR WAVEGUIDE AS A FUNCTION OF FREQUENCY AND WAVEGUIDE DIAMETER. The dotted lines are the ratio of frequency (f) to the cutoff frequency (f_c) of the TE_{01} mode and are an indication of the number of spurious modes which can propagate. For instance a guide with $f/f_c = 0.3$ can propagate about 9 other TE_{mn} modes and one with $f/f_c = 0.1$ can propagate more than 40 modes.

It is anticipated that at the end of this project we will be able to conclude that the costs are either: 1) excessive to the point where further studies are not worthwhile or 2) low enough to justify some preliminary experimental work. It is probably going to be impossible to make any firm statements of the positive feasibility of such a system without experimental work.

Project 0414: EMISSION OF ELECTRONS IN SOLIDS

Tri-Service Contract Nonr-225(24)
Project Leader: H. Heffner
Staff: M. Cowley

The final report on this project is in preparation.

Project 0415: UTILIZATION OF OPTICAL MASERS

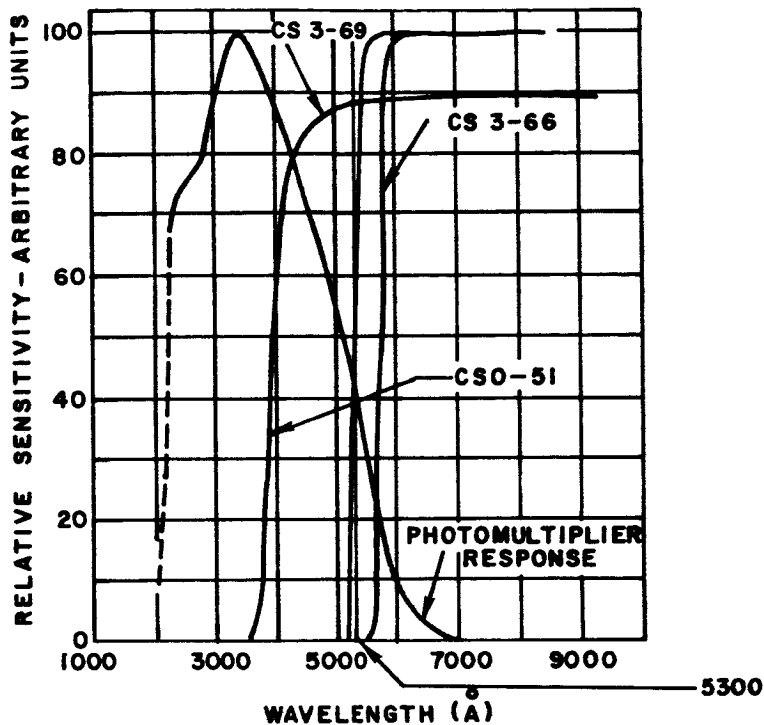
Tri-Service Contract Nonr-225(24)
Project Leader: H. Heffner
Staff: H. Sonnenberg

The object of this project is to investigate possible ways of utilizing the unique properties of the laser.

The experiment proposed in the last report appears to have been successful. Consistent results were obtained in the following manner:

The laser beam was focused onto the silver surface, by a lens which was held by a micromanipulator to allow fine adjustment of the area of the beam on the metal surface. The film was oriented such that the angle of incidence was near the optimum ($\theta_{inc} \approx 80^\circ$. See Fig. 30 of last quarter's report). Critically adjusting the area such that consistently no photomultiplier readings were obtained when the reflected beam was passed through a filter CS 3-66 to remove second harmonic, and then replacing this filter with a CS 3-69 Filter (See Fig. 19) which just passes the second harmonic, an indication of second harmonic appears to have been obtained.

In the first experiment of this type, approximately 40 pictures with consistent results were obtained. Consistent here means that every time the CS 3-66 Filter was inserted, no photomultiplier readings were obtained, and when the CS 3-69 Filter was substituted, readings were obtained. From Fig. 19 we see that substituting the CS 3-66 Filter for the CS 3-69 Filter reduces the area under the photomultiplier response curve by about a factor of 1/2, which has the effect of lowering the sensitivity of the detector to broadband radiation by the same factor. So it is conceivable when only one or two photons are detected that the consistency in results may have been due to such an effect. To rule out this possibility, a CSO - 51 Filter (See Fig. 19) was substituted for the other two filters, and the number of photons per pulse compared to the case in which the



33020

FIG. 19. SUPERPOSITION OF FILTER CHARACTERISTICS ON THE PHOTOMULTIPLIER CHARACTERISTIC. The second harmonic is at 5300 Å.

CS 3-69 Filter was used. The results were essentially identical, verifying that the radiation being detected is confined to the region between the two Filters CS 3-69 and CS 3-66. On the average, about two to three photons per laser pulse were obtained, which corresponds to approximately 10^{-15} watts of second harmonic power. This is within about one order of magnitude of the calculated second harmonic power.

In later experiments, the results obtained were not as decisive as in the first experiment, but on a statistical basis, the results were always positive.

At present, a scheme in which counters are to be used to collect data is being set up. This technique may enable us to determine experimentally the behavior of the second harmonic upon the angle of incidence, and

depending upon how well this scheme works, it may be possible to verify the quadratic intensity dependence and the inverse area dependence of the second harmonic.

$$P_{2w} \approx \frac{P_w^2}{A} \times 10^{-24} .$$

Project 0558: INVESTIGATION OF NOISE IN ELECTRON GUNS

Army Contract DA 36-039 AMC-00094(E)
Project Leader: A. E. Siegman
Staff: M. O'Flynn

Technical Report No. 0558-1 by Michael O. O'Flynn, entitled "Monte Carlo Investigation of Noise in an Incipient Space-Charge Diode," is in process of publication. Upon its completion and distribution this project will be terminated.

Project 0572: INFRARED AND SUBMILLIMETER MASER STUDIES

Air Force Office of Scientific Research Grant No. 323-63
Project Leader: A. E. Siegman
Staff: Guido Francois

This project presently aims at mixing into an appropriate crystalline material a visible laser output with infrared or far infrared radiation in order to obtain sidebands of the laser light. This will allow measurement of the relevant nonlinear dielectric matrix elements of various crystalline materials and evaluation of the possibilities for difference frequency generation at infrared frequencies and for optically pumped parametric oscillations. These are also important quantities for evaluating the light modulation capabilities of the materials.

In the course of this quarter we have completed the theory of the influence of a gaussian beam spread on the angular spectrum of the second harmonic power generated in a KDP type crystal. Various experiments have shown excellent agreement with this theory. These experiments have required the development of special equipment for studying the transverse profiles of cw laser beams in detail. A first attempt has been made

to measure the coefficient d_{36} in ADP. Also, a commercial firm has agreed to try growing a single crystal of AgNO_3 . This material is the most promising one for the mixing of the 3.39μ and the 6328 \AA lines of the He-Ne laser.

The second-harmonic power generated by a single plane wave in a crystalline material, oriented at or near the index matching angle, follows a $[(\sin \psi)/\psi]^2$ law, where $\psi = \alpha \rho$ and ρ is the angular deviation from the index matching angle. The constant α ranges from 10^3 to 10^4 . A cw laser beam can be expanded in a set of plane waves. If the beam is diffraction-limited and has a uniphase wavefront with gaussian intensity distribution, its plane-wave expansion will have a gaussian distribution. The total harmonic output generated by the beam is the superposition of a continuous set of elementary plane harmonic waves, each of which results from the two-by-two interaction of the fundamental waves. The angular spectrum of the harmonic output as a function of the crystal orientation ψ is given by:

$$P^{2\omega} = P_o^{2\omega} \frac{(d^2/2)^2}{(d^2/2)^2 + (r\lambda/2\pi)^2} \times \int \left[\frac{\sin(\psi + \Psi)}{\sin \psi + \Psi} \right]^2 e^{-\Psi^2/2\sigma^2} d\Psi \quad (1)$$

The constant d is defined in the focus of the diffraction-limited beam as the radius at which the field of the laser beam is down by a factor e from its value in the center of the beam. The parameter r represents the distance from the flat mirror to the crystal.

Several experiments have confirmed the following facts predicted by (1):

1. The dependence of the harmonic output on the spacing r between a plane of collimation or focus and the crystal is given by

$$\frac{(d^2/2)^2}{(d^2/2)^2 + (rd/2\pi)^2}$$

2. The angular dependence is given by the convolution integral of (1); and this angular dependence is independent of the spacing of the crystal from the laser.
3. The standard deviation σ of the gaussian function can be calculated and the experimental patterns can be reproduced on the computer if one uses the proper value of σ .

In order to measure the exact size of the laser beam, we have mounted a small detector (.0015" diam.) on a two-dimensional micropositioner. The detector is a silicon solar cell mounted behind a thin Be-Cu plate which had previously been perforated by a pulsed ruby laser. The horizontal motion of the positioner is driven by a stepmotor and the range is determined by two limit switches with micrometer screw adjustment, as in Fig. 20. The forward and the return speed are individually adjustable. A 4-pole, double-throw relay commands the entire cycle of motion. Figure 21 gives a few horizontal scans of a laser beam. The different curves are taken at different settings of the vertical micrometer of the micropositioner.

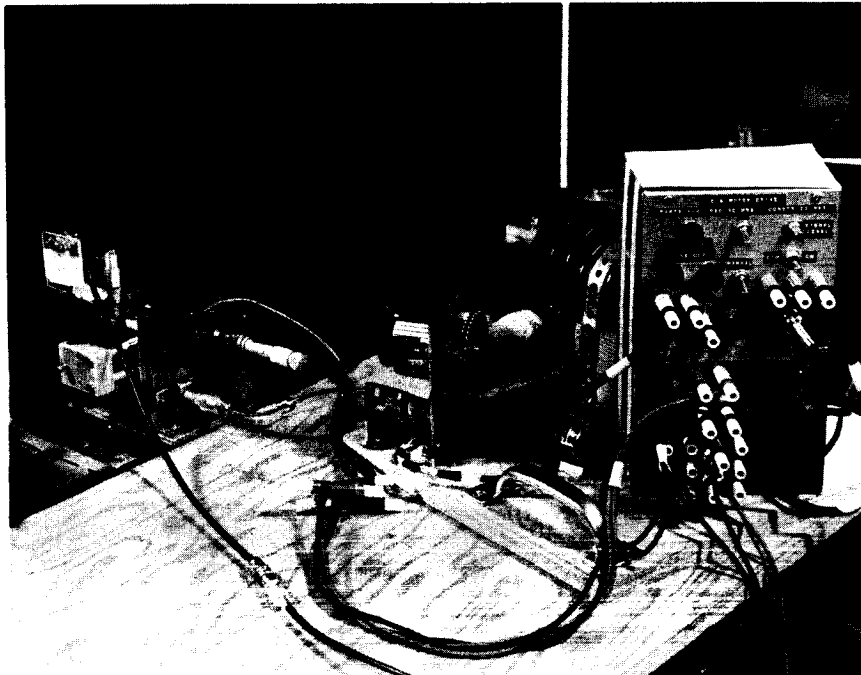


FIG. 20. EQUIPMENT FOR STUDYING THE TRANSVERSE PROFILE OF CW LASER BEAMS.

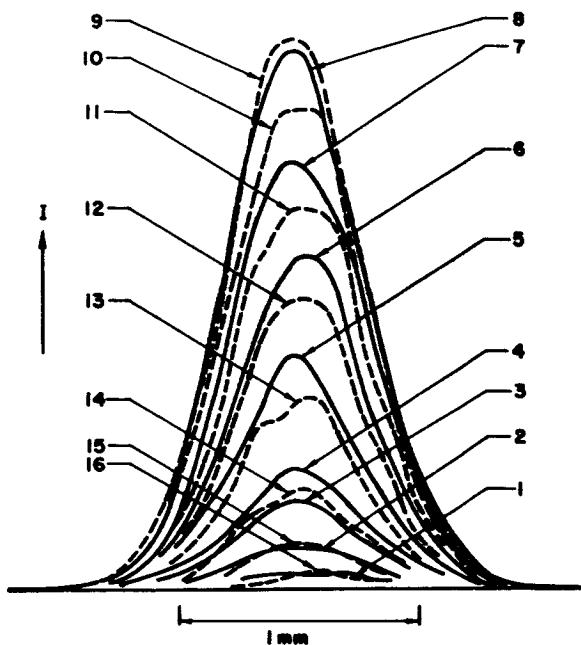


FIG. 21. CURVES 1 THROUGH 16 GIVE THE TRANSVERSE POWER DENSITY IN A LASER BEAM. Each curve results from a horizontal scan. Scans are made at vertical intervals of 0.1 mm.

33021

We have used this equipment to make a complete record of the beam used in the measurement of d_{36} in ADP. In order to do so, we have driven the vertical micrometer at the rate of 1/8 rpm. The amplified photodetector output was sent to a dc to frequency converter. The output of this instrument was then recorded on magnetic tape. The radio-science division of the Stanford Electronics Research Laboratories has then transferred the information on to punched cards. A computer program which will process the information and produce a contour plot is in preparation.

Besides requiring a knowledge of the exact pattern of the laser beam, the measurement of d_{36} also depends on a delicate and difficult calibration of the photomultiplier. Rather than project a precisely known amount of energy at or near 3164 \AA on the cathode of our photomultiplier, we have compared the second harmonic output of the crystal with a known amount of fundamental light. We are presently studying the problem of determining the ratio of the quantum efficiencies of the photomultiplier at 3164 \AA and 6328 \AA .

Project 0576: MICROWAVE LIGHT MODULATION METHODS

Air Force Contract AF33(657)-11144

Project Leader: S. E. Harris

Staff: O. P. McDuff, L. M. Osterink,
J. Markiewicz, H. Hayami

This project will investigate methods for the modulation and demodulation of light at microwave frequencies, with particular emphasis on frequency modulated light.

Work during the previous quarter has been directed toward the development of a complete theoretical understanding of the FM laser [Ref. 1] and an experimental demonstration of similar operation in an argon laser having appreciably larger fluorescent linewidths than the He-Ne laser of Harris and Targ.

A. THEORY

A first-order theory has been obtained for the stable FM operation of a laser having an intracavity phase perturbation driven at a frequency which is approximately but not exactly that of the axial mode spacing. These results appeared in Applied Physics Letters in November, 1964, entitled "FM Laser Oscillation - Theory," by S. E. Harris and O. P. McDuff. The basis of these calculations was the self-consistency equations of Lamb [Ref. 2]. Here, one assumes a cavity electromagnetic field of the form

$$E(z,t) = \sum_n E_n(t) \cos [\nu_n t + \phi_n(t)] U_n(z)$$

where E_n , ν_n , and ϕ_n are the amplitude, circular frequency, and phase of the nth mode and $U_n(z) = \sin(n\pi z/L)$. By assuming a dielectric perturbation having a time-varying susceptibility at the modulation frequency ν_m and occupying a length a of the laser cavity, the contribution

¹S. E. Harris and Russel Targ, Applied Physics Letters, November 15, 1964.

²W. E. Lamb, Jr., Physical Review, 134, A1429 (1964).

of the dielectric perturbation to the polarization of the nth cavity mode is obtained. Assuming that the driving frequency ν_m is approximately but not exactly equal to the cavity mode spacing $\Delta\Omega$ (e.g., $\nu_m - \Delta\Omega = \Delta\nu$), neglecting all mode coupling effects between those except immediately adjacent modes (other terms are smaller by $\sim \Delta\nu/\Delta\Omega$), and assuming that the linear atomic susceptibility χ_n'' of the laser medium cancels the losses of a given mode, we obtain recursion relations which have the steady-state solution

$$Q_n = n\pi$$

$$E_n = J_n(\Gamma)$$

where

$$\Gamma = \frac{1}{\pi} \frac{\Delta\Omega}{\Delta\nu} \delta$$

and δ is the peak single-pass phase retardation of the dielectric perturbation.

It is worth noting that this solution does not represent a sweeping of the frequency of each mode across the doppler linewidth. In the absence of coupling of one mode to another, this individual-mode FM is important. It would occur if the dielectric perturbation were distributed uniformly spatially over the whole cavity. In the above solution, this individual-mode FM is a higher order effect and is neglected.

The series form of solution obtained above has been cast into closed form. We had, rewriting in terms of a center frequency $\Omega_0 = N_0 \pi z/L$ of the FM signal

$$E(z, t) = \sum_{n=-\infty}^{\infty} J_n(\Gamma) \cos[(\Omega_0 + n \nu_m) t + n \pi] \sin \frac{(N_0 + n) \pi z}{L}$$

Using various trigonometric and Bessel identities, one obtains a traveling-wave form

$$E(z, t) = \frac{1}{2} \left\{ \text{Sin} \left[\Omega_0 t + \frac{N_0 \pi z}{L} + \Gamma \text{Sin} \left(v_m t + \frac{\pi z}{L} \right) \right] \right\} \\ - \frac{1}{2} \left\{ \text{Sin} \left[\Omega_0 t - \frac{N_0 \pi z}{L} + \Gamma \text{Sin} \left(v_m t - \frac{\pi z}{L} \right) \right] \right\}$$

Each term in this equation represents a carrier traveling at light velocity but which is phase modulated, the phase term traveling at a slightly different velocity. The net result is a traveling phase-modulated signal whose phase relative to some reference point changes slowly with time. The total field is seen to be the sum of a (+) traveling and (-) traveling wave. In standing-wave form, the solution becomes

$$E(z, t) = \text{Cos} \left[\Omega_0 t + \Gamma \text{sin } v_m t \cos \frac{\pi z}{L} \right] \\ \times \text{Sin} \left[\frac{N_0 \pi z}{L} + \Gamma \cos v_m t \sin \frac{\pi z}{L} \right]$$

As this shows, the total field at no point inside the cavity is FM except at the ends where the amplitude is zero. This means that one wants to couple out of the cavity only one of the traveling waves. A nonperfect end mirror does this approximately while a brewster-angle polarizer inside the cavity also does this, in effect, when taking the reflection of the orthogonal polarization.

It has been noted that if the dielectric perturbation is multiple-frequency, a more complicated recursion relation for the E_n results but that the lower-order Bessel terms in the expansion of a multiple-frequency-modulated FM signal satisfies this recursion relation. An obvious application is the synthesis of waves with prescribed frequency vs time characteristics.

Basic problems which are being studied are the effects of saturation of the laser medium and the quenching of the original modes of the unperturbed laser by the FM mode of operation described. In the place of each of these original modes, there appears the sideband of the FM signal detuned from it by $n\Delta\nu$.

B. EXPERIMENT

A stable table for use in the FM experiments is essentially complete. It consists of 8 layers of ordinary 2"x4"x8" cut bricks separated by fiber pads and topped with a 4'x8'x10" granite surface plate. The whole structure floats on 18 innertubes.

An electro-optic modulator using KDP has been constructed. It uses a 1-cm-long crystal with the electric field along the optic axis. Single-pass phase retardation $\delta = 0.12$ has been measured at 120 Mc, the expected $\Delta\Omega$ of the argon laser to be used.

A photo-multiplier detector has been completed and tested; a scanning spherical mirror interferometer is being built; and, preparations to convert FM to AM using both a birefringent discriminator and a Michelson interferometer have been made.

Preparations are being made to operate the system on a pulsed, high-peak power basis.

Various other miscellaneous parts for the argon laser setup have been ordered and/or received. The laser itself is expected to be delivered during January.

Project 0577: MICROWAVE PHOTOTUBES AND LIGHT DEMODULATORS

Army Contract DA 36-039 AMC-00094(E)

Project Leader: A. E. Siegman

Staff: J. R. Kerr

This project has investigated methods for demodulating coherent light signals which are carrying broadband microwave frequency or amplitude modulation with particular emphasis on microwave phototubes, photomixers, and similar devices.

This project has been successfully completed, with experimental results in good agreement with theory. The original FM phototube concept for demodulating frequency modulated light using an optical dispersing element and a transverse-wave phototube has been verified, and additional types of interactions and "aperture effects" have also been experimentally observed and theoretically explained, using the same experimental tube.

The final report has been completed, and the project is terminated with this report.

Project 0581: INFRARED MODULATION BY FREE CARRIER ABSORPTION

Air Force Contract AF04(695)-536

Project Leader: A. E. Siegman

Staff: J. A. Tellefsen

The purpose of this project is the study of the modulation characteristics of an infrared modulator tube which utilizes the infrared absorption by free carriers generated on a semi-conductor surface by electron bombardment.

A. EXPERIMENTAL SETUP

The basic experimental setup was reported in the last quarterly report. The experiments we have performed have mostly been with the modulator tube as described in that report, with few exceptions. The tube has been slightly redesigned for two important needs. First, a decision was made to incorporate a small vac-ion pump into the glass envelope because several of the earlier set-backs, as reported previously, were caused by small leaks in the glass. There are a number of seals imbedded in the over-all structure which, because of the necessary heat treatment, could be possible leak sources. Incorporating a vac-ion pump together with a pump-speed indicator allows us to measure how good the vacuum is at any time. Secondly, but related to this same problem, we decided to get rid of the doubtful epoxy window seals used previously, and substitute a graded quartz-to-glass seal. The distance between the two quartz windows was thereby increased slightly.

Some time after the pump was put in, another crack was discovered near the seal where the sample contact feeds through, and the glass eventually broke. The seal is now reinforced, and contact to the tungsten pin is made via a light spring clip. Each time the glass envelope is opened and the cathode is exposed to atmospheric pressure, a new electron gun assembly must be inserted.

We have done some breadboard experiments to find a suitable grid-pulsing circuit. We still feel that there is more to be done with the one we are now using. The problems arise from the fact that we need fast and large pulses applied at -2KV. We have built a coupling circuit that enables us to observe the current pulses through the plate circuit. According to the simple theory there is a linear relation between the absorption coefficient and the plate current. Our method consists of inserting a current probe inside an isolated housing. Furthermore, other high-voltage couplers and meters have been built. A glass cage completely surrounding the modulator tube will prevent any accidental touching of high-voltage cables.

The beam steering was not to our satisfaction due to misalignment of the gun structure. We therefore had to increase the dc supply to be able to control the position of the beam spot. We are considering an auxiliary deflection method by the means of magnetic coils. In the current setup we have approximately half the sample area at our disposal.

The optical system is also receiving new consideration. In the current setup we are using a large Spectra-Physics Laser Model 112. Integrated output power at 3.39μ is 4 to 5 milliwatts. With the detector, the same as described earlier, we are able to scan the laser beam and to see the mode pattern in great detail. The laser mount, the modulator mount, as well as the detector, are all furnished with micro-positioners enabling three-dimensional adjustments to be made. This system has also been used to evaluate the optical properties of some of the other semiconductor samples available. A few look very promising.

B. RECENT EXPERIMENTAL RESULTS

At the moment of writing this report, some preliminary observations of what is believed to be free carrier modulation have been observed. However, it is too early to give any quantitative data. The problems encountered, besides those mentioned above, have to do with the fact that 3.39 μ laser beam is invisible; there are no other methods by which the radiation can be viewed than through detectors of the kind we are using. Therefore, no visual means can be used in aligning the various components.

C. PLANS FOR THE FUTURE

We hope within a short time to have removed some of the problems now blocking our efforts to directly evaluate the performance of the modulator tube. The detector circuitry as well as the grid modulator will be re-examined and improved upon. We will try to use infrared lenses to collimate the beam to the active spot. This should improve the performance. There are other electrical problems to be tackled too, mainly in connection with the high voltage supply network.

Project 0582: OPTICAL PHASE- AND FREQUENCY-MODULATION TECHNIQUES

Air Force Contract AFO4(695)-536

Project Leader: S. E. Harris

Staff: C. M. McIntyre

As reported last quarter, the most important practical consideration involved in the construction of an optical network using 1 cm calcite crystals is the maintenance of temperature within 0.05 °C. A proportional temperature controller is being used for this purpose. This quarter, better thermal contact between the temperature sensing element and the surface being controlled, and better insulation of the test unit helped achieve the desired stability. To determine the stability, the output intensity of a Senarmont compensator was monitored to measure the variation in retardation of a single crystal with time. This variation has been held to 1/100 of a wave over a period of up to 6 hours. Other tests indicating the stability were performed including measuring the retardation with the Senarmont compensator on successive runs with the controller

turned off and then on between each run. The position of the analyzer for a minimum output remained constant within one degree (corresponding to a constant retardation within $1/180$ of a wave). The achievement of this control was necessary before the compensating crystals could be worked on.

As noted previously, each stage of the network will consist of a 1 cm calcite crystal and a quartz compensating plate. The quartz plate will be used to control the overall retardation of the stage. Now that the desired temperature control has been obtained, polishing of the quartz plates has begun. Each stage in the filter must be the same length within a retardation of $2\pi n$ (where n is a small integer) at the desired temperature. The accuracy required in polishing the quartz is obtainable in our laboratories. The procedure consists of polishing the quartz plates, measuring the retardation of the stage at the controlled temperature, calculating the amount of material that has to be removed from the quartz, and repeating the above steps until the desired retardation has been reached. This work will be continued next quarter. When the plates are completed, the network can be assembled and tested. The temperature control for the larger volume of the assembled network may necessitate being even more careful with insulation, but no serious problems are anticipated.

A computer program for the synthesis procedure was initiated this quarter and is now being written. This program will be designed to allow synthesis from either an electric field or an intensity characteristic. There will also be a check (or analysis) program.

It should also be mentioned that other means of temperature control are being investigated for future application.

Project 0592: LASER PHOTOMIXING STUDIES

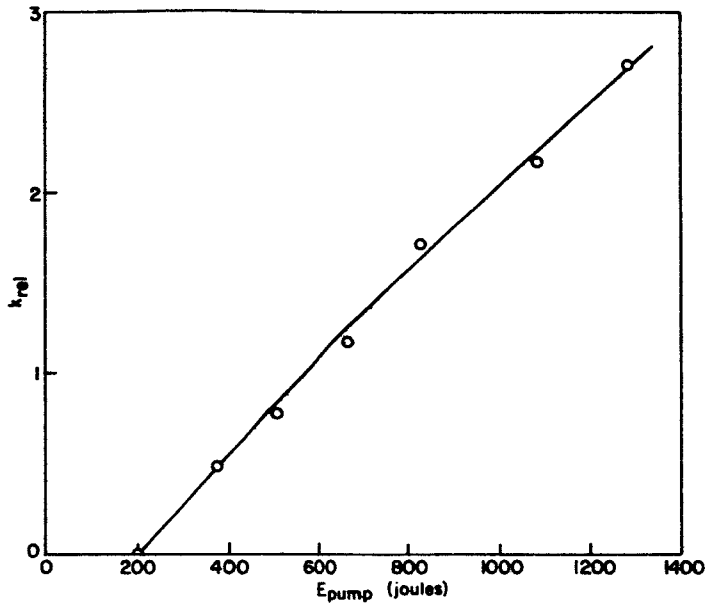
Signal Corps Contract DA 36-039 SC-90839
Project Leader: A. E. Siegman
Staff: J. Allen, J. O'Brien

The purpose of this project, which is now terminating, was to study optical maser characteristics and photoelectric mixing, particularly at microwave difference frequencies. Emphasis was placed on the mixing of signals derived from two separate lasers, using one laser as a frequency reference for studying the other.

We have considerably improved the agreement between theory and experiment for the ruby laser oscillation delay time analysis presented in a preceding QRR. It may be recalled that while the theory is presented in terms of delay time and actual pump power absorbed by the rod, the quantities measured in the experiment are the delay time and the input energy to the pump flash lamp, as determined by the voltage of the capacitor bank that is discharged into the flash lamp. In order to compare theory and experiment, it is necessary to know the relationship between the pump power k of the theory and the measured input energy E . This can be done in the following way: by using a calibrated photomultiplier, and filters passing only light in the two pump bands of ruby, a relative k , k' , may be determined for various values of E , which gives k' as a function of E . Presumably geometry determines a multiplicative factor between this k' and the k of the theory so that in a quotient of two k 's the factor cancels out. Thus, $k'(E)/k'(E_{th}) = k/k_{th}$, where E_{th} is taken as the lowest input energy for which lasing can be obtained, and k_{th} is the theory's threshold k -value. The relative quantity $k'(E)$ has been determined carefully by Nelson and Remeika [Ref. 1] for the same kind of flash lamp used in our experiments. Their results are shown in Fig. 22. Making use of their data, and the method of the preceding discussion, we have plotted our experimental data and the results of the theory together in Fig. 23 where it is seen that there is general agreement in magnitude and scope between theory and experiment.

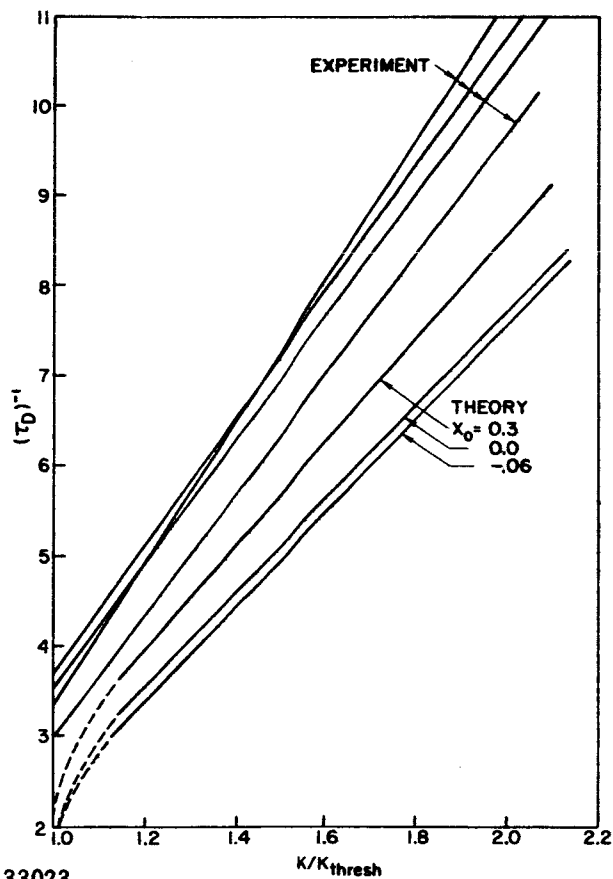
Some further discussion of this portion of the work will be given in the final report which has also been in preparation in the past quarter. This report summarizes the work on a large number of topics which has been carried out under this contract during the past two years.

¹D. F. Nelson and J. P. Remeika, J.A.P., 35, 3 (Part 1), Mar 1964, p. 522.



33022

FIG. 22. EXPERIMENTAL CURVE AT $k_{\text{rel}}(E)$ (FUNCTIONAL NOTATION) FROM NELSON AND REMEIKA'S PAPER.



33023

FIG. 23. COMPARISON BETWEEN THEORY AND EXPERIMENT FOR LASER DELAY TIME.

Project 0816: STUDY OF TRANSIENT PHENOMENA IN LOW PRESSURE GAS
DISCHARGE PLASMAS

Air Force Contract AF33(615)-1504

Project Leader: H. Derfler

Staff: T. Simonen, S. Puri, A. Y. Sader

I. OBJECTIVES

The purpose of this project is to study the excitation and detection of an impulse propagating through a plasma.

This program comprises:

1. A theoretical investigation of impulse propagation in terms of plasma waves taking into account geometrical effects, magnetic fields and collisions.
2. An experimental study of suitable means to excite and detect longitudinal space-charge waves in low-pressure gas discharge plasmas, in particular of the Bohm and Gross variety. Parallel-plane grids and coaxial probes immersed in the plasma will be used as transmitter and detectors. Schemes to excite and detect plasma waves with external electrodes will be studied.
3. Attempts to distinguish experimentally between Landau damping and collision damping of space-charge waves in a fully ionized cesium plasma.
4. An investigation of the possibilities of using electron beams, light, or laser action to excite or detect collective interaction in a low-pressure gas-discharge plasma.

II. INTRODUCTION

This is the third quarterly report and covers the period for 3 August 1964, to 3 November 1964. It describes the response of a Maxwellian electron plasma to an oscillating sheet dipole. The excitation and propagation of Bohm and Gross waves and the Van Kampen modes are described. Numerical results are given to illustrate the combined effects of Landau damping and collision damping on the propagation of the Bohm and Gross waves. The excitation and propagation of the Van Kampen modes discussed in this report have not previously been discussed in the literature. Work on a cesium diode to be used in future propagation experiments is described.

III. THEORETICAL WORK

A. FREQUENCY RESPONSE

The signal received by a pair of closely spaced unloaded grids, ($d \ll \lambda_d$), at a distance l from an identical pair of transmitting grids was given by equation* (9-44) [Ref. 1] as

$$\frac{V_2(\omega)}{V_1(\omega)} = - \frac{d}{2\pi} \int_{-\infty}^{\infty} \frac{e^{-ikl} dk}{1 + P(\omega, k)} \quad (1)$$

In the first quarterly report [Ref. 1] we investigated this response for an electron plasma having a spherical-shell velocity distribution. Such a plasma does not exhibit Landau damping nor does it support Van Kampen modes.

This quarter we considered the response (1) in a Maxwellian electron plasma. In order to illustrate the basic principles we considered again an open-circuited output and the condition $d \ll \lambda_d$. These conditions can be interpreted as describing the electric field

$$E(\omega) = \lim_{d \rightarrow 0} V_2(\omega) / d \quad (2)$$

excited by an oscillating dipole charge sheet with a voltage drop

$$V(\omega) = \lim_{d \rightarrow 0} V_1(\omega) \quad (3)$$

An oscillating sheet could be experimentally realized by a transversely modulated sheet electron beam shot across the plasma.

* 9-44 refers to QSR 9, Eq. 44.

¹ QSR No. 9, Project No. 0816, p. I-84, March 1964.

The propagator for a Maxwellian electron velocity distribution can be expressed in the Mittag-Leffer expansions [Ref. 2] (10-24) and (10-25).

$$\frac{1}{1 + P(\omega, k)} = \Omega' \sum_{n=-\omega}^{\omega} \frac{C_n^{\pm}}{K - K_n^{\pm}} \quad \begin{array}{l} + K < 0 \\ - K > 0 \end{array} \quad (4)$$

The K_n are the roots of the dispersion relations (10-19) and (10-20). The C_n are the corresponding residues (10-23). We split the integral (1) at $K = 0$ and use (4) to obtain

$$\frac{E(\omega)}{V(\omega)} = \frac{\Omega'}{2\pi\sqrt{2\lambda}_d} \sum_{n=-\infty}^{\infty} \left[C_n^+ \psi(1, 1; -iK_n^+ L) - C_n^- \psi^*(1, 1; iK_n^{-*} L) \right] \quad (5)$$

where ψ is the confluent hypergeometric function of the second kind [Ref. 3] as defined by:

$$\psi(1, 1; x) = \int_0^{\infty} \frac{e^{-xt} dt}{1+t} \quad \begin{array}{l} -\pi < \phi < \pi \\ -\frac{\pi}{2} < \phi + \arg(x) < \frac{\pi}{2} \end{array} \quad (6)$$

As it stands, this integral defines a function with a logarithmic branch cut along the negative real x -axis. On the other hand, we note that as a function of frequency the arguments $x_n^+ \equiv -iK_n^+ L$ and $x_n^- \equiv i(K_n^-)^* L$ of the ψ functions in Eq. (5) never cross the positive imaginary axis, that is $-3\pi/2 < \arg(x) < \pi/2$. We thus have to use the analytic continuation of the ψ function in the range $-3\pi/2 < \arg(x) < -\pi$.

Power series representations are

$$\psi(1, 1; x) = -e^x \left[\ln \gamma x + \sum_{n=1}^{\infty} \frac{(-x)^n}{n!n} \right]$$

²QSR No. 10, Project No. 0816, p. I-85, June 1964.

³A. Erdelyi, et al, Higher Transcendental Functions, 1, p 256, McGraw-Hill, New York, 1953.

or

$$\psi(1,1;x) = -e^x \ln \gamma x + \sum_1^{\infty} \sigma(n) \frac{x^n}{n!} \quad (7)$$

where

$$\gamma = 1.781072\dots \quad \sigma(n) = 1 + 1/2 + \dots + 1/n$$

$$-\frac{3\pi}{2} < \arg(x) < \frac{\pi}{2} .$$

The appropriate asymptotic expansion is

$$\psi(1,1;x) \sim \sum_0^N \frac{(-1)^n n!}{x^{n+1}} + \Lambda i\pi e^x \quad (8)$$

$$\begin{array}{l} \text{Re } x > 0 \quad \Lambda = 0 \\ \text{Re } x < 0 \quad \left\{ \begin{array}{l} \text{Im } x < 0 \quad \Lambda = 0 \\ \text{Im } x = 0 \quad \Lambda = 1 \\ \text{Im } x > 0 \quad \Lambda = 2 \end{array} \right. . \end{array}$$

The discontinuous factor Λ is a consequence of Stokes Phenomenon [Ref. 4] and does not represent a true discontinuity of the function. In fact near the negative real axis the asymptotic expansion is not good enough in which case an appropriate power series must be used, Eq. (7).

Using Eq. (8) we find that the voltage response for large distances is asymptotically proportional to

$$\psi \sim \frac{1}{iK_n^{\pm} L} \pm \Lambda i\pi e^{-iK_n^{\pm} L} . \quad (9)$$

⁴P. M. Morse and H. Feshbach, "Methods of Theoretical Physics," McGraw-Hill, New York, 1953, 1, p. 609.

Whenever $-\pi < \arg(K_n^+) < -\pi/2$ or $-\pi/2 < \arg(K_n^-) < 0$ the analytic continuation is included ($\Lambda = 2$). The first term of Eq. (9) represents the Van Kampen modes while the second term represents Bohm and Gross waves. Because the Van Kampen modes decay as L^{-1} rather than exponentially they would be expected to predominate for sufficiently large distances and certainly below the critical frequency where the imaginary parts of the wavenumbers K_n become dominant.

B. NUMERICAL COMPUTATIONS

1. Fried and Contes Z-function

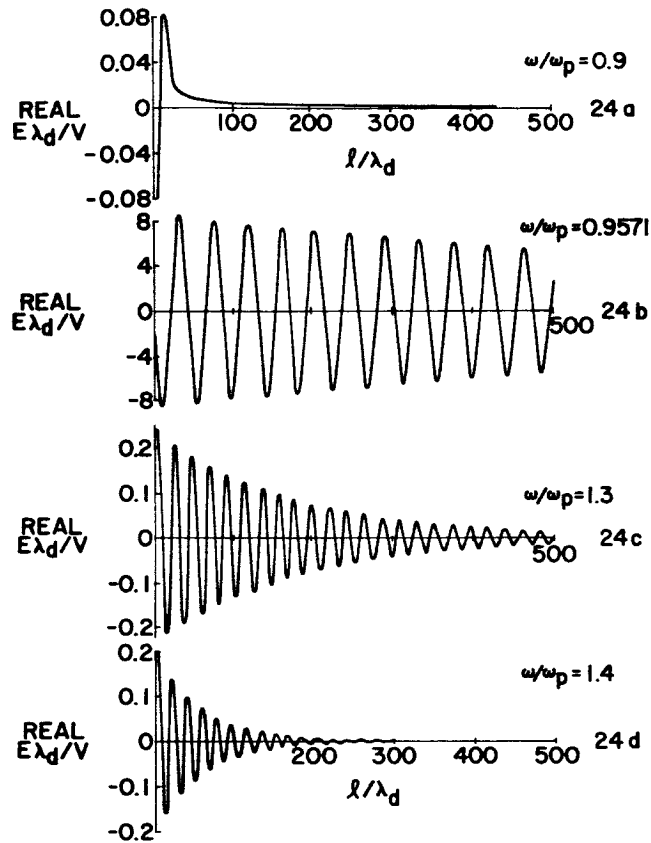
Numerical computations for a plasma having a Maxwellian electron velocity distribution involve the Z-function [Ref. 5] and (or) its first few derivatives. For these computations and to facilitate future work an efficient computer program was written for finding Z and its first four derivatives. The program is written so that there is no loss of accuracy as there is when recurrence relations are used to find higher derivatives.

2. Calculation of Frequency Response

The electric field $E(\omega)$ excited by an oscillating dipole sheet of strength $V(\omega)$ as given by Eq. (5) has been calculated for a set of frequencies as a function of position. Figure 24a-d illustrate this response for a plasma having a collision frequency $\nu/\omega_p = 10^{-4}$ and a drift $\Delta = V_d \cdot \langle (V - V_d)^2 \rangle^{-1/2} = 0.3$. The wave numbers for such a plasma were given in QSR No. 10, Fig. 48. Below the critical frequency, Fig. 24a, only the Van Kampen modes propagate and decay as L^{-1} . Above the critical frequency but below the plasma frequency, Fig. 24b, the Bohm and Gross waves are only slightly damped. Above the plasma frequency, Figs. 24c and 24d, the Bohm and Gross waves become increasingly Landau damped.

The electric field as a function of frequency at a fixed position $l/\lambda_d = 100$ is shown in Fig. 25. The level of the received signal in db, $20 \log_{10} |E(\omega)/E(\omega_c)|$, is referred to the signal received at the critical frequency. This diagram illustrates the effective passband.

⁵B. D. Fried and S. D. Conte, "The Plasma Dispersion Function," Academic Press, New York, 1961.

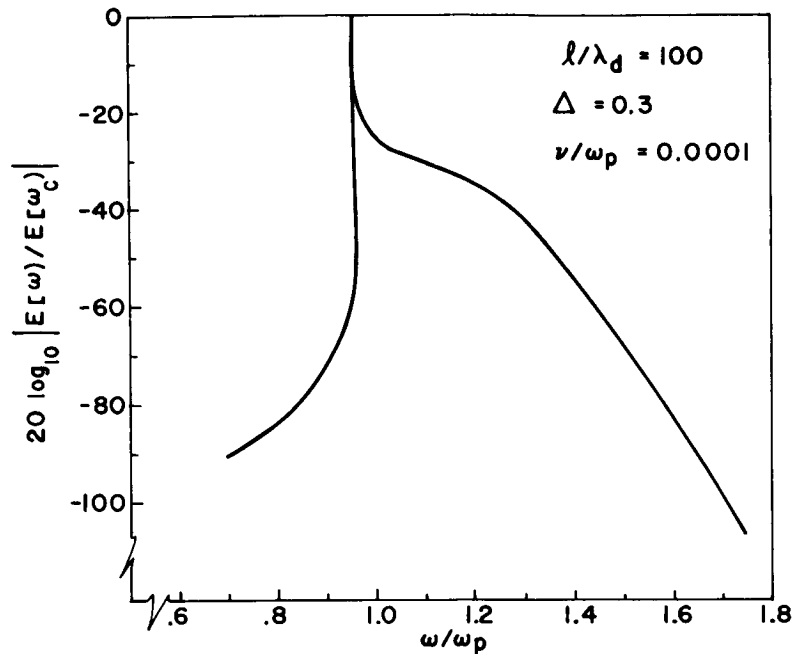


32441

FIG. 24. ELECTRIC FIELD EXCITED BY AN OSCILLATING DIPOLE SHEET AS A FUNCTION OF DISTANCE. Plasma: Drifting Maxwellian, $v_d/v_T = 0.3$, $\nu/\omega_p = 10^{-4}$, $\omega_c/\omega_p = 0.9567$.

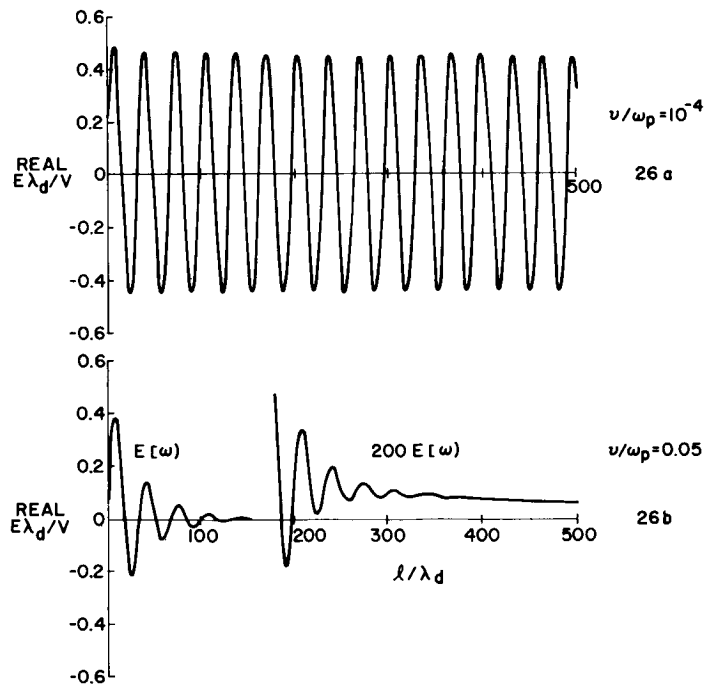
The collision frequency $\nu/\omega_p = 10^{-4}$ is typical of a highly ionized cesium plasma and of the relatively collision-free plasma used by Malmberg and Warton [Ref. 6]. Figure 26 compares the response of such a plasma with that of a plasma having the collision frequency $\nu/\omega_p = 0.05$ typical of a mercury-vapor discharge. Figure 26b is expanded to illustrate the effect of Van Kampen waves from which their L^{-1} decay can be seen.

⁶J. H. Malmberg and C. B. Warton, Phys. Rev. Letts., 13, 6, p. 184, 10 August 1964.



32439

FIG. 25. WAVE ENERGY EXCITED AT A FIXED DISTANCE FROM AN OSCILLATING DIPOLE SHEET AS A FUNCTION OF FREQUENCY. Plasma: Drifting Maxwellian, $V_d/V_T = 0.3$, $\nu/\omega_p = 10^{-4}$, $l/\lambda_d = 100$, $\omega_c/\omega_p = 0.9567$.

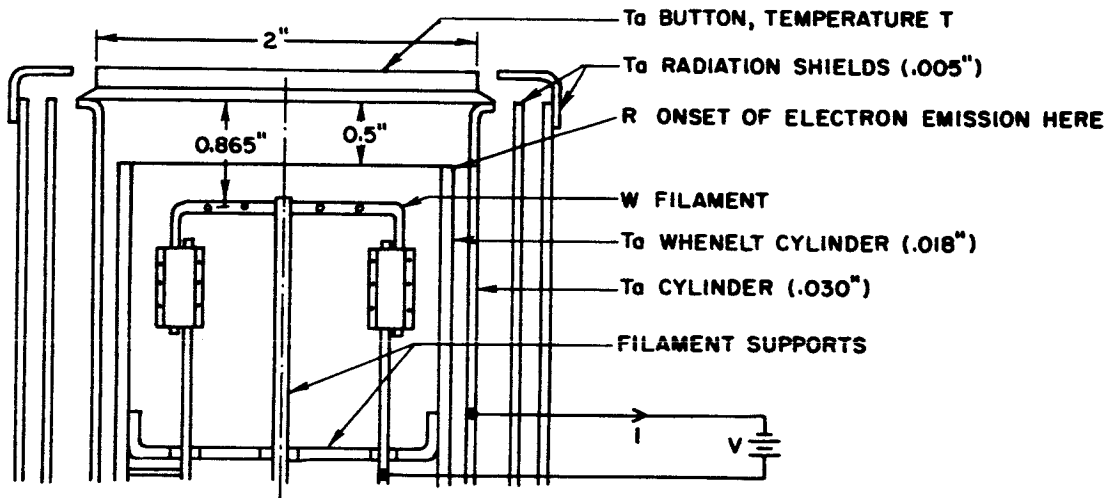


32440

FIG. 26. EFFECT OF COLLISIONS ON ELECTRIC FIELD EXCITED BY AN OSCILLATING DIPOLE SHEET AS A FUNCTION OF DISTANCE. Plasma: Drifting Maxwellian, $V_d/V_T = 0.2$, $\omega/\omega_p = 1.1$.

IV. EXPERIMENTAL WORK

Work to boost the power available from the current regulated power supply used in heating the tantalum emitter has been completed. To increase the efficiency of the heater we introduced radiation shields as shown on Fig. 27. We also increased the thickness of the Wehnelt cylinder (now 0.018") to enhance thermal conduction losses and thereby lower its temperature. By these measures we could boost the emitter temperature by 100 °K but thermal runaway still occurred beyond an emitter temperature of $T = 2250$ °K. Figure 28 shows the measured space-charge-limited voltage-current characteristic with a sharp break due to the onset of temperature-limited emission from the Wehnelt cylinder. The following attempts were made to further cut down the electron emission from the Wehnelt cylinder.

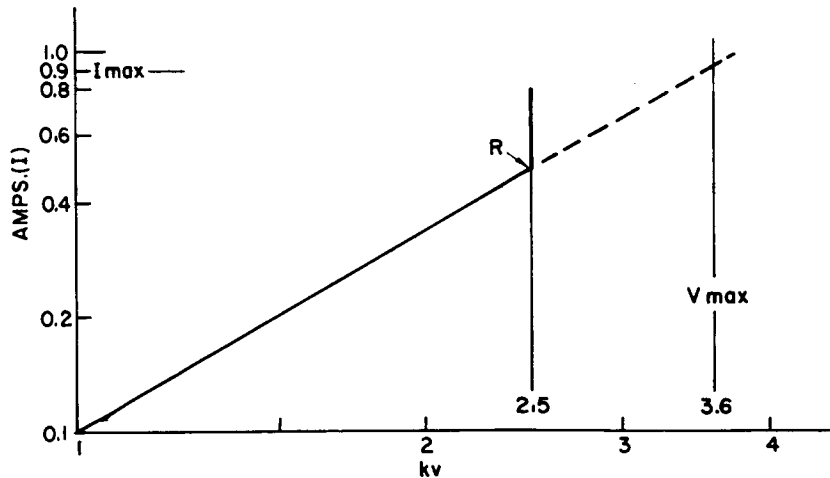


33024

FIG. 27. HEATING BY ELECTRON BOMBARDMENT. Thermal runaway occurs due to onset of electron emission at R.

A. SCHOTTKY EFFECT AND FIELD EMISSION

A lip was introduced to round off the top edge of the Wehnelt cylinder. This did decrease the runaway temperature showing that Schottky effect and field emission are negligible as compared to the increase in effective area of emission by the presence of the lip.



33024

FIG. 28. BOMBARDER CHARACTERISTICS. Thermal runaway starts at R, at temperature $T = 2250^{\circ}\text{K}$.

B. SAND BLASTING

The Wehnelt cylinder was sand blasted to enhance radiation cooling. This had the adverse effect of increasing the electron emission presumably due to a larger effective surface area of emission and Schottky effect on sharp corners.

C. CARBURIZING

It has been reported in the literature [Refs. 7,8] that carburization of tantalum was successfully used to suppress electron emission from grids in transmitter tubes. Based on this fact several attempts have been made to form a layer of TaC on the Wehnelt cylinder by heating it to 1400°C in an atmosphere of CO or CO_2 at pressures ranging from a few mm Hg up to 1 atmosphere. In all cases the cylinder warped badly or even broke like an eggshell due only to thermal stresses. This method of increasing the work function was therefore abandoned.

⁷M. Knoll, "Material and Processes of Electron Devices," Springer, Berlin, 1959, p. 96 and p. 385.

⁸K. Becker and H. Ewest, Zeitschrift f. Techn. Physik, 11, (1930), p. 148 and p. 216.

D. RHENIUM PLATING

Currently we are considering electroplating the Wehnelt cylinder and its surrounding with Rhenium. Rhenium has a work function of 5.1 volts as compared to 4.1 volts for tantalum and therefore should solve our problem, deferring thermal runaway beyond the working temperature of 2500 °K.

V. DISCUSSION AND FUTURE WORK

It was found in Sec. IIIB, Fig. 25, that the passband of propagation for a plasma with a gaussian distribution of velocities is drastically reduced as compared with the passband found earlier, [Ref. 2], Eq. (53), for a plasma with a spherical-shell distribution of velocities. This effect, due to Landau damping, relaxes the problems associated with the broad-band design of the circuit and thus makes the experimental study of impulse propagation in such a plasma feasible. Currently we are removing the restriction $k \ll \lambda_d$ in order to compute the coupling efficiency of the probes as a function of frequency. These data are needed before a specific broad-band circuit, suitable for a cesium plasma, can be designed.

Work on the cesium plasma diode to be used in this experiment is in progress. We hope in particular that the problem of thermal runaway can be solved by electroplating the Wehnelt cylinder with Rhenium as described in Sec. IV.

Finally we note that the continuous-wave experiment by Malmberg and Warton [Ref. 6] satisfies our condition $k \ll \lambda_d$ and does exhibit the effect of Landau Damping. We are conducting some computations, specifically designed to compare our theory with their experimental data.

Project 0832: RF BEHAVIOR OF PLASMA DIODES

Army Contract DA 36-039 AMC-00094(E)
Project Leader: H. Derfler
Staff: M. Omura

The purpose of this project is the study of oscillations and waves in plasmas near thermodynamic equilibrium.

In the past QRR's we were primarily concerned with the dc potential and the number densities of various species between two thermionically emitting parallel planes. We now consider some rf phenomena in such a system by using the hydrodynamic equation of motion for the electrons.

A. HYDRODYNAMIC EQUATION

A derivation of the hydrodynamic equation of motion is given by Rose and Clark [Ref. 1]. The equation is derived by taking appropriate averages of the Boltzmann equation. If zero drift velocity, zero collision frequency and isotropic velocity distribution are assumed, the zeroth and the first-order equation of motion for the electrons become

$$- n_o e \bar{E}_o = \nabla P_o \quad (1)$$

$$n_o m \frac{\partial \bar{u}}{\partial t} = - n_o e \bar{E}_1 - n_1 e \bar{E}_o + \bar{j} \times \bar{B}_o - \nabla P_1 \quad (2)$$

where the subscripts o and 1 denote zeroth and first-order quantities respectively. The effect of the temperature is taken into account by the pressure terms ∇P_o and ∇P_1 . For Maxwellian velocity distribution we have

$$P_o = n_o kT$$

and hence

$$- n_o e \bar{E}_o = kT \nabla n_o$$

or

$$\nabla \phi_o = \frac{kT}{e} \frac{\nabla n_o}{n_o} \quad (3)$$

¹D. Rose and M. Clark, Plasmas and Controlled Fusion, The M.I.T. Press, Cambridge, Mass. (1961) Chapters 4 and 6.

Equation (3) yields the scale-height law which had been assumed in deriving the dc quantities. For the rf pressure adiabatic compression is assumed and thus

$$P_1 = \gamma n_1 kT \quad (4)$$

and γ is set to 3.

If $e^{i\omega t}$ time variation is assumed for the first-order quantities, Eq. (3) becomes

$$i\omega n_o m \bar{v}_1 = -n_o e \bar{E}_1 - n_1 e \bar{E}_o + j_1 X \bar{B}_o - \gamma k T \nabla P_1 \quad (5)$$

Equation (5) plus Maxwell's equations give us enough equations to solve for \bar{E}_1 . Before we go on, however, we shall make further simplifications by assuming the dc magnetic field to be zero and that the quasi-static approximation is valid. By using the following relations

$$\bar{I}_1 = \bar{j}_1 + i\omega \epsilon_o \bar{E}_1$$

$$j_1 = n_o e \bar{v}_1$$

$$\nabla \cdot \bar{E} = \rho_1 / \epsilon_o$$

$$\omega_p^2 = (n_o e^2 / m \epsilon) = \text{plasma frequency}$$

$$v_\theta = (kT/m)^{1/2} = \text{thermal velocity}$$

Eq. (5) becomes

$$\gamma v_\theta^2 \nabla \left(\frac{\rho_1}{\epsilon_o} \right) + \frac{e \bar{E}_o}{m} \frac{\rho_1}{\epsilon_o} + (\omega^2 - \omega_p^2) \bar{E}_1 = \frac{-i\omega}{\epsilon_o} \bar{I}_1 \quad (6)$$

or

$$\gamma v_{\theta}^2 \nabla(\nabla \cdot \bar{E}_1) + \frac{eE_0}{m} (\nabla \cdot \bar{E}_1) + \omega^2 \left[1 - \frac{\omega_p^2}{\omega^2} \right] E_1 = - \frac{i\omega}{\epsilon_0} \bar{I}_1. \quad (7)$$

We now look for resonances with $\bar{I}_1 = 0$. Possible resonances with $I_1 \neq 0$ will be considered at a later time.

B. BOUNDARY CONDITION

Consider the geometry shown in Fig. 29. We shall assume that the emitting walls are perfect conductors and that the dc quantities (i.e., electron density, ion density and the potential) vary only in the direction normal to the walls. Under these conditions the first-order quantities can be shown to vary in the form $A_1(x)e^{\Gamma z}$ where x is the direction normal to the emitters and z is the parallel direction. In particular, we get for the first-order charge density

$$\rho_1(x, z) = \rho_1(x) e^{\Gamma z}. \quad (8)$$

If we take the z component of Eq. (6) we get

$$(\omega^2 - \omega_p^2) E_{1z} = - \frac{\gamma v_{\theta}^2}{\epsilon_0} \frac{\partial \rho_1}{\partial z} = \frac{\Gamma \gamma v_{\theta}^2}{\epsilon_0} \rho_1. \quad (9)$$

Since $E_{1z} = 0$ at the wall, ρ_1 must also be zero. Consequently, from Poisson's equation the following equivalent boundary condition is obtained.

$$\left. \frac{\partial E_{1x}}{\partial x} \right|_{\text{wall}} = \left. \left(\frac{\rho_1}{\epsilon_0} - \frac{\partial E_{1z}}{\partial z} \right) \right|_{\text{wall}} = 0$$

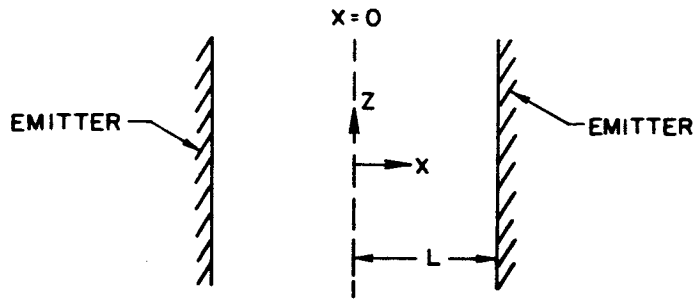


FIG. 29. ELECTRON AND ION EMITTER GEOMETRY.

C. RESONANCES

For a wave in resonance between the two walls, we have

$$\frac{\partial}{\partial y} = \frac{\partial}{\partial z} = 0. \quad (10)$$

Equation (10) and the condition $\nabla \times E_1 = 0$ require that E_{1z} and E_{1y} be zero. Thus we are left with the following differential equation for resonance.

$$\gamma v_\theta^2 \frac{d^2 E_{1x}}{dx^2} + \frac{e}{m} E_0 \frac{dE_{1x}}{dx} - (\omega_p^2 - \omega^2) E_{1x} = 0 \quad (11)$$

By using the following relations and definitions

$$E_0 = \frac{-d\phi}{dx} = -\frac{kT}{e} \frac{d\eta}{dx}$$

$$\omega_{po} = \text{plasma frequency at } x = 0$$

$$\lambda_0 = \sqrt{2} v_\theta / \omega_{po}$$

$$\xi = x / \lambda_0$$

$$\omega_p^2 = \omega_{po}^2 e^\eta$$

Equation (11) is normalized to

$$\frac{d^2 E_{1x}}{d\xi^2} + \frac{1}{\gamma} \frac{d\eta}{d\xi} \frac{dE_{1x}}{d\xi} - 2 \left[e^\eta - \frac{\omega^2}{\omega_{po}^2} \right] E_{1x} = 0 \quad (12)$$

Solutions of Eq. (12) were obtained numerically and some of the results are presented here.

In Fig. 30 the amplitudes of E_{1x} for the first six resonances are shown for molybdenum emitters 1 cm apart at $T = 2200^\circ\text{K}$ (See QRR No. 8 [Ref. 2] for the dc solution). It should be noted that near the wall, where the electron density is high, the rf electric field is small.

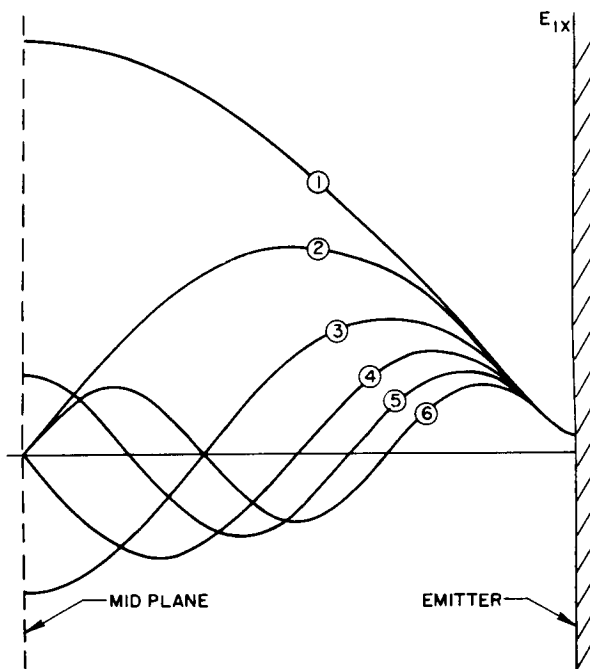


FIG. 30. ELECTRIC FIELD AMPLITUDES OF THE FIRST SIX RESONANCES FOR MOLYBDENUM EMITTERS SPACED 1 CM APART AT $T = 2200^\circ\text{K}$. Modes are numbered and corresponding frequencies are given in Table I.

In table (1) the first six resonance frequencies are given for different temperatures. For lower temperatures the resonances are spread

²QRR No. 8, 1 Jan - 31 Mar 1964, Project 0832, pp. I-64 - I-74.

TABLE 1. THE FIRST SIX RESONANCE FREQUENCIES OF THE PLASMA BETWEEN TWO MOLYBDENUM EMITTERS AS A FUNCTION OF TEMPERATURE. The electric field is symmetric about $X = 0$ for odd numbered modes and anti-symmetric for the even numbered modes.

		MODE 1	MODE 2	MODE 3	MODE 4	MODE 5	MODE 6
T	$\omega_{po}/2\pi$	ω_1/ω_{po}	ω_2/ω_{po}	ω_3/ω_{po}	ω_4/ω_{po}	ω_5/ω_{po}	ω_6/ω_{po}
1800	1.10×10^7	1.55	2.72	3.88	5.06	6.18	7.40
1900	1.27×10^7	1.54	2.70	3.87	5.03	6.14	7.32
2000	1.96×10^7	1.28	1.93	2.66	3.40	4.12	4.89
2100	4.45×10^7	1.06	1.23	1.46	1.73	2.03	2.33
2200	9.79×10^7	1.013	1.053	1.115	1.196	1.293	1.403
2300	2.02×10^8	1.003	1.013	1.029	1.051	1.078	1.111

apart and as the temperature is increased the percentage separation of two adjacent resonances decreases. In Fig. 31 graphs of $L/\lambda_0 \sqrt{\omega^2/\omega_{po}^2 - 1}$

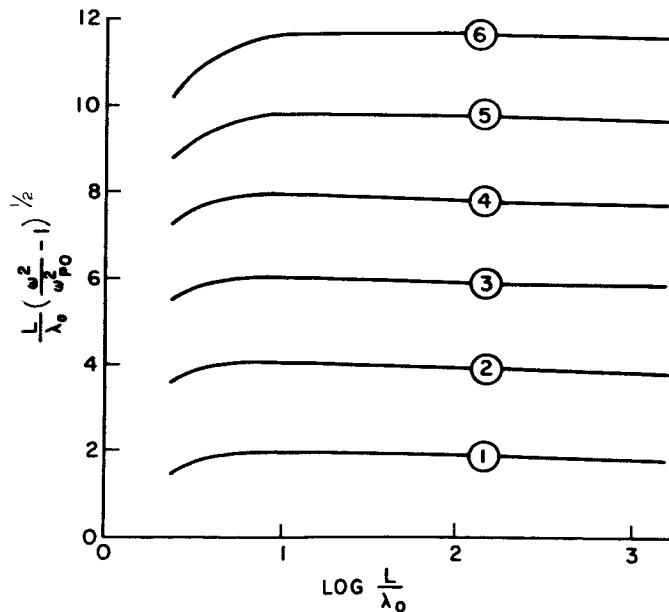


FIG 31. PLOTS OF $L/\lambda_0 (\omega^2/\omega_{po}^2 - 1)^{1/2}$ VS $\text{LOG } L/\lambda_0$ FOR THE FIRST SIX MODES.

vs $\log L/\lambda_0$ are given. The quantity $L/\lambda_0 \sqrt{\omega^2/\omega_{po}^2 - 1}$ is approximately a constant for each mode indicating that $\sqrt{\omega^2/\omega_{po}^2 - 1}$ is approximately proportional to λ_0/L . This result is not surprising because in the case of uniform plasma, Eq. (11) yields the following dispersion relation

$$\gamma v_{\theta}^2 k^2 = \omega^2 - \omega_{po}^2$$

or

$$\left(\frac{\pi}{\lambda}\right)^2 = \frac{1}{\gamma \lambda_0^2} \left(\frac{\omega^2}{\omega_{po}^2} - 1 \right)$$

where λ is the wavelength. At resonance

$$\frac{N\lambda}{2} = 2L$$

where N is an integer and hence at least in the uniform case the quantity $L/\lambda_0 [\omega^2/\omega_{po}^2 - 1]^{1/2}$ is expected to be a constant.

D. COMMENTS

The resonances described above are very similar to the Dattner resonances found in the positive column of a discharge (see for example, an analysis of Dattner resonance made by Parker [Ref. 3]). The difference lies in the fact that in a positive column the electron density decreases toward the wall, whereas in the plasma we are investigating, the opposite is true. Consequently, in the case of positive column, the rf field is strong near the sheath where the density is low while in our case the field is strong near the center of the plasma.

The analysis we have made does not take into account Landau damping. By taking the averages of the Boltzmann equation to derive the hydrodynamic equation, all the details which affect the velocity distribution and hence the mechanism which lead to Landau damping are ignored. Presumably Landau

³J. V. Parker, "Resonance Oscillations in a Hot Non-Uniform Plasma," TR No. 20, Calif. Inst. of Tech.; Pasadena, Calif., May 1963.

damping is important whenever the wave length becomes comparable to the Debye length. At low temperatures we do encounter cases where the Debye length becomes comparable to the emitter separation. In these cases the "Q" of the resonances may be quite low and resonances undetectable. We have also neglected collisions in our analysis. We noted earlier [Ref. 2], however, that the collision frequency in the plasma we are considering may be very low.

If these resonances can be detected readily, the data can be used for diagnostic purposes.

Project 0833: DC STATES OF PLASMA DIODES

National Aeronautical and Space Administration
Grant NsG 299-63
Project Leader: H. Derfler
Staff: ----

The purpose of this project is the study of stationary potential distributions between parallel-plane electron and ion emitting surfaces.

In QRR No. 10 we summarized the basic equations to be used in an attempt to explain the anomalous open-circuit voltages in low-pressure cesium diodes, in terms of "coverage instabilities." As a first step toward this objective we checked our basic assumptions against experimental data. Using the equations due to Gyftopoulos and Levine [Refs. 1, 2, 3] we computed the rates of evaporation of cesium ions (γ_p) and neutral cesium atoms (γ_a) from a tungsten surface at a temperature of $T = 848^\circ\text{K}$. These data are shown in Fig. 32, together with experimental data due to Taylor and Langmuir [Ref. 4]. At first glance we notice that the theoretical value of the ion emission γ_p is roughly a factor

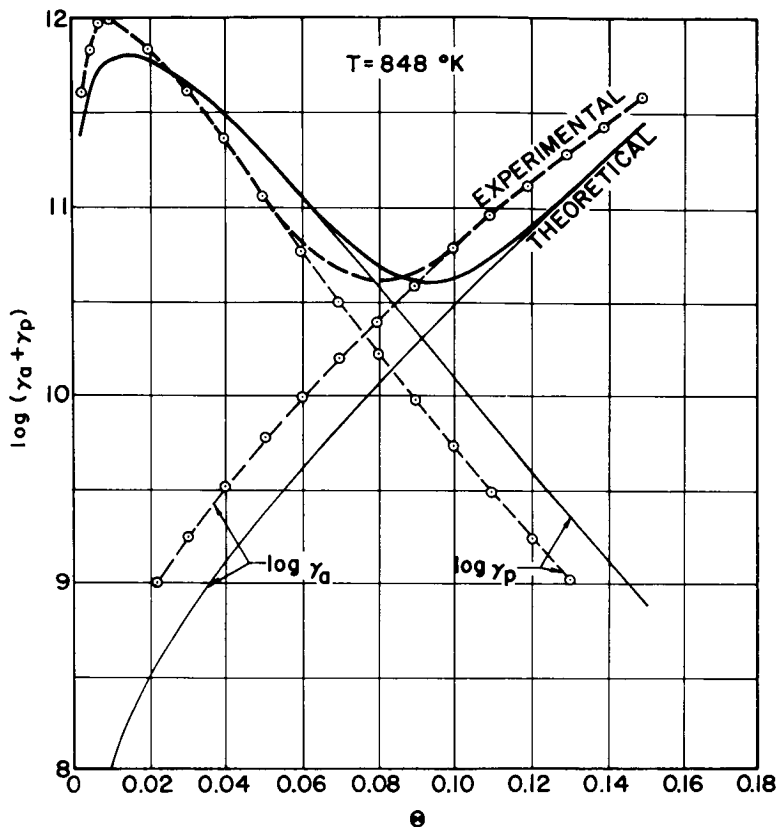
$$\gamma_{p,th}/\gamma_{p,exp} = \exp(0.829) = 2.28, \quad \theta = 0.1 \quad (1)$$

-
- ¹E. P. Gyftopoulos and J. D. Levine, J. Appl. Phys., 33, 1962, pp. 67-73.
²J. D. Levine and E. P. Gyftopoulos, Surface Phys., 1, 1964, pp. 171-193.
³J. D. Levine and E. P. Gyftopoulos, Surface Phys., 1, 1964, pp. 225-241.
⁴J. B. Taylor and I. Langmuir, Phys. Rev., 44, 1933, p. 440, Fig. 19.

too large, and the emission of neutral atoms by a factor

$$\gamma_{a,th}/\gamma_{a,exp} = \exp(-0.691) = 0.502, \quad \theta = 0.1 \quad (2)$$

too small.



32604

FIG. 32. ION (γ_p)-, ATOM (γ_a)-, AND PARTICLE ($\gamma_a + \gamma_p$)- EMISSION RATES IN $\text{CM}^{-2} \text{SEC}^{-1}$ VS THE FRACTION θ OF THE IONIC MONOLAYER COVERING A TUNGSTEN SURFACE AT $848 \text{ }^\circ\text{K}$.

—Theoretical values after Gyftopoulos and Levine
 ----"Experimental" values after Taylor and Langmuir

The following factors may affect this discrepancy:

- a) The experimental mass constant $A_{exp} = 60 \text{ A}\cdot\text{cm}^{-2} \cdot \text{Grad}^{-2}$ (for $1200 < T < 2000 \text{ }^\circ\text{K}$) [Ref. 5] is smaller than the theoretical mass constant

⁵W. B. Nottingham, "Thermionic Emission," article in Encyclopedia of Physics, XXI, p. 175, Springer, Berlin, 1956.

$A_{th} = 120 \text{ A} \cdot \text{cm}^{-2} \cdot \text{Grad}^{-2}$. This effectively increases the electron work function ϕ_e :

$$\phi_{e,eff} = \phi_e + \frac{kT}{e} \ln A_{th}/A_{exp} \quad (3)$$

Replacing ϕ_e by $\phi_{e,eff}$ in Eqs. (2) and (3) of QRR 10, we find that γ_p increases still further and γ_a decreases accordingly, thus widening the gap between experimental and theoretical values.

b) Changes in the frequency of vibration ν of the absorbed particles or the number of absorption sites σ_f affect the magnitude of γ_a and γ_p in the same direction. An adjustment of these parameters can thus not fit both γ_a and γ_p to the experimental data.

c) It has been shown by Luke and Smith [Ref. 6] that the polarizability $\alpha = 5.5 \times 10^{-24} \text{ cm}^3$ of a cesium ion is effectively increased upon absorption:

$$\alpha_{eff} = \frac{2\alpha}{1 - \frac{2\alpha}{z_0^3}} = 18.7 \cdot 10^{-24} \text{ cm}^3 \quad (4)$$

where z_0 is of the order of 2 ion radii. These authors thus obtain a correction to the electron work function given by

$$\Delta\phi_{e1} = \frac{-8.75 \theta}{1 + 1.77 \theta^{3/2}} \quad (5)$$

Following Gyftopoulos and Levine [Ref. 1] we used instead

$$\Delta\phi_{e2} = \frac{-7.31 \theta G(\theta)}{1 + 1.22 \theta^{3/2}} \quad (6)$$

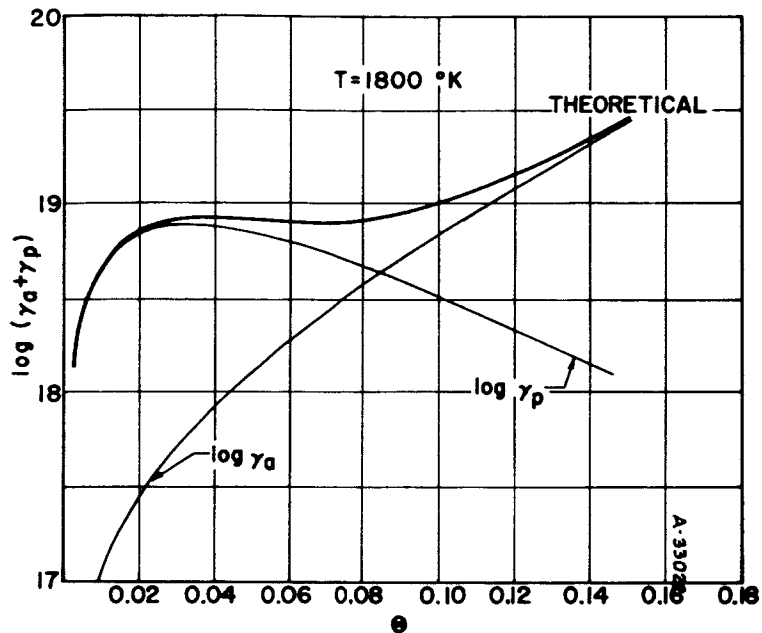
⁶K. P. Luke and J. E. Smith, NASA Technical Note D-2357, Lewis Research Center, Cleveland, Ohio, 1964.

For small θ the difference between Eq. (5) and (6) is roughly $\Delta\phi_{e1} - \Delta\phi_{e2} \sim -1.44 \theta$ which for $\theta = 0.1$ is equal to -0.144 volt = 1.97 kt/e at $T = 848^\circ\text{K}$. A comparison with Eqs. (1) and (2) shows that the polarization effect proposed by Luke and Smith would shift the theoretical values in the right direction and indeed overshoot the experimental data. Obviously the polarizability may be adjusted such as to yield a best fit of γ_p and γ_a to the experimental data. From a theoretical point of view this is not a very happy proposition and, pending further investigation, we shall continue to use the Theory of Gyftopoulos and Levine.

e) The "experimental" data shown in Fig. 32 have been obtained by Taylor and Langmuir through measurement of ion currents and subsequent extrapolation to zero electric field. It was assumed by these authors that the electric field at the cathode must vanish under conditions of thermal equilibrium. This is by no means obvious and a cathode sheath, associated with a finite electric field at the cathode, is indeed compatible with the conditions of thermal equilibrium. The existence of such a sheath in front of the emitter would in fact explain the ambiguity encountered by Taylor and Langmuir in their process of extrapolation.

The error introduced by this process may very well be of the order of 1 kt/e and thus explains the discrepancies observed in Eqs. (1) and (2).

The sheath effect just described is amenable to calculations within the frame work of the theory outlined in QRR No. 10 and we shall pursue this matter in the future. For the time being we use the theory of Gyftopoulos and Levine to obtain rates of atom and ion emission at $T = 1800^\circ\text{K}$ as shown in Fig. 33. It is in this temperature range that Breitwieser observed anomalous open-circuit voltages in cesium plasma diodes as described in QRR No. 7. It is seen from Fig. 33 that at these temperatures a slight increase in the total particle emission rate, $\gamma_a + \gamma_p$, strongly increase the coverage θ of the emitter surface with ions. With it goes a rapid increase in electron emission which, in turn, reduces the height of the potential maximum in front of the emitter. Less ions are thus fed back to the emitter and so θ decreases again. Calculations now in progress will show if this feedback mechanism does indeed give rise to oscillations and if these oscillations can explain the anomalous open-circuit voltages observed by Breitwieser.



32603

FIG. 33. ION (γ_p)-, ATOM (γ_a)-, AND PARTICLE ($\gamma_a + \gamma_p$)- EMISSION RATES IN $\text{CM}^{-2} \text{SEC}^{-1}$ VS THE FRACTION θ OF THE IONIC MONOLAYER COVERING A TUNGSTEN SURFACE AT 1800 °K.

—Theoretical values after Gyftopoulos and Levine

Project 0908: ION AND PLASMA BEAM SOURCES

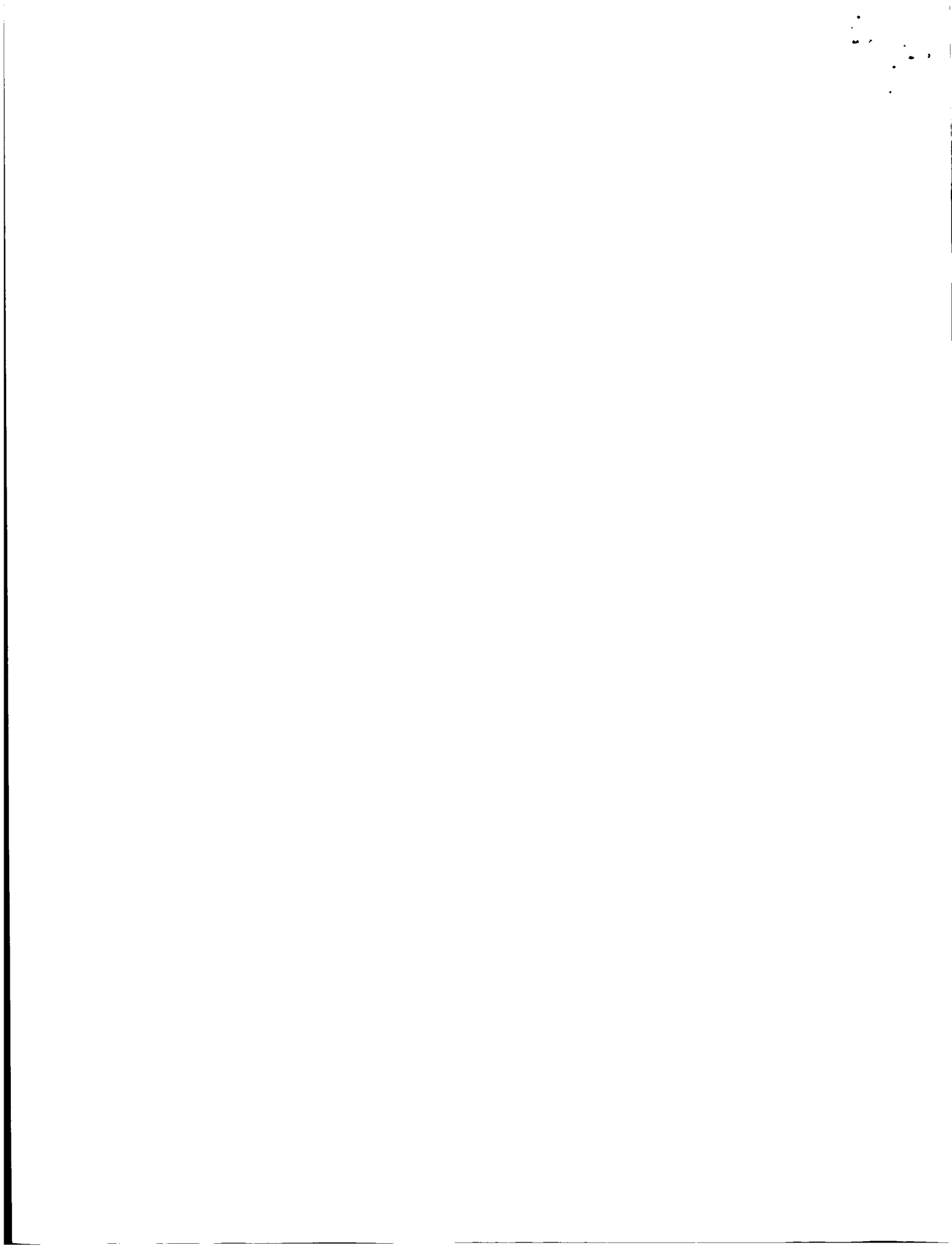
Air Force Contract AF33(657)-11144

Project Leader: R. P. Lagerstrom

Staff: J. Shiue

The purpose of this project is to produce ion and plasma beam sources suitable for high-vacuum plasma experiments. Thermionic emission of lithium ions from lithium-alumino-silicates such as spodumene and eucryptite has been under specific investigation.

A final report is in preparation.



Project 4651: PHYSICAL PRINCIPLES OF MAGNETIC ADAPTIVE COMPONENTS

Air Force Contract AF33(657)-11586

Project Leader: J. B. Angell

Staff: R. C. Woodbury

The purpose of this project is to study properties and basic operating mechanisms of square-loop magnetic materials suitable for use in magnetic adaptive components. Of particular interest is the 50 percent Ni-Fe grain-oriented material used by H. Crafts in his second-harmonic adaptive component.

To review briefly, the achievement of variable gain with memory stems from the correlation of magnetic remanence of the core with the second-harmonic content of the time-varying flux when driven with a small sinusoidal H field. Adaption from one second-harmonic amplitude level, or gain state, to another is achieved by the application of a dc field, which causes the gross flux level to change linearly with time. The latter is achieved only if the material has a relatively square hysteresis loop and strong eddy-current damping.

Major effort during the past quarter has centered on a final report covering the adaption mechanisms in 50 percent nickel-iron. In addition, the studies have uncovered the following information:

1. A theoretical analysis has been made of the generation of second harmonic in materials which do not possess residual domains to any appreciable extent. In such cases, a gross rotation of the magnetization is the principal contributor to small flux changes which result from small alternating fields. In both of the two situations considered, the alternating field is applied in the major magnetization direction or parallel to the sense direction. It is assumed in the first case considered that a small dispersion of the grain orientation exists relative to the major direction. When a gaussian distribution is also assumed, the resulting second-harmonic component in flux density response to a sinusoidal field is

$$B_{m2} = \frac{3}{2} B_s \sigma^2 \left(\frac{HM_s}{2K_a} \right)^2$$

σ is the standard deviation of the misalignment angle (radians) of the crystal grains and K_a is the anisotropy energy. An interesting side-light is that the above component represents about 15 percent of the measured second-harmonic signal from 50 percent nickel-iron.

In the second case it is assumed that a random orientation of the crystal grains exist but that the saturation magnetization of each grain lies in the nearest easy axis to the major magnetization direction. The resulting second-harmonic component of flux density response to the sinusoidal field is

$$B_{m2} = 0.17 B_s \left(\frac{HM}{2K_a} \right)^2$$

2. Further investigations of the mechanisms behind the anomalous hysteresis or so-called big step-little step ratio have also been made. Two separate effects are actually responsible for what has been commonly termed anomalous hysteresis.

The first effect is the creation of new switching walls upon reversal of the adaption or switching direction. The presence of new walls causes the rate of flux change to increase; hence the step size in a step-wise adaption characteristic will increase with the reversal in the direction of switching.

The second effect is the movement of existing walls in a potential well of asymmetrical shape. When the reversal in switching field occurs, the asymmetry of the well aids the movement of the wall over a characteristic distance, δ_A , which gives rise to a larger adaption rate immediately following the reversal in switching direction.

Project 4657: SELF-REPAIRING CIRCUIT TECHNIQUES

Air Force Contract AF33(657)-11586

Project Leader: J. B. Angell

Staff: J. S. Eggenberger*

The object of this project is to develop effective means of using digital magnetic memory arrays in which there are some defective storage elements.

*I.B.M. Resident Scholar

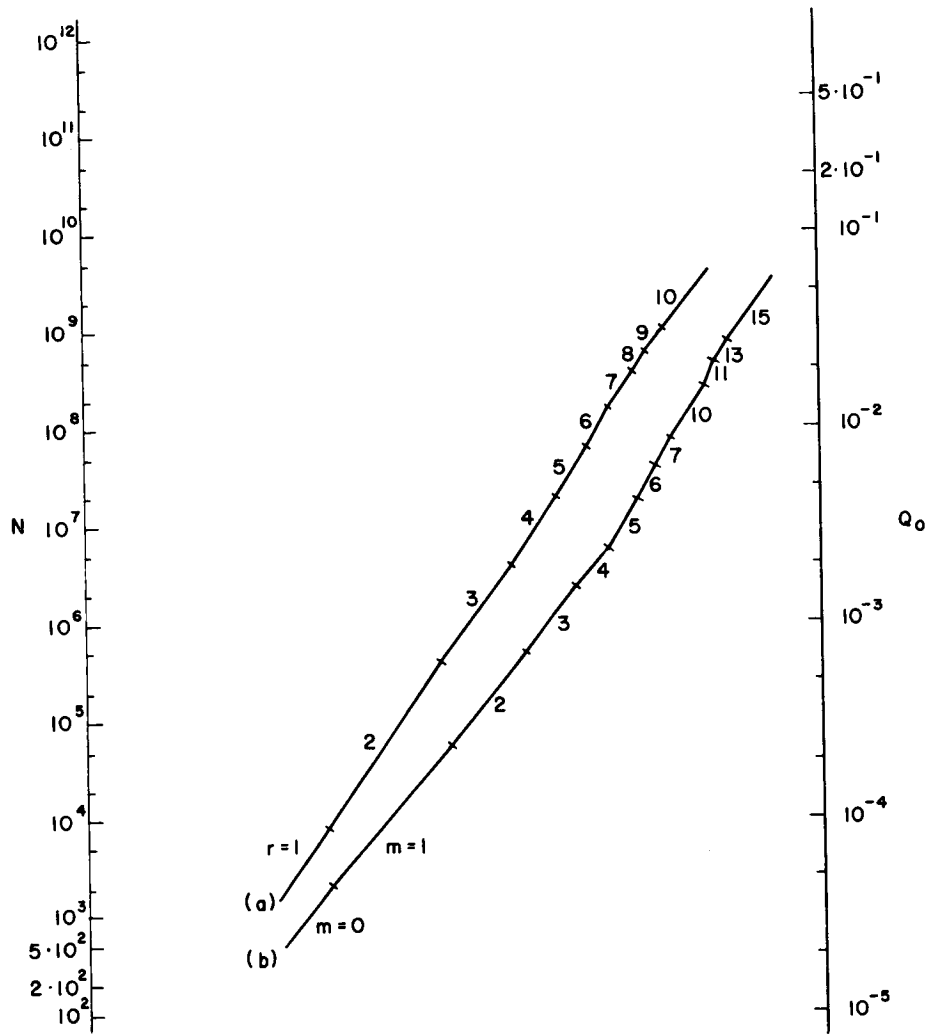
Three methods for accomplishing this goal have been considered. These are:

1. Error-correcting codes, including duplication and more complex codes.
2. Error detection, along with feedback to locate the defective elements.
3. Alternate location, wherein an alternate group of elements is substituted for any group containing a defective element.

For each method, there is an optimum redundancy. Too small a redundancy results in a large probability of an uncorrected error. In the case of an uncorrected error, the array must be discarded and the cost increases due to manufacturing shrinkage. Concise techniques have been evolved for determining the optimum redundancy and attendant array cost for each method.

As an example of the techniques evolved, Fig. 34 is a code selection nomograph for duplication and for the Bose-Chaudhuri $n = 63$ codes. The Bose-Chaudhuri codes have been used as examples in that they are good examples of efficient error-correcting codes. The left axis is the number of bits to be stored in the completed array, and the right axis is the defect probability for individual elements. A straight line connecting the number of bits to be stored with the element defect probability crosses the duplication curve (a) and the $n = 63$ curve (b). The region of curve (a) which this line crosses indicates the optimum number of times to repeat each bit, the region of curve (b) indicates the optimum number of errors to correct using the Bose-Chaudhuri $n = 63$ codes. Similar segmented lines can be constructed for other families of codes.

Several interesting points are apparent from Fig. 34. It is seen that if high redundancy is indicated, the element defect probability has much more influence on the choice of code than does the number of bits. Also, for high element defect probability and low array size, repetition can be more efficient than more complex codes. For example, consider an array of $2 \cdot 10^5$ bits, with an element defect probability of 0.05. Seven-fold duplication is optimum, for a redundancy of 7. However, in the $n = 63$ codes, the (63,7) code is optimum, for a redundancy of 9.



a. r-fold duplication

b. Bose-Chaudhuri code, $n = 63$, $m =$ error correcting

FIG. 34. CODE SELECTION NOMOGRAPH.

Similar techniques have been evolved for the error detection with feedback and alternate location methods. The analytic work on this project has been completed and a final report is in preparation.

Project 4715: TRANSIENT PERFORMANCE OF TRANSISTOR SWITCHES
UNDER HIGH LEVEL INJECTION

Tri-Service Contract Nonr-225(24)
Project Leader: J. F. Gibbons
Staff: P. Kamas

The purpose of this project is to study the transient behavior of transistor switches as they proceed from the OFF condition into the saturated condition.

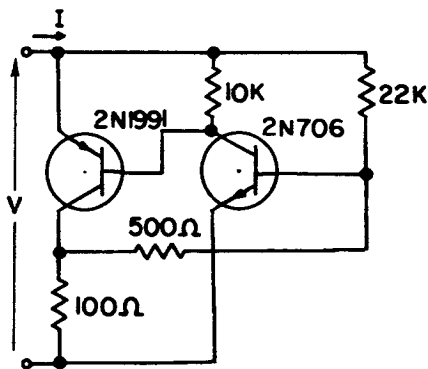
This project has been inactive this past quarter.

Project 4813: APPLICATION OF SOLID-STATE PHENOMENA TO
MICROSYSTEMS

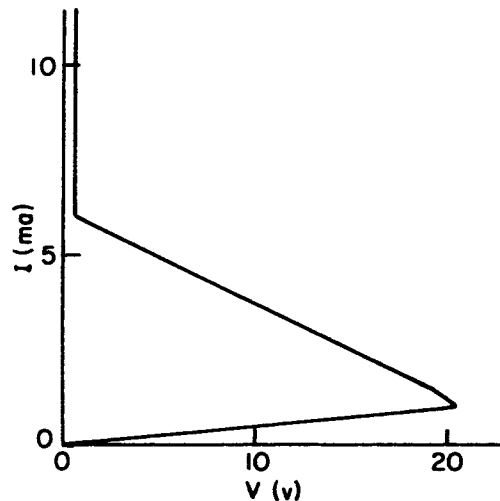
Office of Naval Research Contract Nonr-225(44)
Project Leader: J. G. Linvill
Staff: M. Nagata

The object of this project is to apply physical phenomena of solids to systems which must be small to perform their necessary function. Further, the intent is to establish suitable models of the phenomena useful to the application and to evaluate the limits of performance which are imposed by the properties of the solids used.

During the course of consideration of optical control of switches, a very simple two-transistor negative resistance circuit was obtained by M. Nagata. (Fig. 35.)



(a) NEGATIVE RESISTANCE CIRCUIT



(b) MEASURED V-I CHARACTERISTIC

33025

FIG. 35. NEGATIVE RESISTANCE CIRCUIT AND V-I CHARACTERISTIC.

The circuit has a number of interesting properties. No internal batteries are required. The characteristics are very insensitive to changes in transistors. The linearity of the negative resistance characteristic is surprisingly good. The break points depend upon stable quantities.

A report describing the properties in detail, giving measurements and outlining possible applications is in preparation.

Project 4818: APPLICATIONS OF ELECTRO-OPTICAL PHENOMENA IN SOLIDS

Office of Naval Research Contract Nonr-225(31)
Project Leader: J. G. Linvill
Staff: J. W. Hill

The purpose of this project is to evaluate the presently available photo-optical solid-state components and to find ways of interconnecting these components to construct a set of static and dynamic logic circuits. "Circuits" in this case include optical connections, the close proximity of photon emitting and detecting units, and also longer range optic fiber coupling. Conventional electrical circuit connections are used as well.

Work on this project is absorbed into Task 4820 and 4821. This project is closed with this period. Mr. Hill is presently working on Project 4819.

NEW PROJECT

Project 4819: TACTUAL COMMUNICATION

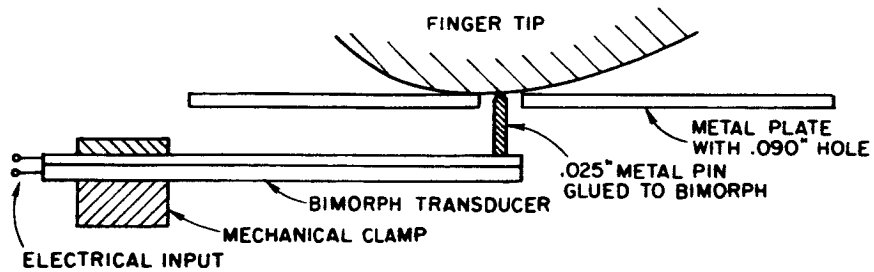
Office of Naval Research Contract Nonr-225(44)
Project Leader: J. G. Linvill
Staff: J. W. Hill

The purpose of this project is to investigate the principles of tactual communication and to evaluate the implementation of such communication using solid-state phenomena and devices.

Earlier work under the contract supporting this project dealt with a piezoelectric dynamic embosser. A technical report* describing this work in detail is presently available.

*G. J. Alonzo, "Development of a Piezoelectric Dynamic Embosser for Use as a Reading Machine," Stanford Electronics Laboratories, Technical Report 4813-4, March 1964.

In the problem of designing a transducer to apply a vibratory signal to the human finger tip, the mechanical impedance that the skin represents to the transducer is an essential variable. This quarter quantitative measurements have been made to determine this impedance. The physical arrangement of the bimorph transducer and finger is shown in Fig. 36. The results obtained using this apparatus are shown in Fig. 37 a and b.



33026

FIG. 36. THE PHYSICAL MEASURING SET UP.

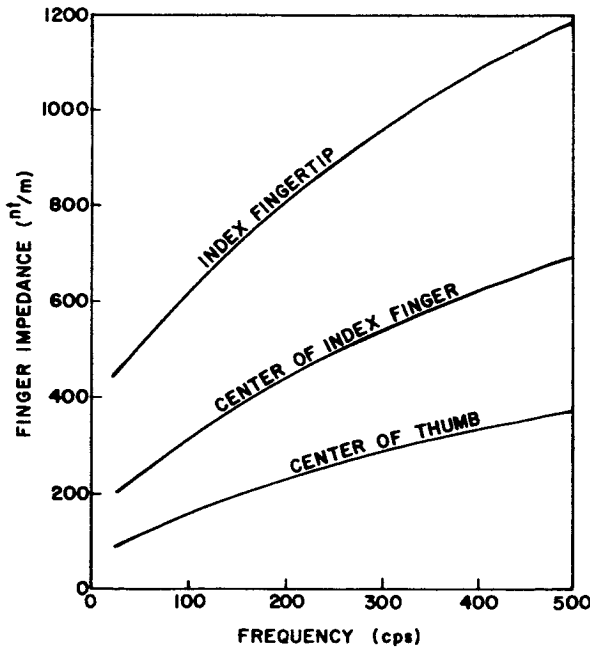


FIG. 37a. MAGNITUDE OF SKIN IMPEDANCE.

33027

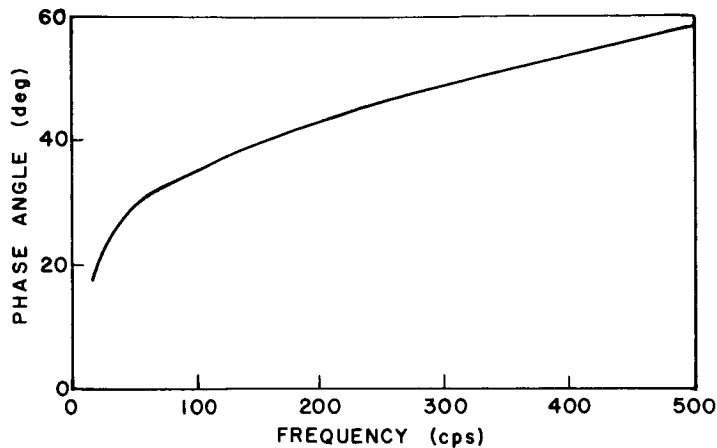


FIG. 37b. PHASE ANGLE OF SKIN IMPEDANCE.

33028

As is readily apparent from these graphs taken from different parts of one person's finger there is a wide range of impedances depending on the part of the finger measured. There is also an additional ± 50 -percent variation in the same measurements made on different people. Thus, we can only place the impedance of the human fingertip in a range of impedances whose limits are more than an order of two apart.

A report on the detailed methods used to calculate this impedance is in preparation.

NEW PROJECT

Project 4820: LIGHT DETECTION AND AMPLIFICATION IN SEMICONDUCTORS

Office of Naval Research Contract Nonr-225(31)

Project Leader: J. G. Linvill

Staff: H. W. Ruegg

The purpose of this project is to study means of achieving fast, high-gain light detection with semiconductor structures.

A. CONVENTIONAL SEMICONDUCTOR JUNCTION DETECTORS

During this quarter the performance of conventional semiconductor devices as photodetectors was investigated. Specifically, the dependence of operating speed on device parameters, the required power gain and photon flux density were calculated for the photodiode, the phototransistor and the field-effect transistor used as light activated switches.

The switching time of a photodiode was found to be proportional to the required power gain and inversely proportional to the incident photon-flux density.

The switching time of a phototransistor can be approximated by the sum of the charging time of the collector-base capacitance and the rise time of the "intrinsic transistor." The charging time of the collector-base capacitance is approximately proportional to the voltage gain and inversely proportional to the photon flux density. The rise time on the other hand is approximately proportional to the current gain. It is therefore possible to achieve a minimum switching time for given device parameters by optimizing the current gain and voltage gain contribution to the required power gain.

A field-effect transistor can also be operated as a light detecting-amplifying device. The switching time again is proportional to the required power gain, but was shown to be, to a first order approximation, independent of the incident photon-flux density.

In order to estimate the capabilities of these three detecting-amplifying devices, their performance in optoelectronic logic building blocks as drivers of injection luminescent diodes was investigated theoretically [Ref. 1]. The power gain required from the detecting-amplifying devices in this case is equal to the fan-out of the logic circuit divided by the overall quantum efficiency associated with photon generation and light transport.

Assuming reasonably optimistic state-of-the-art parameter values for silicon devices, the propagation delays through opto-electronic logic blocks were calculated for different gain requirements and different power consumptions. In Fig. 38 the estimated propagation delays for a photodiode (2), a phototransistor (4) and a field-effect transistor (5), are plotted vs power consumption per simple logic function (NOR, NAND), for an overall quantum efficiency of 1 percent and a fan-out of 5. Also

¹H. Ruegg, "The Gain Element in Optoelectronic Logic Building Blocks,"* Technical Report No. 4820-1, Stanford Electronics Laboratories, Nov 1964.

*Paper presented at the Symposium on Optical and Electro-Optical Information Processing Technology, Boston, Nov 9-10, 1964. Also published as TR No. 4820-1.

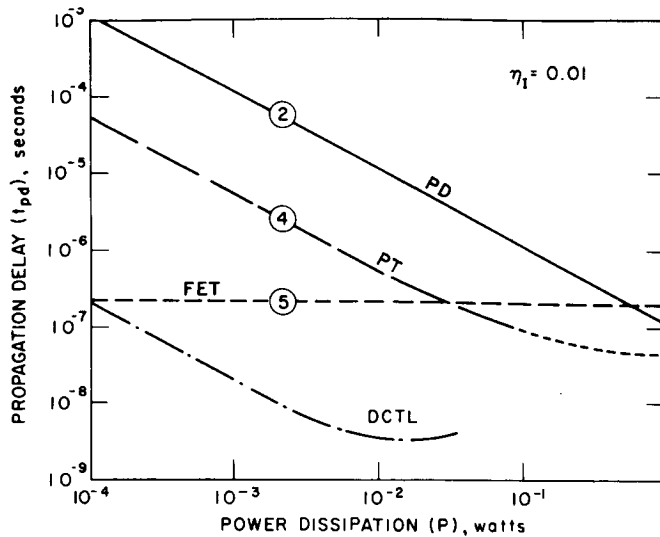


FIG. 38. ESTIMATED PROPAGATION DELAY FOR THREE "STATE-OF-THE-ART" OPTOELECTRONIC LOGIC BUILDING BLOCKS VS POWER DISSIPATION.

included in Fig. 38 is the power vs delay curve for conventional direct coupled logic (DCTL) obtained with 2N709 transistors. It is seen that, with present-day quantum efficiencies, the optoelectronic systems considered are by at least two orders of magnitude slower than an all electronic system operating at the same power level.

The only two possibilities to improve the situation are to either increase the overall quantum efficiency considerably or else to find a much faster detecting-amplifying device. We have chosen to explore the second possibility.

B. CARRIER MULTIPLICATION BY SECONDARY IONIZATION

Secondary ionization of carriers in a high-field region is an inherently fast gain mechanism which might conceivably be utilized to increase the external quantum efficiency of a semiconductor junction detector. The following two possibilities are presently being considered:

1. Linear amplification can be obtained by biasing a junction detector close to breakdown and thus achieving a carrier multiplication factor which is high but finite. The practical difficulty is the very steep

increase of the multiplication factor from essentially 1 to infinity over a voltage range of a few percents of the breakdown voltage of the junction. However, recent measurements on silicon [Ref. 2] indicate that for small fields the ionization coefficient for holes is by orders of magnitude smaller than the ionization coefficient for electrons. A rather gradual increase of the multiplication factor with applied voltage should therefore result for wide junctions if care is taken that only electrons are injected into the depletion region. The effect might be enhanced by a field distribution in the depletion layer which favors the ionization by electrons.

2. A nonlinear threshold type amplification might be achieved by increasing the multiplication factor in a junction from a finite value to infinity. (Light-triggering avalanche breakdown.) Such an increase of the multiplication factor can be achieved by changing the field configuration in the junction. For a constant applied voltage the field configuration can be influenced by changing the space charge in the multiplying junction or in a region which is in electrical contact with this junction. The light generated carriers themselves might directly cause the additional space charge or else they might only be the agents to change the charge state of traps.

Project 5002: HIGH-FIELD TRANSPORT PROBLEM

National Science Foundation Contract NSF-GP 1033

Project Leader: G. L. Pearson

Staff: C. Y. Duh

This project is concerned with the theoretical studies of high-field transport properties in n-type semiconductors.

The integral equation which governs the function of the appearing rates per unit energy range has been previously derived as

$$S(E'') = \int_{E=0}^{\infty} K(E'', E', \vec{\epsilon}) S(E) dE \quad (1)$$

where

$$K(E'', E', \vec{\epsilon}) = \int_{E'=0}^{\infty} M(E'', E') A(E', E, \vec{\epsilon}) dE'$$

²C.A. Lee, et al, "Ionization Rates of Holes and Electrons in Silicon," Phys. Rev., 134, p. A761 (May 1964).

The physical significances of the symbols were given in last quarter's report. For the zero field case, $\vec{\epsilon} = 0$, solution Eq. (1) will result in the Maxwellian distribution of carriers.

In the presence of electric field, the solution of Eq. (1) becomes extremely difficult. Analytic solution of $S(E)$, the rate of appearance at energy E , has been attempted without success. The main difficulty lies in the area of proper construction of the kernel $K(E'', E', \vec{\epsilon})$. For most general cases with least assumption, it is almost impossible to construct the kernel $K(E'', E', \vec{\epsilon})$. Even under certain simplified assumptions that constant mean free path is assumed to characterize the scattering processes, and the δ -function approximation is used for the emission and absorption processes, it is still unable to achieve the analytic solution of $S(E)$ from Eq. (1).

An experiment which utilizes the $n^+ - n - p^+$ or $n^+ - p - p^+$ structure to measure the maximum drift velocity of the hot carriers has been considered. Plans during the next quarter will be directed toward the manufacturing of the structure appropriate for our experimental purposes. Photo-mask techniques will be employed.

Project 5059: HOT ELECTRONS IN THIN METAL FILMS

Air Force Contract AF33(657)-11586
Project Leader: J. L. Moll
Staff: P. H. Bardell

This project is concerned with experimental and theoretical studies of high-energy electrons in thin metal films.

The final report on this project by P. H. Bardell, Jr., entitled "Hot-Electron Transport in Thin Copper Films," dated August 1964, is in process of publication. Upon its distribution, this project will be closed.

Project 5101: DIFFUSION OF IMPURITIES IN III-V COMPOUND SEMICONDUCTORS

Office of Ordnance Research Grant DA 31-124 ARO(D)-155
Project Leader: G. L. Pearson
Staff: M. G. Buehler

The object of this project is to study the diffusion coefficients, solubilities, and distribution coefficients of II, IV, and VI column

impurities in III-V compound semiconductors. To study the solubility of Zn in InAs, the ratio of the electrically free carrier density to the Zn density is desired. The Zn density is known from radio tracer analysis of Zn^{65} . The electrically free carrier density is given by the Hall coefficient. This report presents the details for measuring the Hall coefficient using a square array of point contacts centered on a thin homogeneous sample

The geometrical arrangement is shown in Fig. 39. The problem has two boundary conditions: current must be parallel to the sample edge and the

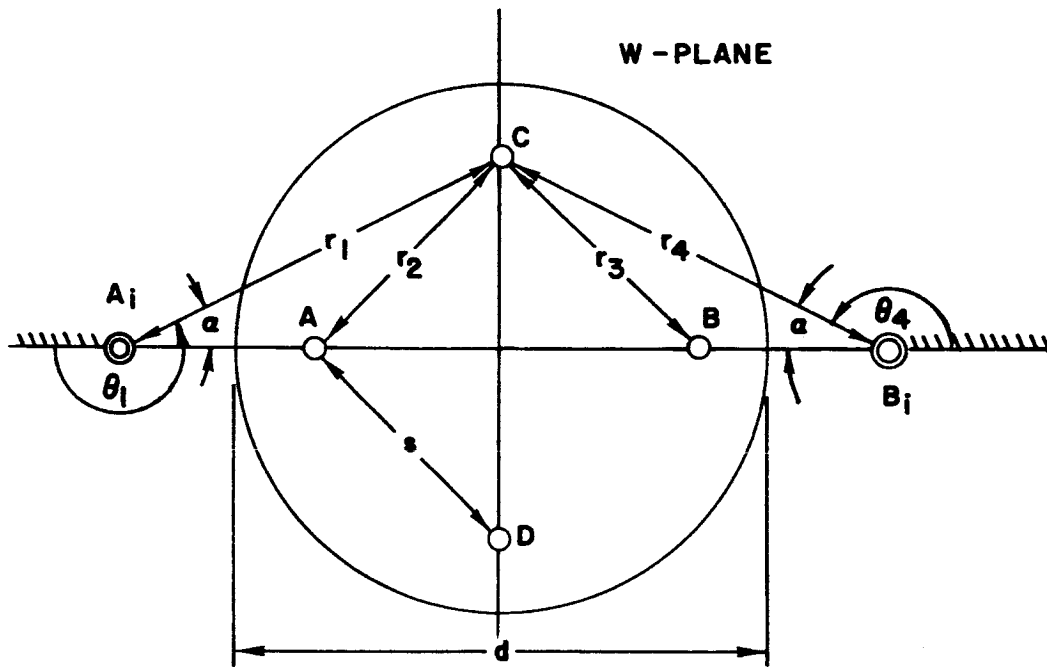


FIG. 39. ILLUSTRATION OF HALL COEFFICIENT MEASUREMENT USING A SQUARE ARRAY OF POINTS CENTERED ON A THIN CIRCULAR SAMPLE. Current sources are A and A_i - sinks are B and B_i . Hall voltage is measured between C and D. The magnetic field is perpendicular to page.

surface integral of the current density about a source point must give the current enclosed. A two-dimensional problem has been assumed where the thickness of the sample w is much less than the probe spacing s .

The current density of a point discharging to infinity then has cylindrical symmetry given by $J = 1/2\pi rw$ where r is the radial distance from the point. To satisfy the boundary condition of current flow parallel to a boundary, image points are located at A_i and B_i . To locate these points the problem is transformed from the unit circle of the W -plane to the right-half Z -plane. The bilinear transformation $W = (Z - 1)/(Z + 1)$, $Z = (1 + W)/(1 - W)$ is used.

The equations for current flow in a magnetic field are given by Barron and MacDonald [Ref. 1]. For a thin isotropic conductor in a perpendicular magnetic field B , the conduction charges are acted upon by the electric field E and the Lorentz force. If the net Lorentz force acts perpendicular to both J and B then

$$\bar{J} = \sigma(B) \bar{E} + \sigma(B) R(H) \bar{J} \times \bar{B} \quad (1)$$

where $\sigma(B)$ is the conductivity and $R(H)$ the Hall coefficient. For steady state

$$\bar{\nabla} \bar{J} = 0, \quad \bar{\nabla} \times \bar{E} = 0. \quad (2)$$

From Eq. (2), $\bar{E} = -\bar{\nabla}\phi$ which leads in two dimensions to Laplace's equation $\nabla^2\phi = 0$.

The solution is a matter of matching boundary conditions in accordance with the current flow given by Eq. (1). In Fig. 40 current points A and A_i have been transformed into the Z -plane using the bilinear transformation. Point A is seen to be a Corbino current source with a radial electric field and current paths that are logarithmic spirals. A boundary condition in the Z -plane is that no net current may cross the vertical axis. To satisfy this boundary condition an image point A_i is created whose current paths are image logarithmic spirals. The electric field for the image point A_i is found from Eq. (1), and the potential is found from $\bar{E} = -\bar{\nabla}\phi$.

¹T. H. K. Barron and D. K. C. MacDonald, Physica, 24, S102 (1958).

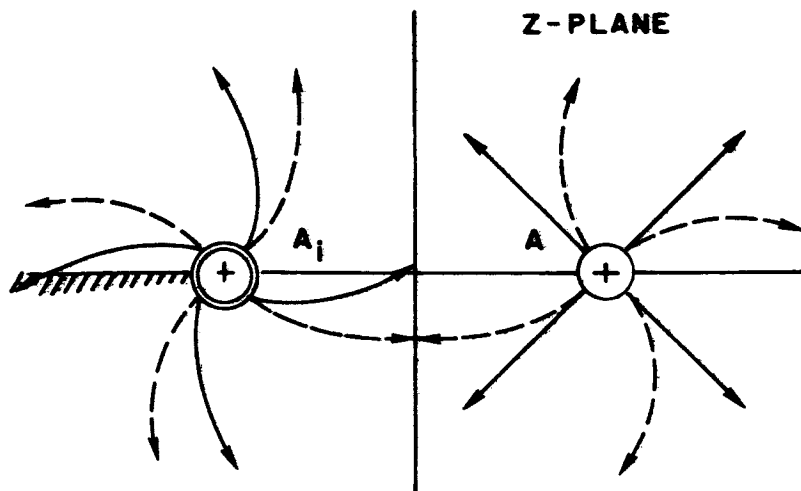


FIG. 40. BOUNDARY CONDITION IS SATISFIED ALONG VERTICAL AXIS BY ADJUSTING THE CURRENTS (DASHED LINES) FROM A_i TO IMAGE THOSE FROM A . Solid lines represent electric field from sources.

The potentials for the sources shown in Fig. 39 are

$$\varphi_{A_i} = K_1 \ln r_1 + K'_1 \theta_1$$

$$\varphi_A = K_2 \ln r_2$$

$$\varphi_B = -K_2 \ln r_3$$

$$\varphi_{B_i} = -K_1 \ln r_4 - K'_1 \theta_4$$

where K_1 , K'_1 , and K_2 are constants. The potentials φ_{A_i} and φ_{B_i} are multivalued; hence, a cut is made in the W -plane extending from $-\infty$ to A_i and B_i to ∞ . The angles θ_1 and θ_4 are then measured in the counter-clockwise sense from the cut.

The potential difference between C and D, V_H , may now be computed and it is seen that along the vertical axis all potentials cancel except the angular-dependent part of φ_{A_i} and φ_{B_i} .

$$V_H = 2 K_1' [(\pi + \alpha) - (\pi - \alpha)] \quad (4)$$

It can be shown that

$$K_1' = \frac{R_H BI}{\pi W} \quad (5)$$

so that the Hall coefficient is

$$R_H = \frac{V_H W}{IB} \frac{\pi}{4\alpha} \quad (6)$$

It can also be shown that the position of the image point A_i related to the probe spacing s and diameter d is such that

$$\tan \alpha = \frac{2s^2}{d^2} \quad (7)$$

Combining Eq. (6) and (7), we obtain

$$R_H = \frac{V_H W}{IB} \cdot \frac{\pi}{4 \arctan \left(\frac{2s^2}{d^2} \right)} \quad (8)$$

A correction factor is now defined as follows:

$$C_H = \frac{\pi}{4 \arctan \left(\frac{2s^2}{d^2} \right)} \quad (9)$$

Equation (9) was verified experimentally using 0.12 ohm-centimeter, n-type Ge at room temperature. First, a large sample, 0.750" in diameter and 0.010" thick, was measured in a magnetic field to 10^4 gauss. Two smaller samples were then cut from this large disk. Probe spacing was 0.106". The smallest sample, 0.200" diameter, was measured using the van der Pauw technique [Ref. 2] with contacts on the periphery. Experimental correction factors were then calculated by comparing the van der Pauw measurement to the square-array measurement.

A recently published analysis by Lange [Ref. 3] using the image current sources with radial current paths undisturbed by the magnetic field leads to:

$$C'_H = 2\pi / [\pi + 4 \arctan (2s^2/d^2)] \quad (10)$$

for the same geometry.

A comparison between Eqs. (9) and (10) and experiment is shown in Fig. 41. It is seen that the new theory, as given by Eq. (9), follows the experimental data points. For $d/s > 5$, the correction factor is approximated by:

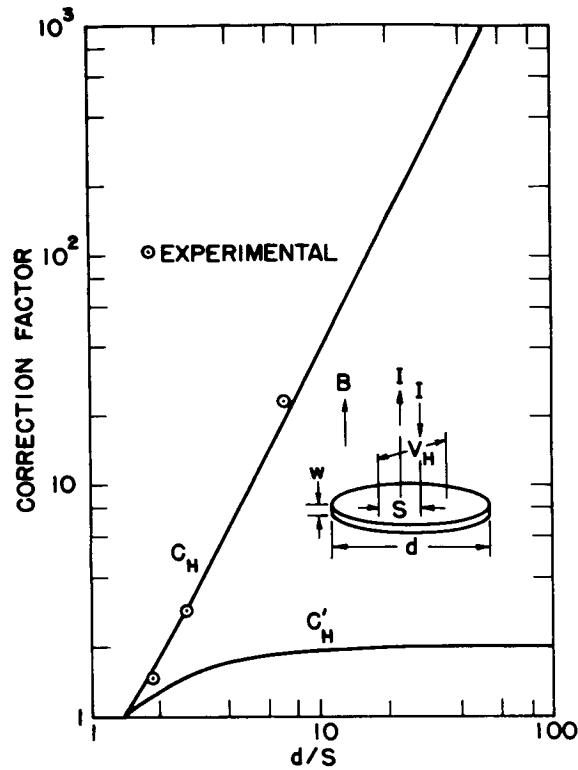
$$C_H = \frac{\pi}{8} \left(\frac{d}{s}\right)^2 = 0.393 \left(\frac{d}{s}\right)^2 \quad (11)$$

As d/s approaches infinity, C_H becomes infinite, and according to the new theory, the Hall potential approaches zero. In contrast, the old theory, as given by Eq. (10), predicts a value of 2 for C'_H as d/s approaches infinity, so that the Hall potential reaches the non-zero value of $R_H IB/2W$. This shows clearly the necessity for modifying the current-flow patterns by the magnetic field when d/s is greater than 1.414.

It is planned to extend the analysis either experimentally or, if possible, analytically to cover the case where the sample thickness is

²L. J. van der Pauw, Phillips Tech. Rev., 20, 220 (1959).

³J. Lange, J. Appl. Phys., 35, 2659 (1964).



d/S	$\sqrt{2}$	1.5	2.0	2.5	3.0	4.0	
C_H	1.000	1.081	1.694	2.535	3.590	6.316	
d/S	5.0	7.5	10.0	15.0	20.0	40.0	∞
C_H	9.836	22.06	39.30	88.34	156.9	628.3	∞

32235

FIG. 41. HALL-EFFECT CORRECTION FACTORS USING A SQUARE ARRAY OF POINTS CENTERED ON A THIN CIRCULAR SAMPLE. The new theory is given by C'_H , the old theory by C_H .

comparable to and larger than the probe spacing. Such information is desired to determine when the thin-sample approximation is no longer valid.

The material presented in this report has been published in part in the literature [Ref. 4].

⁴M. G. Buehler, W. Shockley and G. L. Pearson, Appl. Phys. Letters, 5, 228 (1964).

Project 5103: ANOMALOUS DIFFUSION IN COMPOUND SEMICONDUCTORS

Office of Ordnance Research DA 31-124 ARO-D-155
Project Leader: G. L. Pearson
Staff: R. Mehta

The purpose of this project is to make a theoretical study of various parameters leading to anomalous diffusion characteristics of impurities into compound semiconductors.

Technical Report No. 5103-1 by Rajendra Mehta has been published. The project is now closed.

Project 5107: PROPERTIES OF GaAs P-N JUNCTIONS

Tri-Service Contract Nonr-225(24)
Project Leader: G. L. Pearson
Staff: D. J. Dumin

This project is concerned with the study of some of the properties of GaAs diodes. The temperature-dependent properties of the forward and reverse currents are being studied. Other diode properties will be incorporated into these studies as time progresses.

Technical Report No. 5107-1 by David J. Dumin has been published. The project is now closed.

Project 5108: A STUDY OF GaAs $P_x 1-x$.

National Aeronautics and Space Administration
Grant NsG-555
Project Leader: Gerald L. Pearson
Staff: Yen-sun Chen

The object of this project is to evaluate the optical, electrical and metallurgical properties of the GaAs $P_x 1-x$ alloy. Among evaluations of particular interest to us are the investigation of the crystal structure and its imperfections by the Kossel-line technique and by that of the lattice absorption spectra as the mole fraction of GaAs, x , varies from 0 to 1.

Due to the efforts in this quarter, we are now able to grow single crystal of GaAs $P_x 1-x$ over the whole composition range; and these crystals are very free of the free carrier absorption in the long wavelength region to make our measurement of the lattice absorption spectra possible. The following is a summary of the work performed in this quarter.

A. CRYSTAL GROWTH

The method of open-tube epitaxial vapor growth [Ref. 1] is now under full control to supply us the samples needed in this project. Of the twelve runs made during this period, the last seven yielded good single crystals with composition ranging from 30 percent P to pure GaP. The details of these runs are presented in Table 1.

TABLE 1. CRYSTAL GROWTH DATA

Run No.		No. 19	No. 20	No. 21	No. 23	No. 24	No. 25	
Substrate (GaAs)	Temp.	820	820	820	805	805	805	
	Temp. Grad. °C/cm	16	16	16	16	16	16	
	Orientation	(111), (111)	(111), (111)	(111)	(111)	(111)	(111)	
	Angle Against Flow	0°	0°	30°	30°	30°	30°	
Flow of H ₂	By pass cc/min	54	54	90	48	38	31	
	PCl ₃ * cc/min	41	25	28	24	15	7	
	AsCl ₃ ** cc/min	22	48	34	48	67	82	
Composition calculated from flow rates		%P	85	60	70	60	40	20
Growth time		hrs	6	8	8	5.75	6	6
Epitaxial layer	thickness (111) μ	150-300	400	600	425	425	425	
	(111) μ	75	100					
	growth (111) μ/min	.4-.8	.8	1.25	1.25	1.2	1.2	
	rate (111) μ/min	.2	.2					
Lattice constant		Å	5.481	5.520	5.500	5.515	5.556	5.582
Composition		%P	85	65.5	72	67.5	48	35
Energy Gap (for α = 10 cm ⁻¹ , 300 °K)		eV	2.13	2.02	2.07	2.05	1.88	1.72
Free Carrier Absorption			none	some	none	none	none	none

Temperature of Ga source is at 950 °C; Run No. 22 is pure GaP, made by Loescher.

* at 0 °C

** at 25 °C

The general remarks are given as follows:

1. The substrates used are GaAs, (111) oriented. To obtain uniform deposition over the entire surface, we found the best arrangement is to have the substrate inclined at an angle of 30° with respect to the direction of flow.

2. The epitaxial growth on (111) surface of GaAs is not only smoother but also faster than that on (111). The opposite was reported by Prehn

¹ See SEL Quarterly Research Review No. 10 on this project.

and Gibbons [Ref. 2] in their experiments. These can best be appreciated by the pictures presented in Fig. 42a, 42b, and 42c. The two epitaxial layers are grown in one single run with the substrate standing parallel to the flow so both surfaces are exposed at the same time and under the same growth conditions.

3. We were able to grow crystals of a rather wide range of composition at fixed temperature merely by adjusting the flow rates of H_2 through PCl_3 and $AsCl_3$ bubblers. This greatly increased the reproducibility of the process. In [Ref. 2], it was reported the composition of the alloy is extremely temperature-sensitive, which seems to be contrary to the result of our experiment.

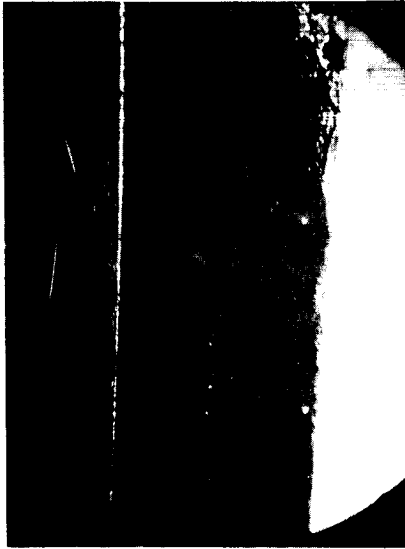
4. It is found that, to remove the epitaxial layer from the substrate, the best etchant is two parts $HNO_3:HF(9:1)$ and one part H_2O . This etchant etches only GaAs but not the alloy up through 65 percent As.

5. The lattice constant, hence the composition, is determined by X-ray diffraction. A powdered sample of a mixture of the alloy and Si is used. The (531) peak of the $GaAs_xP_{1-x}$ alloy is generally situated between the (531) and the (440) peaks of Si. With Cu $K\alpha$ radiation and the peaks of Si as references, an accuracy of 2×10^{-4} in the value of lattice constant is possible; the equivalent accuracy in composition is .5 percent. Figure 43 is a typical example of the measurement.

B. BAND EDGE ABSORPTION

These crystals have very sharp band edge absorption, which is comparable to those of GaP and GaAs. The main factor against using the polycrystals grown in this same system last quarter to evaluate the lattice vibration bands is that we have observed very poor band edge absorption from the transmission data. In Fig. 44, the percent transmission data of a single crystal and a polycrystal grown simultaneously in Run No. 19 are shown; notice that the polycrystal displays not only much poorer band edge absorption but also less total transmission.

²J. Gibbons and P. Prehn, "Epitaxial Vapor Growth of III-V Compounds," Technical Report No. 4711-1, Stanford Electronics Laboratories, Stanford, Calif., Oct 1963.



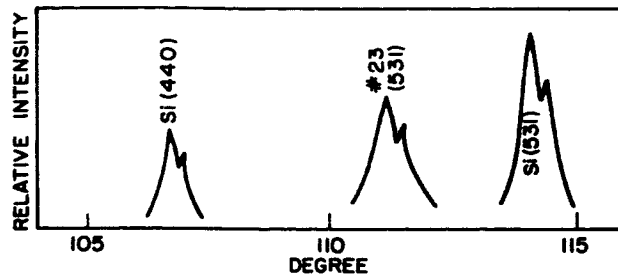
a. Thickness of epi. layers;
left, on GaAs ($\bar{1}\bar{1}\bar{1}$) sur-
face and right, on (111).

b. Crystal grown on (111)
surface of GaAs.



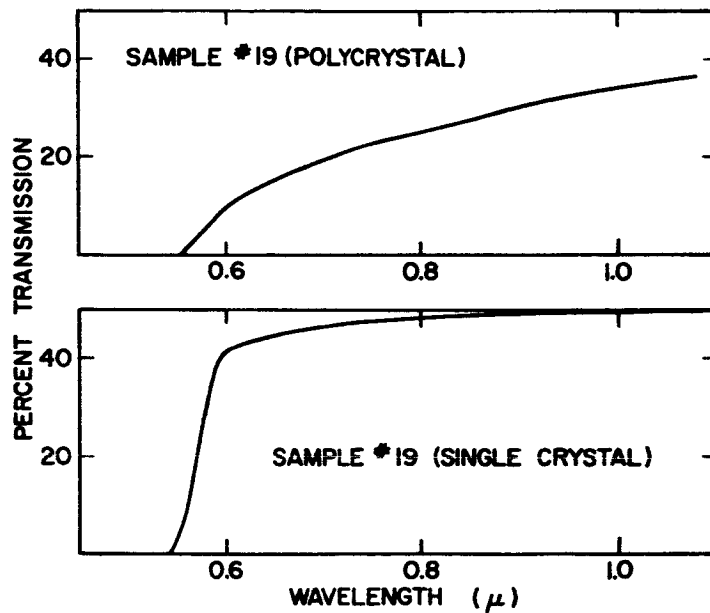
c. Crystal grown on ($\bar{1}\bar{1}\bar{1}$)
surface of GaAs.

FIG. 42. APPEARANCE OF SAMPLE NO. 20 AFTER
GROWTH (ALL 50 \times).



32955

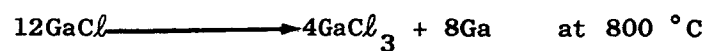
FIG. 43. X-RAY DIFFRACTION PATTERN OF
 POWDERED SAMPLE OF $\text{SiGaAsP}_{x^{1-x}}$.
 ($a_0 = 5.515 \text{ \AA}$)



32956

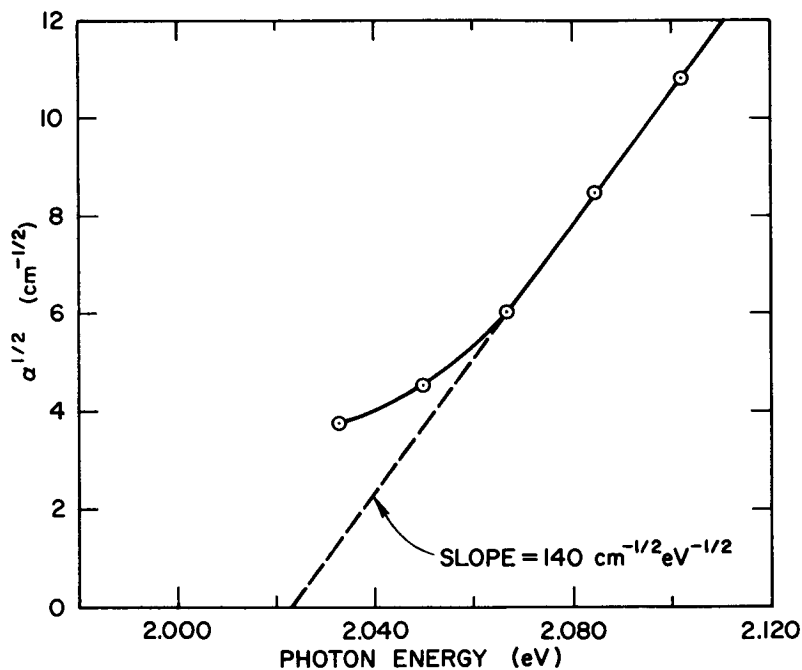
FIG. 44. COMPARISON OF TRANSMISSION DATA NEAR
 BAND EDGE.

At the growth zone, there exist excess Ga atoms; this can be demonstrated by the reactions proposed in Ref. 2:



Thus if no seed is provided in the growth zone, small grains of crystals are grown to form polycrystal leaving room in between grains to catch excess Ga atoms. We believe this is why we have observed such low overall transmission as well as the poor band edge absorption. However, it is possible to detect the combination phonon bands in these polycrystals. This, we believe, is due to the fact that the wavelength of the combination phonons is very small; thus although the crystal is "contaminated" by excess Ga atoms, the grain is still large enough to support the vibration modes.

A typical band edge absorption is presented in Fig. 45 where $\alpha^{1/2}$ is plotted against the photon energy. The slope of this line is comparable to that of GaP reported by Eden [Ref. 3].



32957

FIG. 45. $\alpha^{1/2}$ VS PHOTON ENERGY AT BAND EDGE OF SAMPLE NO. 23.

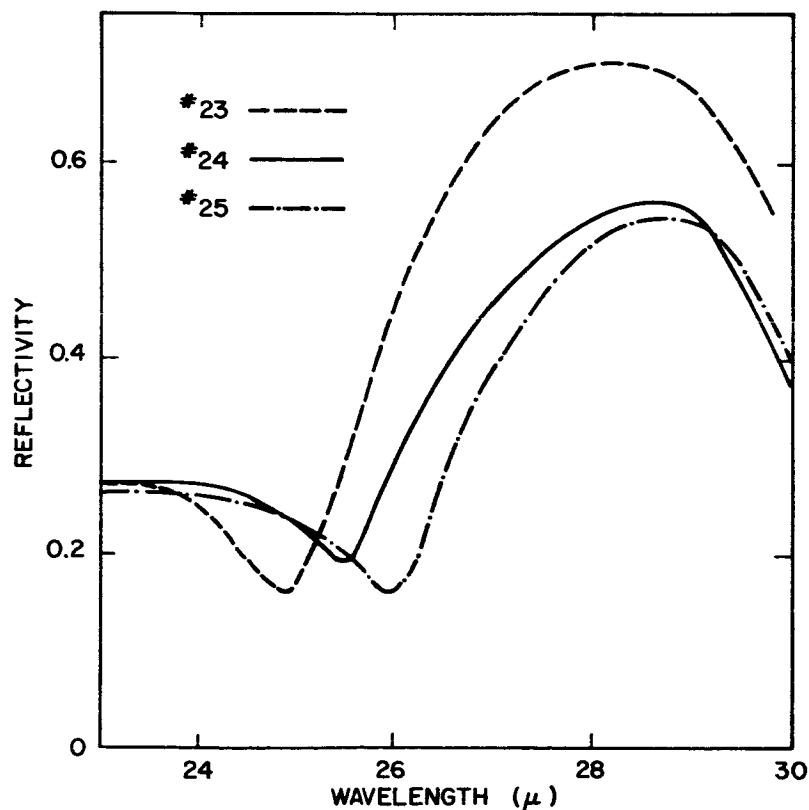
³R. Eden, "Band Structure of Gallium Phosphide," SEL Quarterly Research Review No. 9.

C. LATTICE ABSORPTION SPECTRA

It is purposefully arranged that the crystals we grew should have composition values rather widely separated. The purpose is twofold: 1) to learn the growth process, and 2) most importantly, to have a general understanding of the variation of the lattice absorption spectra over the entire composition range. These crystals were subject to the measurements of the combination bands as well as the restrahlen band. The experimental procedures were described in our previous reports. The results are given below.

1. Restrahlen Band

In Fig. 46, we have plotted the reflectivity vs wavelength in the region of 20μ to 35μ of Sample No. 23, No. 24, and No. 25. The result



32958

FIG. 46. RESTRAHLEN BANDS.

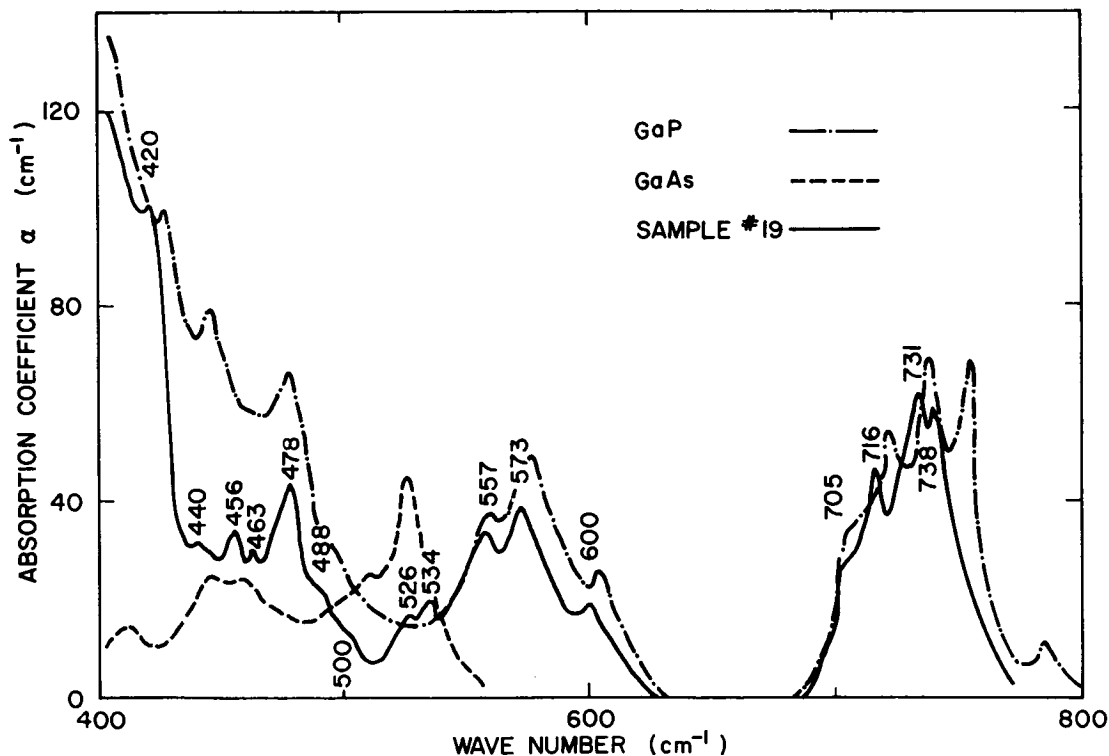
fits very well into our recent data [Ref. 1]. The values of reflectivity just above the restrahlen band are used to help determine the absorption coefficients of the combination bands of various samples.

2. Combination Bands

The absorption coefficient vs wave number in the region of 400 cm^{-1} to 800 cm^{-1} of Sample No. 19, No. 23, No. 24, and No. 25 are given in Figs. 47, 48, 49, and 50 respectively. In each of these figures, the lattice absorption spectra of GaP and GaAs are also given as references. The absorption coefficient α is determined from

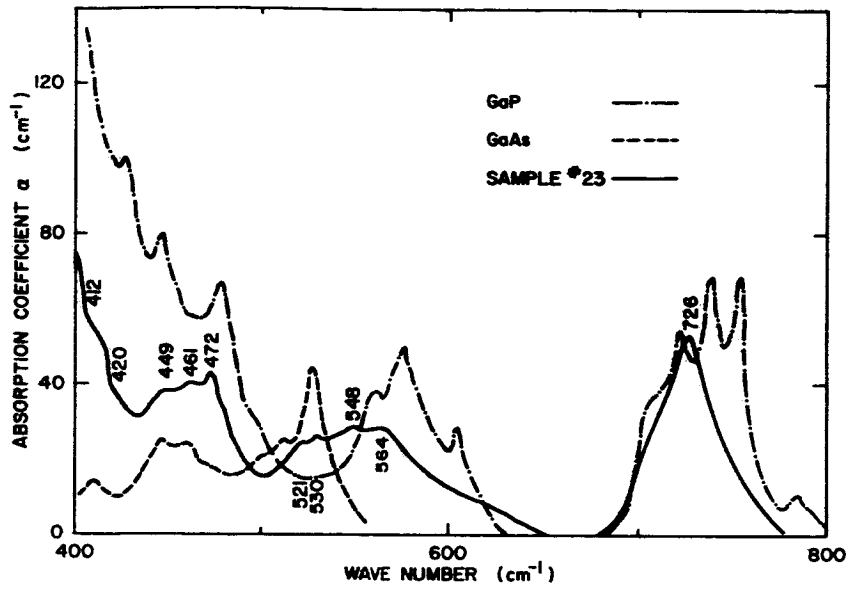
$$T = \frac{(1 - R)^2 e^{-\alpha y}}{(1 - R)^2 e^{-2\alpha y}}$$

where T is the transmission, R is the reflectivity and y is the thickness of the sample.



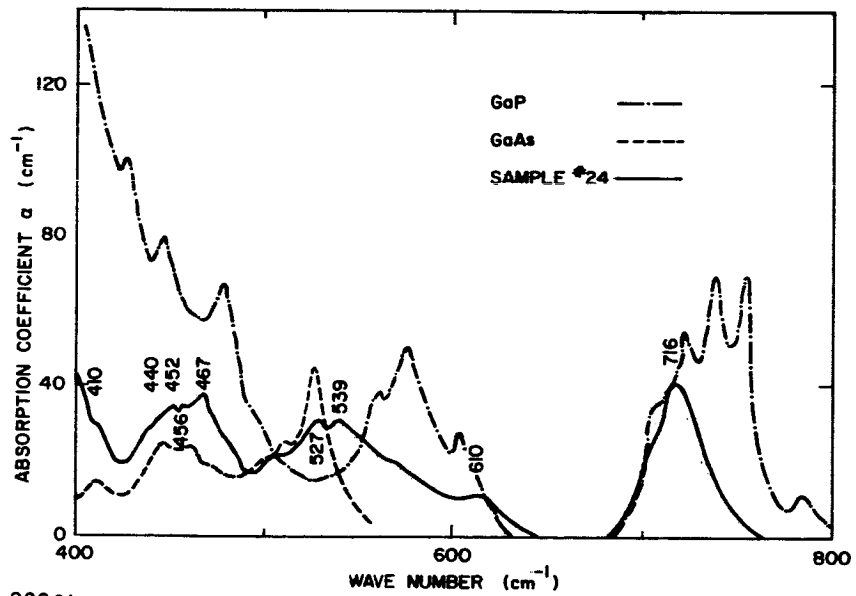
32959

FIG. 47. LATTICE ABSORPTION BANDS OF $\text{GaAs}_{.15}\text{P}_{.85}$ AT 300°K .



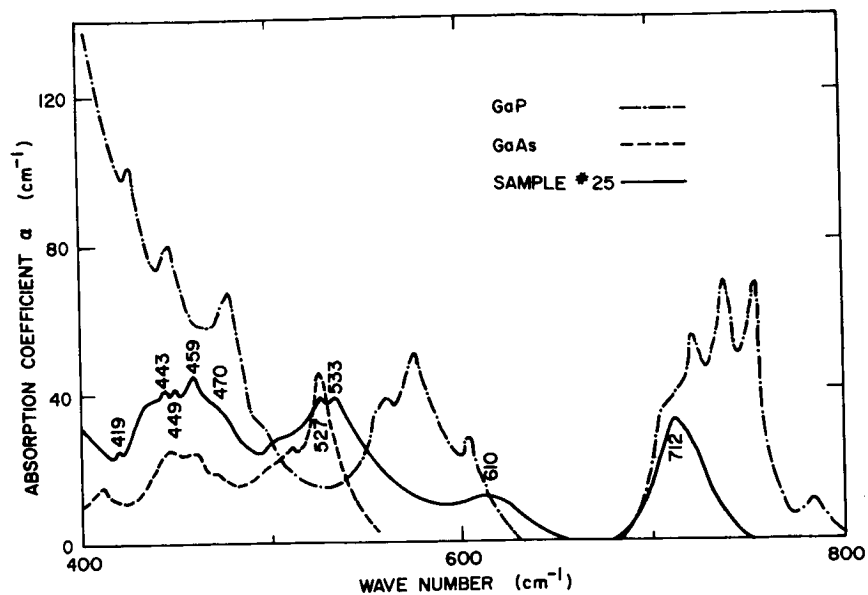
32960

FIG. 48. LATTICE ABSORPTION BANDS OF GaAs_{0.325}P_{0.675} AT 300 °K.



32961

FIG. 49. LATTICE ABSORPTION BANDS OF GaAs_{0.52}P_{0.48} AT 300 °K.



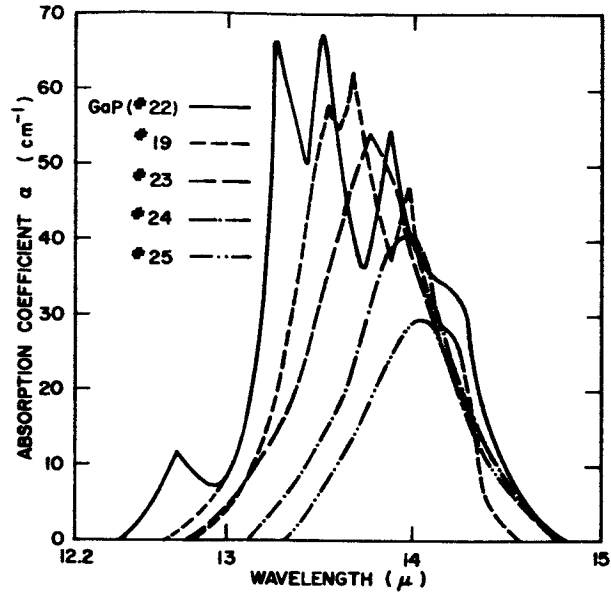
32962

FIG. 50. LATTICE ABSORPTION BANDS OF $\text{GaAs}_{.65}\text{P}_{.35}$ AT 300 °K.

3. Discussion

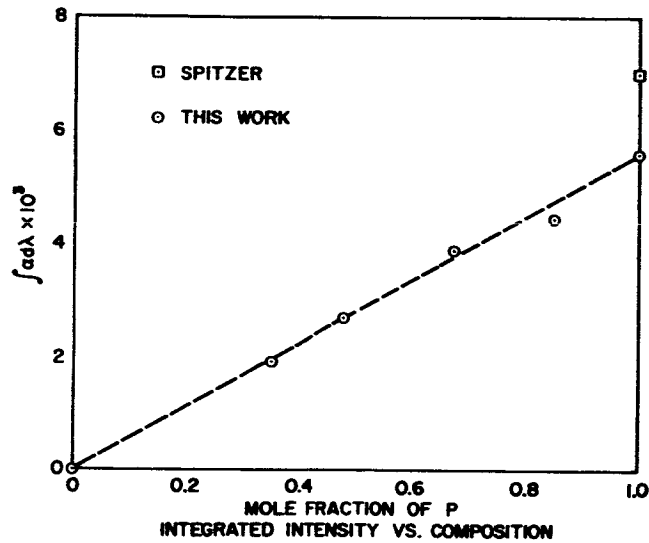
1. The band of GaP at 575 cm^{-1} and that of GaAs at 525 cm^{-1} exhibit a clear superposition in $\text{GaAs}_{x}\text{P}_{1-x}$. The former gradually shifts toward longer wave length and decreases in intensity as x increases; the opposite is true for the latter. In Sample No. 25, these bands almost overlap; they are only 6 cm^{-1} apart.
2. The effect of the fundamental absorption on the total absorption gradually increases as x decreases; this agrees with the observed shifting of the restrahlen band.
3. A new broad band, small in intensity, emerges at 610 cm^{-1} as x increases beyond 0.4. The exact reason is not known.
4. The bands of GaP at 721 cm^{-1} , 739 cm^{-1} and 755 cm^{-1} also shift toward longer wavelength as x increases. But we were unable to resolve the three peaks at $x > 0.3$. Since these bands are quite isolated from any of the GaAs bands, we are able to obtain the dimensionless quantity $\int \alpha d\lambda$ as the integrated intensity [Ref. 4] of this group of peaks. In Fig. 51a, we have plotted α vs λ of these samples in the region of 12μ to 15μ , and in Fig. 51b, the

⁴D. A. Kleinman and W. G. Spitzer, "Infrared Lattice Absorption of GaP," *Phys. Rev.*, **118**, 110, 1960.



32963

FIG. 51a. COMBINATION BANDS OF THE ALLOYED CRYSTAL IN THE REGION OF $13\mu-14\mu$.



32964

FIG. 51b. INTEGRATED INTENSITY VS COMPOSITION.

integrated intensity $\int \alpha d\lambda$ vs composition x . For GaP, the value of $\int \alpha d\lambda \approx 7 \times 10^{-3}$ is given by Spitzer [Ref. 4]; except for this point, the rest of the points form a straight line through the origin. This means that the integrated intensity is in direct

proportion to the mole fraction of phosphorous contained in the crystal, which strongly suggests a clustering model favored also by the superposition of combination bands of GaAs and GaP in the alloyed crystal.

Project 5109: EPITAXIAL GROWTH OF III-V SEMICONDUCTOR COMPOUNDS

National Aeronautics and Space Administration
Grant NsG-555
Project Leader: G. L. Pearson
Staff: J. W. Allen, D. H. Loescher

A. PART I

The purpose of this project is to examine and control the crystallographic and electrical properties of III-V compound semiconducting materials grown epitaxially by vapor deposition. Our interests have been concentrated on the compounds GaP and GaAs.

Semiconductors owe their usefulness in large part to the sensitivity of their properties to the presence of small amounts of impurity. Despite their importance we can only describe these impurities in phenomenological terms at the moment and it is impossible to predict a priori their energy levels, capture cross-sections, optical cross-sections etc., except in the special case of shallow hydrogen-like impurities. As a first step toward the solution of the general problem we are studying the properties of the $3d^n$ transition ions in semiconductors: these have the advantage that the d-shell can be described in terms of perturbed free-ion orbitals. They are also of considerable technological importance. Crystal field spectra (i.e., optical transitions to excited states) have been observed for transition metals in ZnS [Ref. 1], CdS [Refs. 1,2] and ZnSe [Ref.3]. An attempt has been made to relate these spectra to the ground state energies [Ref. 4], which are the ones of importance for electrical properties. Gallium phosphide is a good material for this type of study as its band gap (2.25 eV) makes it suitable for optical and electrical measurements.

¹H. A. Weakliem, J. Chem. Phys., 36, 2117 (1962).

²R. Pappalardo and R. E. Dietz, Phys. Rev., 123, 1188 (1961).

³J. W. Allen, to be published.

⁴J. W. Allen, Proc. Int. Conf. Semiconductors, Paris, 1964.

Optical absorption in GaP containing Fe, Co and Ni has been measured and interpreted as being due to the divalent ions in tetrahedral fields. The crystal field parameter Δ is of the order of 4000 cm^{-1} , while the Racah parameters are reduced to about 0.4 of the free ion value. In addition absorption edges are seen which may be due to charge transfer transitions.

It is planned to extend these measurements to single crystals, and to study the electrical properties such as conductivity and photoconductivity.

B. PART II

In order to achieve the goals outlined in Part I we intend to make a complete study of cobalt in gallium phosphide. Cobalt has been chosen for this study because it should be quite soluble in GaP and because it has a convenient isotope i.e., Co^{60} . The general procedure will be first to measure the solubility, and the diffusion constant, of Co in GaP as a function of temperature and as a function of the conductivity type of the base crystal. Once the data necessary to do predictable diffusions is obtained we plan to prepare samples with various amounts of Co and measure the "energy levels" of Co in GaP. The Hall effect and optical absorption will be used to determine these levels.

The solubility of Co in GaP can be estimated by using a Darken-Gurry plot [Ref. 5]. This plot is based on the experimental evidence that solid solutions form most easily when the atomic radius and electronegativity of the solvent atoms are approximately equal to those of the solute atoms. In the case that the solvent is a compound we use the average value of the atomic radii of the constituents of the compound and also the average electronegativity. The atomic radius of Co is $r(\text{CN}12) = 1.252 \text{ \AA}$ while the electronegativity is $\chi = 1.8 \text{ eV}$. The values for GaP are respectively $r \approx 1.3 \text{ \AA}$ and $\chi \approx 1.85 \text{ eV}$. We see that the values for Co and those for GaP are very nearly the same. While this agreement of atomic radii and electronegativities suggests that Co should be reasonably soluble in GaP,

⁵L. S. Darken and R. W. Gurry, Physical Chemistry of Metals, McGraw-Hill, New York, 1953, p. 86.

it does not guarantee that there will be any solubility. In order to obtain more information on the solubility of Co in GaP, it is necessary to consider the process of solution in more detail.

In order to apply thermodynamics to the problem of estimating the solubility of Co we must create a model of the process of a solute and a solvent forming a solution. The following steps have been suggested [Ref. 6]:

- | | |
|---|-------------------|
| 1. Cobalt atoms leave cobalt crystal, | ΔH_{sCo} |
| 2. GaP bonds are broken and CoP bonds are formed, | ΔH_{chem} |
| 3. The crystal is strained by the substitution of a cobalt atom for a gallium atom, | ΔH_{st} |
| 4. A gallium atom condenses out on the surface of the crystal | $\Delta H_s Ga$ |

The symbol to the right of each step indicates the change in enthalpy due to the process. The quantities ΔH_{sCo} and ΔH_{sGa} are the heats of sublimation of Co and Ga respectively. The bond energy change ΔH_{chem} may be estimated using a result of Paulings [Ref. 7]. The strain energy is discussed fully by Casey [Ref. 8]. Then

$$\Delta H = \Delta H_{sCo} + \Delta H_{chem} + \Delta H_s - \Delta H_{sGa} . \quad (1)$$

Casey has also shown that the concentration of solute atoms may be written in the form [Ref. 8]

$$C = C_o e^{-\Delta H/kT} . \quad (2)$$

Consequently, the calculation of ΔH can provide us with valuable information about the temperature dependence of the solubility. In formula

⁶H. C. Casey, Jr., "Rare Earths in Covalent Semiconductors: The Thulium-Gallium Arsenide System," Stanford Electronics Laboratories, Technical Report No. 5105-1, June 1964, p. 33.

⁷Linus Pauling, The Nature of the Chemical Bond, Cornell Univ. Press, Ithaca, New York, 1960, p. 91.

⁸H. C. Casey, Jr., "Rare Earths in Covalent Semiconductors: The Thulium-Gallium Arsenide System," Stanford Electronics Laboratories, Technical Report No. 5105-1, June 1964, pp. 33-37.

(1) k is Boltzmann's constant and T is the temperature in degrees Kelvin. Performing the calculations of the ΔH 's one finds $\Delta H = 4.4$ eV. This very large value of ΔH means that the solubility of Co in GaP should be a very strong function of temperature. Regrettably, it is not possible to calculate the constant C_o in Eq. (2) with any accuracy. Also the constant is of the order of 10^{25} - 10^{30} , so it cannot be ignored. Consequently, we cannot predict the absolute solubility of Co in GaP, but we can predict the temperature dependence of the solubility. By combining the calculation of ΔH and the results of comparing atomic sizes and electronegativities, we conclude that Co may be quite soluble in GaP and that the solubility should be strongly temperature dependent.

Because of the predicted strong temperature dependence of the solubility, we have begun a program of high temperature diffusions of Co into GaP. We have encountered the difficulty that simple heat treatment at the diffusion temperature, 1160 °C, causes decoration of the grain boundaries in polycrystalline material and also causes absorption on the long wavelength side of the absorption edge of the GaP. This latter effect is also seen in epitaxial single crystal samples subjected to the same heat treatment. Since these effects could mask or confuse the effects of Co, we are trying to find the cause of these effects and eliminate it. Since the effects on the band edge absorption are similar in both the single crystals produced in this laboratory and the polycrystals purchased from Merck and Company, it seems that the effect cannot be due to an impurity in the GaP. The possibility that an impurity, such as copper, is diffusing out of the quartz diffusion ampoule into the material has been considered and is being investigated. As soon as this problem associated with simple heat treatment is solved, the work on Co diffusions will be continued.

In order to have GaP for diffusion studies, it has been necessary to produce our own epitaxial crystals. We are now able to produce large (approximately 3 cm²) pieces of GaP about 17 mils thick in six hours. The epitaxial system has been described by Chauvy in previous editions of this report [Ref. 9]. The next step in the epitaxial growth will be

⁹ D. Chauvy, Quarterly Research Review No. 8, SEL-64-038, Stanford Electronics Laboratories, Mar 1964.

the development of a procedure to grow doped single crystals. Of the three common n-type dopants (Te, S, and Si), the last one, in the form of SiCl_4 , appears to be most easily introduced into the present system. After producing single crystals with various doping densities, it will be possible to study the effect of the doping density on the solubility of Co in the crystals.

In conclusion, we have begun a program to study the effects of Co as a dopant in GaP. At this time, we are producing epitaxial single crystals into which to diffuse Co. Also work on high temperature diffusions has been progressing.

Project 5110: THE EFFECTS OF GAMMA RADIATION ON SILICON SEMICONDUCTOR DEVICES

Office of Ordnance Research DA 31-124 ARO(D)-155
Project Leader: G. L. Pearson
Staff: D. Landis*

The purpose of this work is to study the effects of gamma radiation on silicon semiconductor devices, to relate the observed device changes back to the effects of radiation on silicon material, and to use this information to find methods for predicting the amount of damage a given device would experience in a radiation environment.

Vitovskii, et al [Ref. 1], using Hall measurements, have observed three gamma-induced energy levels in the forbidden band of silicon. They are an acceptor level at $E_c - 0.18$ volts, a donor level at $E_v + 0.23$ volts, and an acceptor level "near" $E_c - 0.5$ volts, for which they find an introduction rate of about 10^5 levels/cm per Rad(C)/cm². Since Si becomes intrinsic after receiving enough radiation, there should also be a radiation-induced donor level near the center of the forbidden band. This level has been observed for some types of radiation, but not yet for gamma radiation. Since these deep levels largely control the permanent radiation damage to devices such as unijunction and field-effect

*Lockheed Fellow.

¹N. A. Vitovskii, T. V. Mashovets, and S. M. Ryvkin, "Energy Spectrum of a Gamma-Radiation Induced Defect in Silicon," Sov. Phys.--Solid State, 4, 10, Apr 1963, p. 2085.

transistors, affect saturation voltages in many devices, and should have a major effect on the recombination characteristics in junctions and base regions of transistors, they are being studied.

One method of studying the introduction rates and energies of radiation-induced defect levels is to measure the resistivity of the silicon as a function of radiation dose. If n-type silicon is irradiated, the deep acceptor level will remove electrons from the conduction band. The change in resistivity gives a measurement of the number of electrons removed. The condition of charge neutrality gives

$$n = N_D^+ - N_A^- , \quad (1)$$

where n is the number of conduction electrons, N_D^+ is the donor density obtained from pre-irradiation resistivity measurements, and N_A^- is the number of acceptors introduced by the radiation times the fermi factor, $f(E_A)$, which gives the fraction of acceptors occupied by electrons. N_A^- may be calculated from

$$N_A^- = N_A f(E_A) = R \Phi / [1 + \exp[(q/kT)(E_A - E_F)]] , \quad (2)$$

where R is the introduction rate of defects per unit radiation dose (assumed linear with dose), Φ is the total radiation dose, E_A is the energy of the acceptor level, and E_F is the fermi level. E_F may be found from

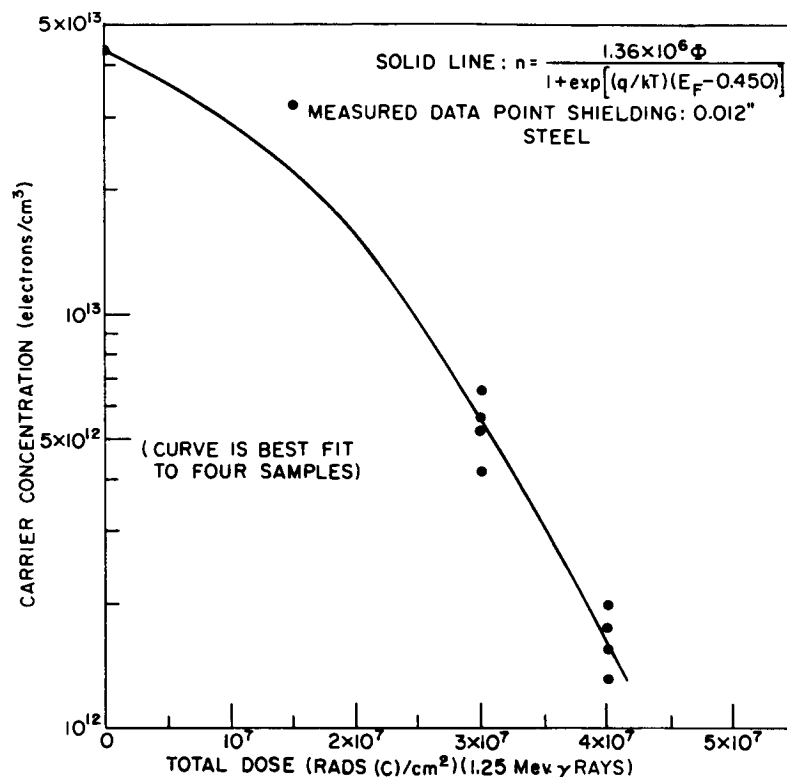
$$E_F - E_i = (kT/q) \ln (n/n_i) , \quad (3)$$

where the symbols have their usual meaning in semiconductor theory. Note that E_F is an experimentally measured variable found directly from the measurement of n .

The parameters R and E_A may therefore be determined from resistivity data as a function of radiation dose. Certain parameters of silicon must be assumed in the analysis of the data. The parameters assumed in the analysis reported here are: the electron mobility (μ_n) is $1450 \text{ cm}^2/\text{volt-sec}$ and is constant since the total number of charged

scattering centers is always less than 10^{14} per cm^3 in this work; the intrinsic conduction electron concentration (n_i) is 1.5×10^{10} electrons/ cm^3 , and the intrinsic fermi level (E_i) is at $E_c - 0.543$ volts.

Two experiments have been performed on high-resistivity n-type silicon. The first consisted of the irradiation of four unijunction transistors [Ref. 2]. The results are shown in Fig. 52. The calculated



33029

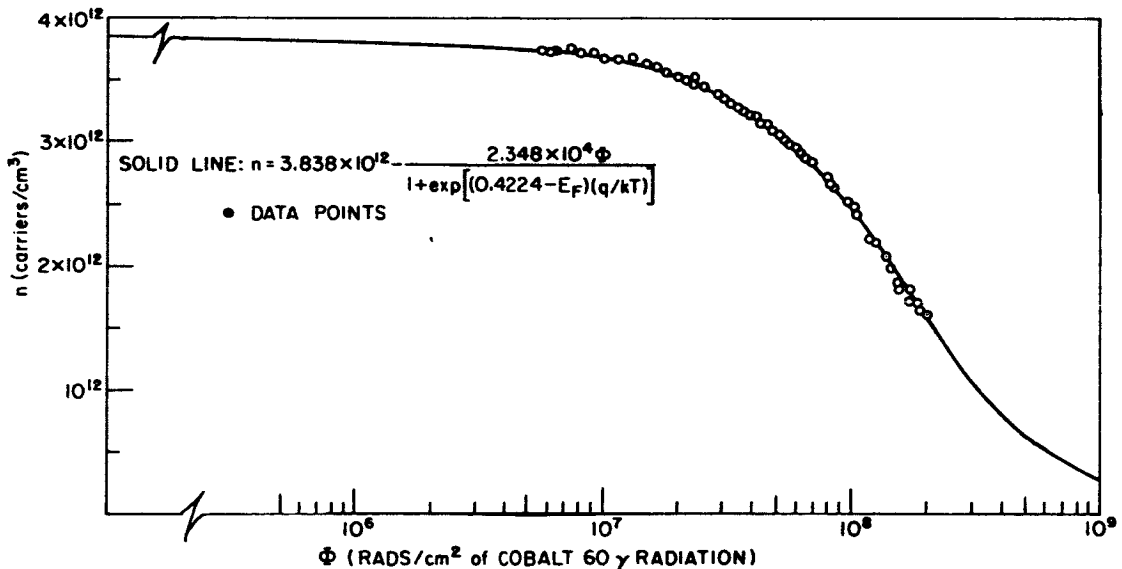
FIG. 52. CARRIER CONCENTRATION VS TOTAL RADIATION DOSE SHIELDED N-TYPE SILICON (UNI-JUNCTION TRANSISTORS).

gamma-induced energy level responsible for the increase in resistivity is $E_A = E_c - 0.450 \pm 0.004$ volts. (The error is statistical probable error of the mean.) The introduction rate of this defect is $1.36 \pm 0.04 \times 10^6$ levels/cm per Rad(C)/ cm^2 . Since all of the data is used in

²The unijunction transistor data was taken by W. D. Rausch of Lockheed Missiles and Space Company. We are grateful for his allowing us to use the data.

the calculations, the goodness of fit of the assumed mathematical form for carrier removal cannot be examined. The only other data point available from this experiment is believed to have been taken at a higher temperature than the rest and hence is not usable in the analysis. The unijunction transistor cans provided 0.012" of steel shielding between the radiation source and the silicon chips.

The second experiment is still in progress at the time of this report after some 300 hours of irradiation. The data so far acquired are shown in Fig. 53. A fit to three points of this data gives the energy level



33030

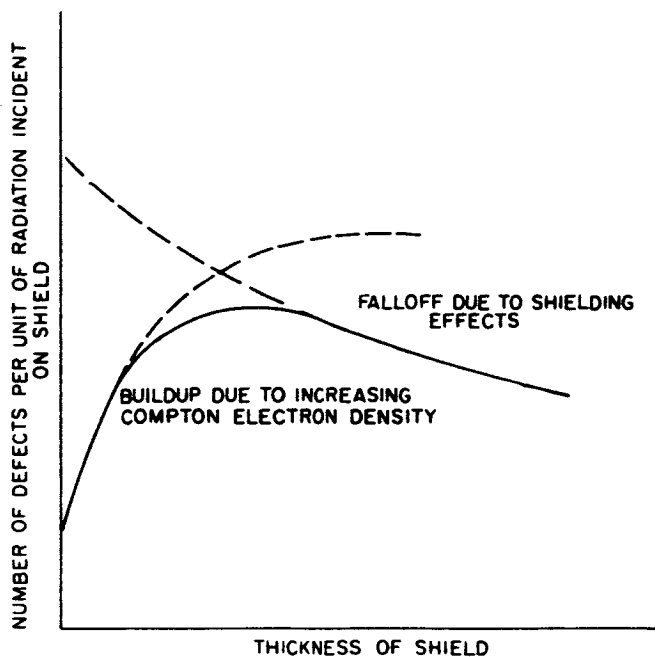
FIG. 53. CARRIER CONCENTRATION VS RADIATION DOSE HIGH RESISTIVITY N-TYPE SILICON.

at $E_c = 0.422$ volts and the introduction rate as 2.35×10^4 levels/cm per Rad(C)/cm². This sample is bare unshielded silicon. The level at $E_c = 0.18$ volts may be significant to a few percent in this experiment,

especially at the lower radiation levels. When the experiment is complete a least-squares fit using the Stanford B-5000 computer will be made on the data to obtain the introduction rates and energies of both defect levels, along with their statistical errors. The more thorough analysis should give a better fit of theory to experiment, particularly at the lower radiation levels.

The difference in defect introduction rates in the two experiments described above is very probably because of the Compton electrons generated in the steel can of the unijunction transistor. From the cross sections involved it is apparent that the only mechanism by which 1.25 Mev gamma radiation can significantly damage silicon is if the gamma ray gives rise to a Compton electron which in turn knocks a silicon nucleus from its place in the lattice, so that the difference in introduction rates noticed is not surprising. At some thickness of material between the radiation source and the sample, the Compton electron and gamma fields will be in equilibrium in the sample of silicon. Calculation of this thickness is mathematically an extremely difficult problem in radiation transport theory; however, a series of experiments scheduled for January should provide a value for the thickness of silicon shielding needed to reach equilibrium in the sample of silicon. The expected results of this experiment are sketched qualitatively in Fig. 54, though the shielding effect (the falloff at large thicknesses) shown in the figure is probably greatly exaggerated. These results, particularly the fact that the introduction rate found above for unshielded silicon was one-fifth of Vitovskii's result, indicate that Vitovskii probably had some shielding between his sample and his Co60 source, a point not mentioned in his paper. It is apparent that for useful predictions of radiation damage, at least from gamma radiation, the thickness and nature of the material between the silicon and the gamma source must be known. For uniformity of results and to insure uniformity of damage through the sample, the radiation experiments should be conducted with a shield thick enough to reach the Compton electron-gamma equilibrium.

An experiment scheduled for the last week in December will search for the hitherto unobserved donor level which should be near the center of the



33031

FIG. 54. SKETCH SHOWING EXPECTED VARIATION OF DAMAGE RATE IN SILICON WITH THICKNESS OF SHIELDING.

forbidden band. This experiment will involve the irradiation of high resistivity p-type silicon.

The experiment on n-type silicon described above requires several minutes to stabilize after the removal of radiation from the silicon sample. This probably indicates the presence of a radiation induced, long lifetime surface trap, possibly the same one which caused a failure in Telstar I [Ref. 3]. The instrumentation presently being used in the experiment requires too long a reading time to allow study of this state, but an automatic data collection system being installed in the Lockheed gamma cell should alleviate this problem.

Attempts to observe characteristics of levels introduced by radiation from junction measurements have so far been inconclusive, probably because of the surface effect mentioned above. Efforts are still being made to acquire or build the guarded junctions described in the last quarterly report, but cost is a problem here.

³ D. S. Peck, R. R. Blair, W. L. Brown, and F. M. Smits, "Surface Effects of Radiation on Transistors," Bell Sys. Tech. Jour., Jan 1963, p. 95.

Project 5111: DIFFUSION OF IMPURITIES IN COMPOUND SEMICONDUCTORS
UNDER PARTIAL PRESSURE OF ONE CONSTITUENT

Tri-Service Contract Nonr-225(24)

Project Leader: G. L. Pearson

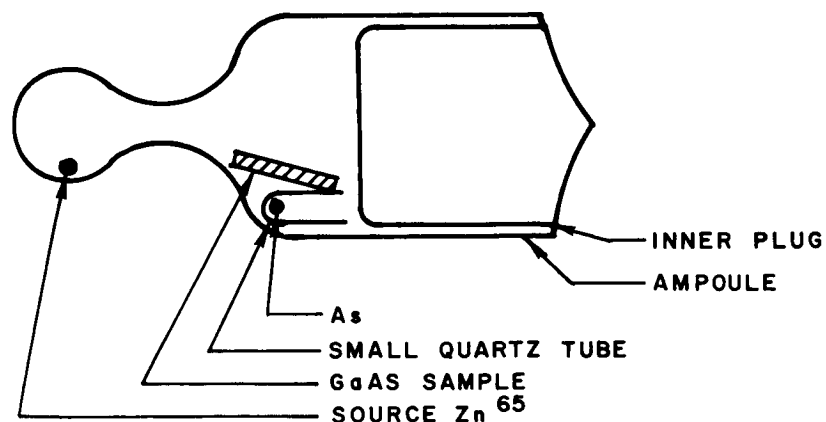
Staff: K. K. Shih

The purpose of this project is to make a study of various parameters leading to anomalous diffusion characteristics of impurities into compound semiconductors as a function of the partial pressure of one constituent.

A. EXPERIMENTAL PROCEDURES

The GaAs samples were n-type single crystals. These samples were lapped parallel and polished; then cleaned and degreased.

The prepared samples were loaded in the clean quartz ampoules, together with the diffusion source Zn^{65} and arsenic. The ampoules were sealed in vacuum. The volume of the ampoules was about 1 to 2 mls.. The amount of diffusion source Zn^{65} was of the order of 2 to 3 milligrams which was calculated to be sufficient to maintain a constant zinc pressure during the diffusion at $900^{\circ}C$ and 90 minutes. In order not to let the sources contact directly with the samples, a special geometry of the ampoules as shown in Fig. 55 has been used.



33032

FIG. 55. A SCHEMATIC DIFFUSION AMPOULE.

The ampoules were then put into a furnace for diffusion at $900 \pm 2^\circ \text{C}$ for 90 minutes. After diffusion, the samples were removed from the ampoules, and they were washed in dilute HCl to get rid of the zinc and arsenic condensed on the surface of the samples. They were cut into circular wafers 0.2 in. in diameter. The sheet resistivity ρ_s was then measured by the four point probe method: its value for a 0.2 in. diameter wafer is equal to $4.1716 \text{ V/I ohms/square}$.

The junction depth x_j was measured by microscope after the samples were cleaved and strained.

The samples were then mounted on aluminum holders. Diffusion profiles were obtained using standard lapping, weighing, and counting procedures. The surface concentration C_0 was determined from these plots.

B. EXPERIMENTAL RESULTS AND DISCUSSION

The GaAs samples except Sample No. 9 had the following properties initially.

1. Boat grown n-type crystal.
2. $N_d = 4.1 - 8.9 \times 10^{15} \text{ cm}^{-3}$, $\mu = 4400 - 4800 \text{ cm}^2/\text{v-sec}$,
 $\rho = 0.15 - 0.36 \text{ ohms-cm}$.
3. [111] orientation.

The weight of the samples, the volume of the ampoules, and the amount of diffusion source Zn^{65} and arsenic which were used in the diffusion experiments were listed in Table 1.

TABLE 1

SAMPLE NO.	1	2	3	4	5	6	7	8	9*
Wgt. of the sample (g)	0.3144	0.3909	0.2989	0.3584	0.2976	0.3592	0.3542	0.3114	0.2642
Net ampoule Vol. (cm ³)	1.49	1.1	1.74	1.24	1.79	1.03	1.29	1.94	0.8
Zn ⁶⁵ (mg)	2.535	3.792	2.745	3.55	2.36	1.687	3.517	2.28	1.85
As (mg)	0	0.342	1.079	1.2	2.68	1.83	8.04	22.61	23.97

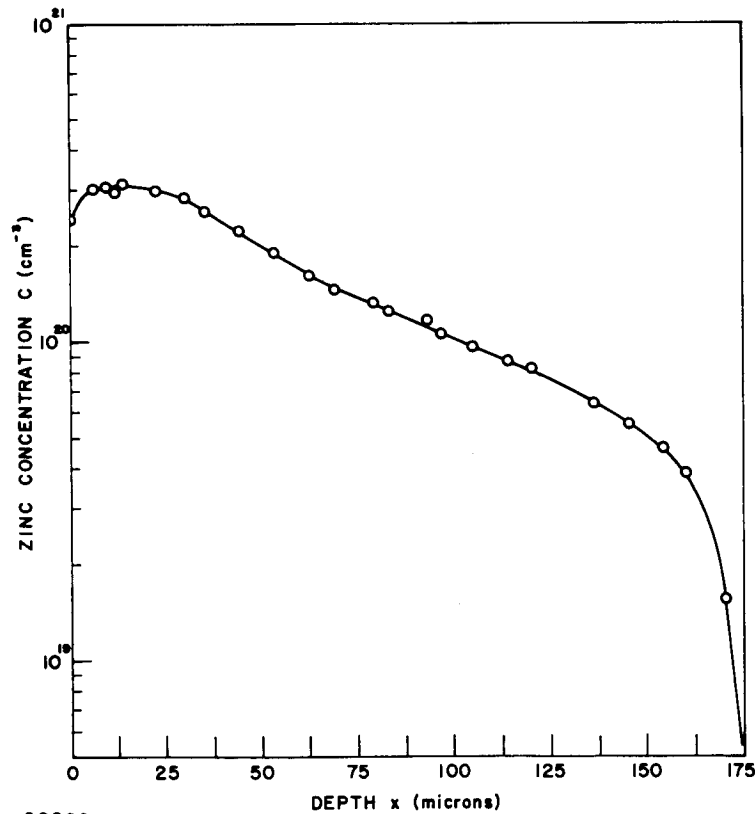
*Sample No. 9 had $N_d = 2.5 \times 10^{16} \text{ cm}^{-3}$, $\mu = 4410 - 5100 \text{ cm}^2/\text{v-sec}$, and $\rho = 0.05 - 0.07 \text{ ohms-cm}$ initially.

If we assume that there is no interaction between zinc and arsenic, or in other words, all the arsenic becomes vapor during the diffusion process, and we also assume that the arsenic pressure is dominated by tetramers, and the contribution due to dimers and monomers are small, then we can calculate the arsenic pressure P_{AS_4} and their values are tabulated in Table II.

TABLE II

SAMPLE NO.	1	2	3	4	5	6	7	8	9
Calculated P_{AS_4} (atms.)	-	0.1	0.2	0.31	0.42	0.57	2	3.75	9.6

The diffusion profiles are plotted in Figs. 56, 57, 58, 59 and 60. The sheet resistivity ρ_s , the junction depth x_j , average conductivity



33033
 FIG. 56. DIFFUSION PROFILE OF Zn IN GaAs AT 900 °C FOR 1.5 HRS WITH NO As ADDED.

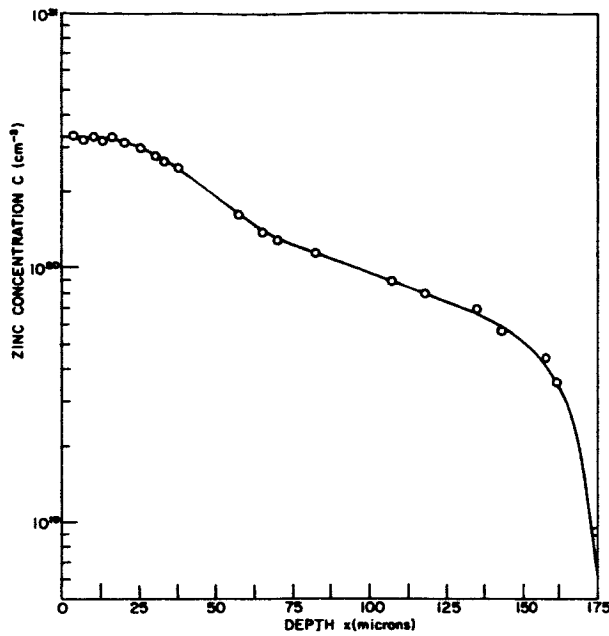


FIG. 57. DIFFUSION PROFILE OF Zn IN GaAs AT 900 °C FOR 1.5 HRS WITH EXCESS As ADDED CORRESPONDING TO P_{AS_4} (CALCULATED) = 0.2 ATMS.

33034

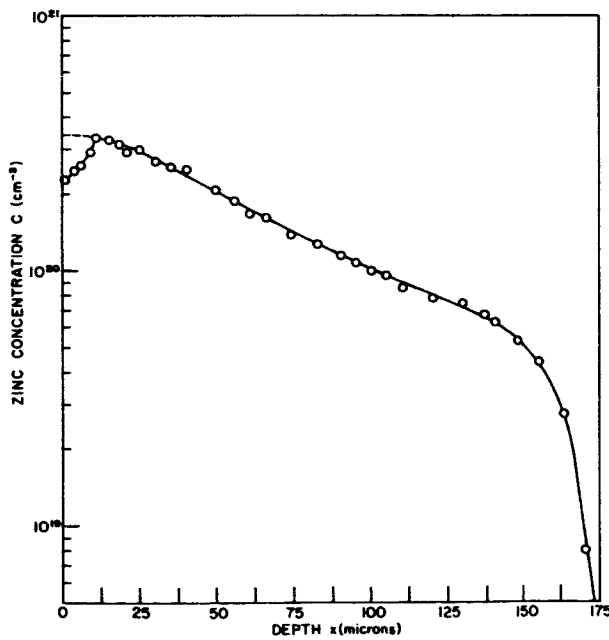


FIG. 58. DIFFUSION PROFILE OF Zn IN GaAs AT 900 °C FOR 1.5 HRS WITH EXCESS As ADDED CORRESPONDING TO P_{AS_4} (CALCULATED) = 0.31 ATMS.

33035

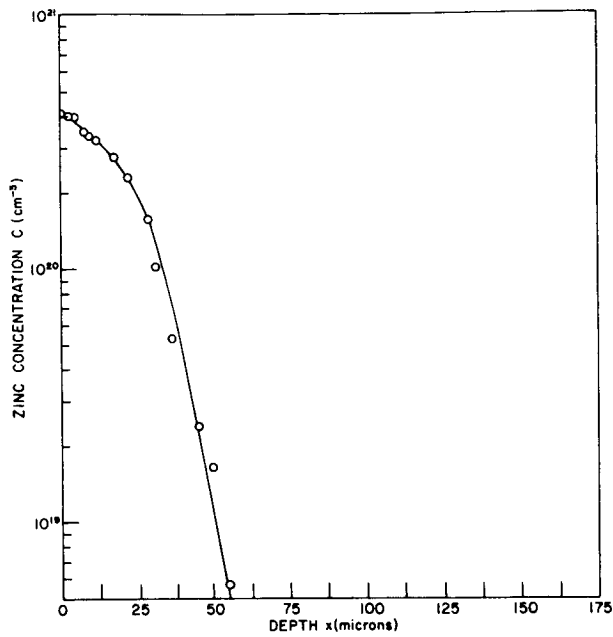


FIG. 59. DIFFUSION PROFILE OF Zn IN GaAs AT 900 °C FOR 1.5 HRS WITH EXCESS As ADDED CORRESPONDING TO P_{AS_4} (CALCULATED) = 0.42 ATMS.

33036

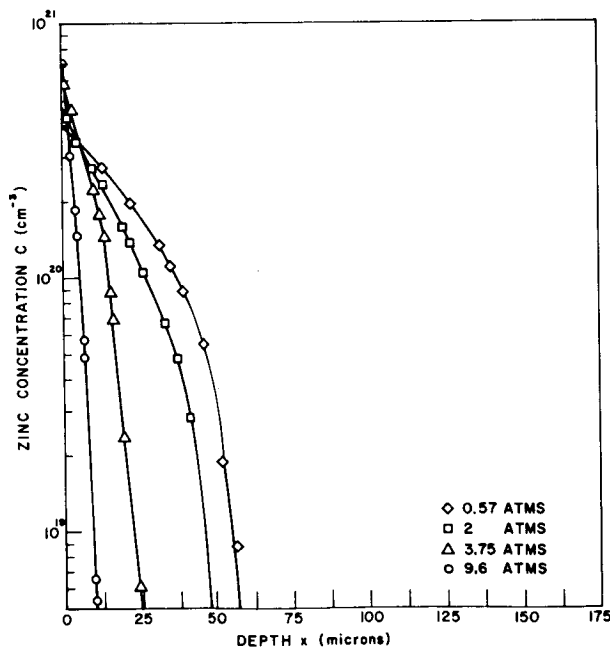
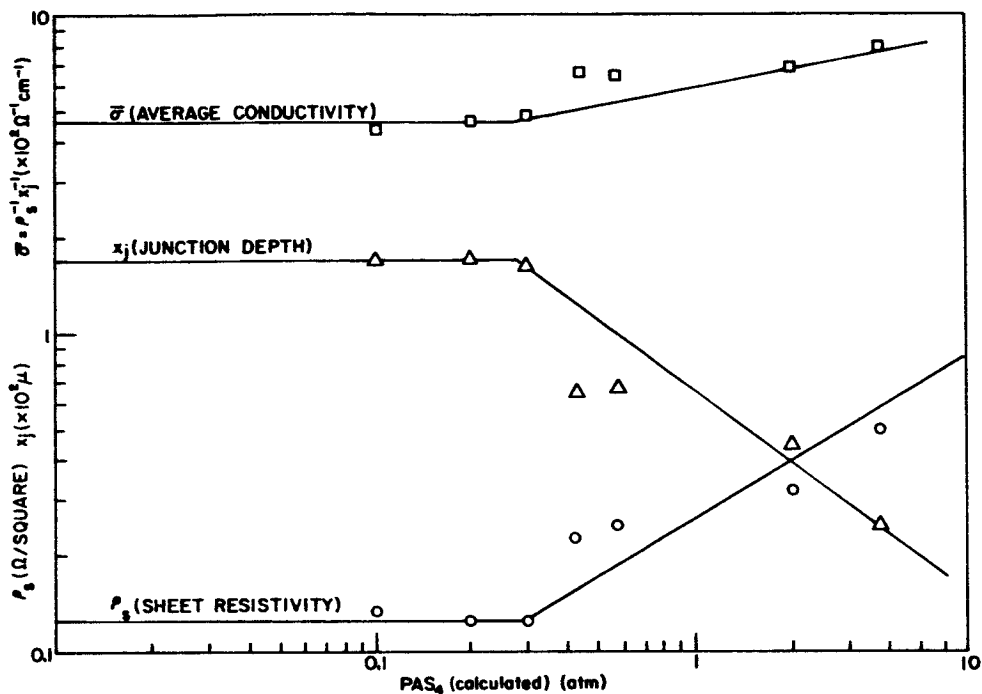


FIG. 60. DIFFUSION PROFILE OF Zn IN GaAs AT 900 °C FOR 1.5 HRS WITH EXCESS As ADDED CORRESPONDING TO P_{AS_4} (CALCULATED) = 0.57, 2, 3.75 AND 9.6 ATMS.

33037

$\bar{\sigma}$ and the surface concentration C_0 vs the calculated arsenic pressure P_{AS_4} are plotted in Figs. 61 and 62.

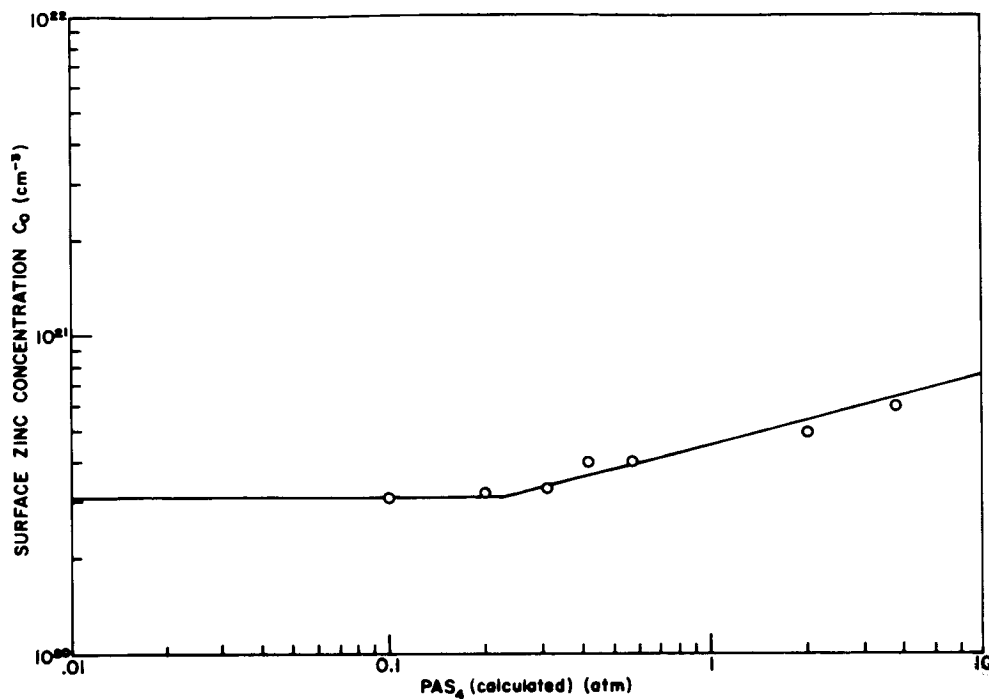


33038

FIG. 61. VARIATION OF ρ_{si} , x_j , AND $\bar{\sigma}$ AS FUNCTION OF ARSENIC PRESSURE FOR Zn DIFFUSION IN GaAs AT $T = 900^\circ \text{C}$ AND $t = 1.5$ HRS ASSUMING THAT THERE IS NO INTERACTION BETWEEN As AND Zn.

The experimental results indicate that there is almost no change for the values of ρ_s , x_j , and C_0 when the calculated arsenic pressure is less than 0.3 atms. Hence the arsenic pressure which we calculated by assuming that there is no interaction between zinc and arsenic at 900°C is not true. There is a possibility of the formation of a second condensed phase. Two such phases are known in Ga-As-Zn ternary system: ZnAs_2 and Zn_3As_2 . However, only the latter would be easy to form under the present condition, since the melting point of ZnAs_2 is 771°C .

After studying the amount of zinc and arsenic used for these experiments, it is found that the weight of zinc is higher than that of arsenic for the cases for which the calculated arsenic pressures are less than 0.3 atms., while for the cases for which the calculated arsenic pressures



33039

FIG. 62. VARIATION OF SURFACE ZINC CONCENTRATION AS FUNCTION OF ARSENIC PRESSURE FOR Zn DIFFUSION IN GaAs AT $T = 900^\circ\text{C}$ AND $t = 1.5$ HRS ASSUMING THAT THERE IS NO INTERACTION BETWEEN As AND Zn.

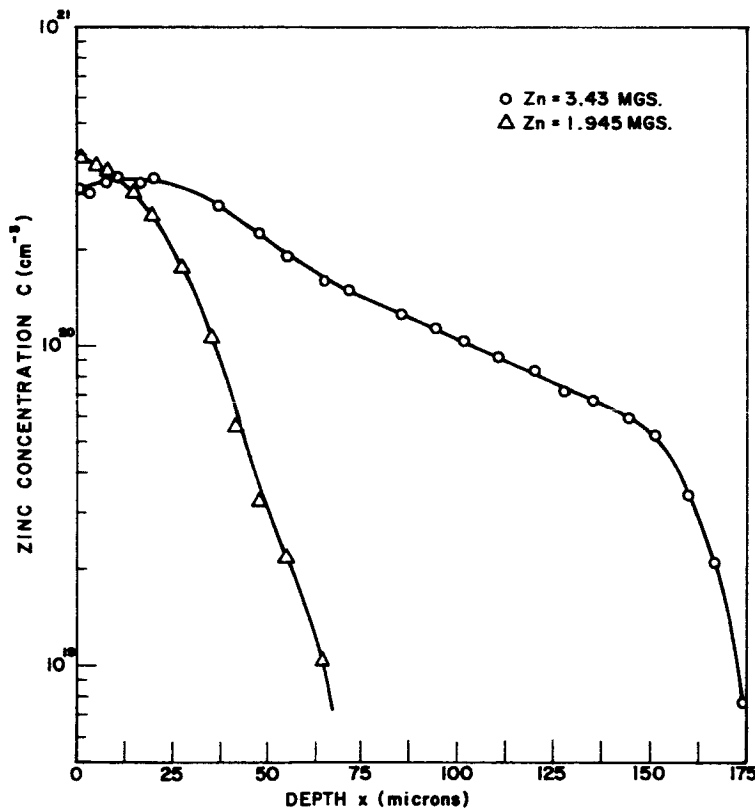
are greater than 0.3 atms., the weight of arsenic is higher than that of zinc. Therefore, we can conclude that the weight of the zinc and the weight of the arsenic are two important parameters in studying the diffusion problems.

Now, we can propose a very crude model to explain the above phenomena as following:

1. If the weight of the zinc is greater than that of arsenic during diffusion, most of the arsenic will combine with the zinc to form solid Zn_3As_2 , and some of the arsenic may mix with the zinc to form zinc-arsenic liquid, and there is almost no free arsenic left. The dissociation pressure of Zn_3As_2 at 900°C is very small so that the total arsenic pressure will be very small, which means that the effect of the arsenic will be small too for this case.
2. On the other hand, if the weight of the arsenic is greater than that of zinc, then most of the zinc will combine with the arsenic

to form solid Zn_3As_2 , and there is almost no free zinc left. For the first order of approximation, the zinc pressure will be determined from the dissociation pressure of Zn_3As_2 , and the arsenic pressure can be determined from the free arsenic left in the ampoule.

In order to obtain some evidence to show that the above is a possible mechanism which could explain the results of our diffusion experiments, two additional experiments have been done. In both cases, we used the same amount of arsenic, which corresponds to 0.53 atms. (calculated arsenic pressure), but different amount of zinc. The results were plotted in Fig. 63. From Fig. 63, we observed that the diffusion profiles are completely different even though the same amounts of arsenic have been



33040
 FIG. 63. DIFFUSION PROFILES OF Zn IN GaAs AT 900 °C FOR 1.5 HRS WITH SAME AMOUNT OF EXCESS As ADDED CORRESPONDING TO P_{AS_4} (CALCULATED) = 0.53 ATMS.

The amount of Zn used = 3.43 and 1.945 mgs respectively.

used for these experiments. For the case that the zinc concentration is higher, the diffusion profile is almost the same as Fig. 56, that is, the excess arsenic did not have any effect in this case since its amount is less than that of zinc. For the other cases when the concentration of zinc is lower, the diffusion profile changes abruptly.

Project 5112: EPITAXIAL GROWTH OF GaP

National Aeronautics and Space Administration
Grant NsG-555

Project Leader: G. L. Pearson, J. L. Moll

Staff: T. Koike

The purpose of this project is to apply the close-spaced epitaxial growth technique to GaP in order to study its optical and electrical properties.

During this quarter some improvements to the experimental system and the method of the growth were sought in order to obtain better control of the growth process.

As reported in the previous report, the temperature was measured both by an optical pyrometer and a thermocouple embedded in one of the carbon blocks. Difficulties in temperature measurements were often encountered since we could not eliminate deposition of the growth materials on the reaction tube wall and pick-up of the rf energy through the thermocouple. Various methods were tested to reduce these interferences. Under all circumstances the real temperatures at the surfaces of the source and the substrate are difficult to measure and certain care must be taken when experimental parameters such as the separation between the source and the substrate are changed.

We have also tried to improve the source material to obtain uniform growth over a longer period of time. The GaP sources used in most of the experiments were purchased from Merck and were composed of relatively large grains. Because of the large grains with different orientations in the source, the reaction does not take place uniformly on the surface of the source and the proper separation between the source and the substrate cannot be kept for a long period of time. To eliminate this effect, pressed-powder sintering was tested by using a few different binder materials. After some preliminary trials we obtained reasonably good results

with paraffin as the binder. The powdered mixture of GaP and GaAs was pressed in a stainless crucible with a stainless piston with a hydraulic press (3,000 pounds per square inch) and then fired in an open tube for several hours at 800 °C. After the firing, the source material was heated for several hours at 1100 °C in a closed ampule with added phosphorus to keep one atmosphere pressure of phosphorus inside the tube. A good single crystal was obtained using this source.

The whole experimental system is now being redesigned for further improvements of the growth method and more experiments on source materials of different compositions are expected.

Project 5207: RADIATIVE LIFETIME MEASUREMENT IN GaAs

Tri-Service Contract Nonr-225(24)
Project Leader: W. E. Spicer
Staff: Jüri Vilms

This project consists of a study of radiative lifetime in uniformly doped p-type GaAs as a function of temperature, by means of photoluminescence and electron lifetime measurement.

Final report is in preparation for publication.

Project 6758: ANALYSIS AND SYNTHESIS OF SOME ADAPTIVE NETWORKS

Tri-Service Contract Nonr-225(24)
Project Leader: B. Widrow
Staff: Donlan Jones

The objective of this project is to attempt to find a mathematical technique which will facilitate the analysis and synthesis of some adaptive networks composed of Adalines and fixed logic.

Further analysis has indicated that a mathematical device called the generalized inverse can be useful in representing least-square-error training procedure applied to Adalines. It is believed that interpretation of this will apply to Ridgway training of Adalines. Investigation of this mathematical device in the synthesis of Adaline networks is being continued.

Not only has the generalized matrix inverse (g.i.) been shown to be a model of least-mean-square-error training of Adalines, but it has also

been used to derive necessary and sufficient conditions for the realizability of a set of patterns used to train Adalines according to Ridgway adaptation. Further, rules have been derived using the generalized inverse which allow for the systematic synthesis of a number of different types of adaptive networks. These networks are Adalines feeding OR, AND, and MAJORITY GATES (Madalines), and also cascaded networks of Adalines.

Present investigation includes the possibility of an Adaline being a matrix generalized inverse taker. Also, relationship of Adalines to the general theory of generalized inverses is being investigated.

A final report is in the process of publication.

Project 6103: PATTERN RECOGNITION AND MACHINE LEARNING

Tri-Service Contract Nonr-225(24)

Project Leader: N. Abramson

Staff: S. Estes, J. McLaughlin, S. Fralick

A. MEASUREMENT SELECTION FOR PATTERN CLASSIFICATION - S. Estes

This period has been devoted almost exclusively to experimental work. First we have investigated the effectiveness of several ordering procedures in selecting measurements for classification by linear discriminants with known normal distributions. Even though the scope of the experiments was limited because of the data which could reasonably be obtained, agreement with the theory was accurate enough that we are inclined to accept the results as typical. For example, on 2000 patterns an error rate of 0.008 (theoretical 0.0075) was observed using 11 selected measurements compared to an error rate of 0.006 (theoretical .0055) on the entire set of 32 measurements. Second, the theoretical result which was previously given for error probability using estimated parameters and linear discriminants was found to be very accurate using training sets with 18 and 32 patterns per class with 32 measurements on each pattern.

Somewhat less effective but still accurate enough to be of value is the prediction of performance using only information available from the training set. The significant problem in this application is in the effect of treating order statistics (obtained by applying the ordering procedures to sample quantities) as if they were simple samples from the underlying distributions.

An extensive discussion of the experiments and theoretical results will be presented in a report which is presently being prepared.

B. MACHINE RECOGNITION OF BINARY PATTERNS - J. McLaughlin

As previously reported, each pattern vector X is regarded as an element of a modulo-2 vector space. Methods of finding the subspace spanned by a training set for a single pattern class can be extended to give a linear, invertible transformation T such that the components of $Y = T(X)$ have the following properties on the training set:

1. A maximum number of transformed measurements (components of Y) are zero on the entire training set.

2. A maximum number of transformed measurements are zero on all but one of the training vectors, consistent with condition 1.
3. A maximum number of transformed measurements are zero on all but two of the training vectors, consistent with conditions 1 and 2.

The method used to find T tends to make additional measurements zero most of the time. The procedure also tends to make the transformed measurements statistically independent. It has been found experimentally (on experiments with handwritten numerals) that the transformed measurements are divided rather sharply into two groups, one group in which the measurements are zero on almost all the training set, and the other group containing measurements which are zero for about half the training vectors. Thus this procedure tends to separate measurements into a good group and a bad group. It is not known why such a sharp distinction occurs. A report on this project is being prepared.

C. LEARNING WITHOUT A TEACHER - S. Fralick

A final report of this portion of Project 6103 is in preparation. For an abstract of this report, see the previous quarterly report.

Project 6105: INFORMATION THEORY

Tri-Service Contract Nonr-225(24)
 Project Leader: N. Abramson
 Staff: N. T. Gaarder

This project is concerned with a variety of problems of information theory. At the present time, we are investigating the design of a detector to process the random field, $y(t, X) = s_i(t, X) + n(t, X)$, the sum of a signal field, $s_i(t, X)$, and a noise field, $n(t, X)$.

The design objective is the minimization of the probability of error in estimating which of the hypotheses:

$$H_0: y(t, X) = s_0(t, X) + n(t, X)$$

or

$$H_1: y(t, X) = s_1(t, X) + n(t, X)$$

is true. Since the detector consists of N point detectors constrained to lie in a plane [the output of a point detector located at position X_i is the random process $y(t, X_i)$], the detector design must consider the processing of the point detector outputs and the configuration of the point detectors. The primary application of the work is in the design of seismometer arrays; however, the results are also applicable to the design of arrays of hydrophones and dipoles.

Two models have been investigated to represent the signal fields, $s_i(t, X)$, $i = 0, 1$. The first model assumes that in the plane occupied by the point detectors, the signal fields are known, spatially homogeneous and isotropic fields [i.e., $s_i(t, X) = s_i(t)$]. The second model assumes that in the plane occupied by the point detectors, the signal fields may be represented as the outputs of a time and space varying random linear filter:

$$s_i(t, X) = \int H(t, X; f) P_i(f) e^{i2\pi f t} df,$$

where $H(t, X; f)$ is a homogeneous and spatially isotropic, zero mean, gaussian random field, and $P_i(f)$ is a known function. The noise field, $n(t, X)$, is assumed to be a spatially homogeneous and isotropic, zero mean, gaussian random field. In addition, it is assumed that the covariance function of the noise, $k_n(\Delta t, \|\Delta X\|) = E[n(t, X) n(t + \Delta t, X + \Delta X)]$, is separable into a temporal covariance function, $k_t(\Delta t)$, and a spatial covariance function, $k_x(\|\Delta X\|)$ [i.e., $k_n(\Delta t, \|\Delta X\|) = k_t(\Delta t) k_x(\|\Delta X\|)$].

A brief description of the results obtained for the first signal model has been given previously (Quarterly Research Review No. 10). A complete description of the results for both signal models is contained in a report, "The Design of Point Detector Arrays," to be published shortly. Included in this report are some new results for the known signal case that display the sensitivity of the detection capability of the system to small changes in the noise covariance function. The detection capability of the system is particularly sensitive when the system is detecting perfectly, or almost perfectly (i.e., singular detection).

Recent effort has been concerned with the physical justification of the various signal and noise models. Under reasonable assumptions, the models have been physically justified; in addition, appropriate forms for the necessary spatial covariance functions have been found. These results are also contained in the forthcoming report.

The analysis of the second signal model has also received effort recently. The results of this analysis, essentially the same as those for the known signal model, are included in the forthcoming report also.

Future effort will be concentrated upon the production of the report.

Project 6203: STATE-LOGIC RELATIONS FOR SEQUENTIAL NETWORKS

Tri-Service Contract Nonr-225(24)
Project Leader: D. L. Epley
Staff: D. L. Starner

This project is a study of the relations between the combinational logic and state-behavior of sequential networks. The goal is a state assignment algorithm, capable of being programmed for a computer, which will handle medium-sized flow tables and capable of producing good results with the expenditure of a reasonable amount of computer time.

Technical Report No. 6203-1 by Duane L. Starner, dated August 1964, entitled "Some State-Assignment Techniques for Large Sequential Circuits," has been distributed and this project is now closed.

Project 6206: MULTI-TAPE SEQUENTIAL MACHINES

Tri-Service Contract Nonr-225(24)
Project Leader: D. Epley
Staff: C. A. Isberg

This project is an investigation of sequential machines with multiple input and output tapes, and their application to sequential transducers involving storage.

A final report is in preparation.

Project 6209: LOGICAL DESIGN OF FAST CIRCUITS

Tri-Service Contract Nonr-225(24)
Project Leader: D. A. Huffman
Staff: ----

The purpose of this project is the development of synthesis procedures by which the response time of logical circuits can be made as low as is theoretically possible. It has application to the design of all digital circuits including a wide variety of coding, control, and other information processing circuits in which the data is encoded in binary form.

This project was inactive the past quarter.

Project 6301: DEVELOPMENT OF SIMULATION FACILITY

Tri-Service Contract Nonr-225(24)
Project Leader: G. F. Franklin
Staff: Jim Kawakami

The purpose of this project is to report, from time to time, the changes and growth of the computer simulation facility available to SEL, maintained by the Systems Theory Group. The purpose of the facility is to permit experimental testing of control and filtering schemes, and data reduction from analog tapes.

Now available is the ability to read, rewind, and write on a 727 digital tape unit. New equipment additions to the facility include a 1/4 inch, 4 track tape recorder and another TR48 analog computer.

Project 6452: MODELING OF LINEAR SYSTEMS

Tri-Service Contract Nonr-225(24)
Project Leader: D. Luenberger
Staff: Lewis Meier

The purpose of the project is to investigate the logical formulations and solutions of the problem of approximating a given linear dynamic system by means of a linear dynamic system of lower order than in the model.

In the last quarterly report the constant coefficient linear approximation problem was defined and the following necessary conditions were derived:

$$G(d_i) = \sum_{j=1}^M \frac{c_j}{d_i + d_j} \quad (1a)$$

$$G'(d_i) = \sum_{j=1}^M \frac{c_j}{(d_i + d_j)^2} \quad (1b)$$

where

$G(s)$ = transfer function of given system

$$\hat{W}(t) = \sum_{l=1}^M c_l e^{-d_l t} = \text{impulse response of approximating system}$$

Equation (1a) was interpreted as follows:

$$G(d_i) = \hat{G}(d_i) \quad (2)$$

where $\hat{G}(s)$ is the transfer function of the approximating system. We may also interpret Eq. (1b) similarly as requiring

$$G'(d_i) = \hat{G}'(d_i) \quad (3)$$

where

$$G'(s) = \frac{dG(s)}{ds}$$

$$\hat{G}'(s) = \frac{d\hat{G}(s)}{ds}$$

During the preceding quarter this work was extended to cover a more general approximating problem where the criterion was minimizing the expected mean square error between the given and approximating systems when their input is a general stationary random process rather than white noise as considered before. The Phillips filter problem, which is the Wiener filter problem with a constraint on the number of dynamic elements, was also considered. In both cases two sets of necessary conditions were obtained very similar in form to Eqs. (1a) and (1b). In fact the solution to the Phillips filter problem is the best approximation to the Wiener filter in the above sense.

We note that both (1a) and (1b) are linear in the c_j 's so that either may be solved by inverting a matrix and then substituted into the other. The result is a highly nonlinear but rational equation for the d_j 's to satisfy. We chose to solve (1a) and substitute it into (1b) and use Newton's method to find iterative solutions of the result. In this manner if we start near the optimal values of the d_i 's we can converge to the optimum values.

The above results may be extended to the cases of complex and multiple roots in the approximating system.

It is hoped that within the next period research on this topic may be completed and the results written up in a report.

Project 6557: THEORY AND DESIGN OF NONLINEAR REACTANCE SUBHARMONIC GENERATIONS

Tri-Service Contract Nonr-225(24)
Project Leader: D. J. Grace
Staff: J. McConnell

A lumped model of the Linvill type has been developed for the junction diode which, when used in the numerical integration computer program, gives close agreement to experimentally observed subharmonic responses. In addition to verification of the mechanisms involved in the experimental circuit, the program and model have been used to illustrate transient buildup of the subharmonic responses and to give some indication of the principal effects of the losses in the diode.

The final report is in process of publication.

Project 6657: STUDIES OF THE DESCRIBING-FUNCTION METHOD OF NONLINEAR NETWORK ANALYSIS

Tri-Service Contract Nonr-225(24)

Project Leader: D. F. Tuttle

Staff: C. S. Burrus

This project is concerned with the analysis of lumped nonlinear circuits. In particular, methods of generating and evaluating approximate solutions are being studied. The original intent was to extend and expand the idea of a describing function. Recent developments, however, have led us to concentrate on the method described in the previous report, and below.

An iterative method for finding an approximate solution to a differential equation has been formulated. The procedure basically consists of finding a special driving function for an auxiliary linear system so that its response will approximate the true response of the nonlinear system. A degree of freedom is available in choosing this linear model, and this is the principal feature of the method. For a first-order equation, this freedom is in the form of a single parameter. The method converges for a wide range of parameter values, and it has been shown that when this parameter is set equal to zero, the method is the same as Picard's method of successive approximations. When the parameter is equal to one, the method is similar to the method of linear perturbations. For values between one and zero, the method becomes far more useful and generates approximate solutions in the form of

$$\tilde{x} = \sum_n \sum_m a_{mn} t^m e^{-\alpha_n t}$$

from an equation of the form $\dot{x} = f(x)$ where $f(x)$ is a polynomial.

An example initial-condition problem was worked for several parameter values, and the rates of convergence compared. It was found that the time interval of interest dictates the "best" parameter value to use.

In applying this method to a second-order equation, several problems have come up; they are primarily involved with choosing a linear model on which to perform the iterations. Equations of the type leading to elliptic

functions as solutions were examined and harmonic-balancing seemed to give very good results. Presently the relation between the Ritz and the Galerkin methods is being studied.

During the next quarter, the application of this procedure to the second-order problem, both driven and undriven, will be continued.

Project 6755: DIGITAL ADALINES

Army Contract DA04(200) AMC-57(Z)

Project Leader: B. Widrow

Staff: M. E. Hoff, Jr.

Present plans call for the construction of a digital Madaline using a high-speed ferrite-core memory. The overall system of the digital Madaline include a ferrite-core memory used to store the weights, a master control clock used to select the proper sequence for reading out the weight bits, a set of shifting accumulators each with a memory read-write circuit, and a computer link. Each shifting accumulator becomes one digital Adaline, performing summation, quantization, storing of the weight changes, and the adaptation of the weights. The computer link enables reading Adaline sums, reading weight values, writing patterns, writing initial weight values, and writing adaptation instructions. Most of the internal digital Adaline arithmetic will be 16-bit binary, so the computer link also includes a binary to B.C.D. converter and a B.C.D. to binary converter.

The complete memory stack, consisting of 16 32×32 ferrite-core memory planes, has been installed. The memory drivers, read-write circuits, and inhibit drivers have been tested and it appears that a one-microsecond memory cycle will be easily achieved. The memory sequence circuits have been completed and tested.

A prototype read-write amplifier and weight computation has been designed and constructed for the digital Adaline. This circuit must now be tested to insure proper performance of all functions. Among these functions are the receiving of data from the ferrite-core memory sense windings and the control of the memory inhibit drivers. When the weights are to be set to particular values or when the weights are to be changed in adaption, the circuit computes the new weight value and correspondingly controls the memory inhibit driver. Completion of the construction of these circuits (16 are required) will finish the memory circuits.

The B.C.D. to binary and binary to B.C.D. converters have been completed and tested. In each case the worst case conversion time is less than 100 microseconds. The average conversion time is approximately 60 microseconds. Thus this conversion will slow the reading of data by the computer by an average of only 20 percent, far less time than would be required to do the conversion in the computer.

The design of the Adaline arithmetic units is nearly complete, and design of the printed circuit cards will commence shortly. Completion of these circuits and the weight computation circuits described above will leave only the control link to the computer to be constructed.

Project 6762: MODEL-REFERENCED ADAPTIVE CONTROL SYSTEMS

Tri-Service Contract Nonr-225(24)
 Project Leader: B. Widrow
 Staff: R. Dressler

This research is concerned with model-referenced adaptive control systems. The model is assumed to be described by an nth-order, time-invariant, linear differential equation. The plant and its adaptive controller are described by an nth-order, time-varying, linear differential equation.

The equation for the model is:

$$\dot{\underline{Y}}(t) = \underline{F}_D \underline{Y}(t) + \underline{D}_D \underline{U}(t), \quad c(t) = \underline{M}_D^T \underline{Y}(t)$$

where, \underline{Y} = n-dimensional state vector

\underline{U} = r-dimensional input vector

C_D = scalar output

The equation for the plant and its adaptive controller is:

$$\dot{\underline{X}}(t) = [\underline{F}_D + \delta \underline{F}_S(t)] \underline{X}(t) + [\underline{D}_D + \delta \underline{D}_S(t)] \underline{U}(t), \quad c(t) = \underline{M}_D^T \underline{X}(t)$$

where, \underline{X} = n-dimensional state vector

\underline{U} = r-dimensional input vector

c = scalar output

δ = scalar constant.

The matrices F_{δ} and D_{δ} consist of the controller's adaptive parameters which are represented by the matrices F_A and D_A respectively, and the time-varying portion of the plant.

Adjustment of the adaptive parameters maintains the error $e(t)$ at approximately zero, (where $e = C - C_D$). The adaption equations have been derived analytically and yield the following for $f_{A_{ij}}$ and $d_{A_{kl}}$, which are elements of F_A and D_A respectively:

$$\dot{f}_{A_{ij}}(t) = -u_{F_{ij}} e(t) y_j(t)$$

$$\dot{d}_{A_{kl}}(t) = -u'_{D_{kl}} e(t) u_l(t)$$

where, y_j = model state variable

u_l = control variable.

The u' are adaptive gain constants and determine stability and rates of convergence for the adaptive system.

Project 6763: ADAPTIVE COMPUTER DIAGNOSIS OF ELECTROCARDIOGRAMS

Tri-Service Contract Nonr-225(24)

Project Leader: B. Widrow

Staff: Donald F. Specht

The purpose of this study is to discover, through adaptive pattern recognition techniques, a method of analyzing electrocardiograms with more accuracy than is presently obtained by the clinical diagnosis. This project is a continuation of an unsponsored project which resulted in a satisfactory method of separating normals from abnormal. Emphasis will now be placed on processing a sufficient number of cases for training of the adaptive computer so that the recognition rate of the machine will markedly exceed that of the present capability of human interpreters. An attempt will also be made to isolate the different diseases.

A report entitled "Vectorcardiographic Diagnosis Utilizing Adaptive Pattern Recognition Techniques," by D. F. Specht, has been prepared and

published. (TR 6763-1 SEL-64-045.) The report includes experimental results, a Madaline adapt procedure not previously published, and an efficient computer simulation program of a many-element Madaline which can accept analog inputs.

Research is being continued under this project which will lead to publishing a dissertation. Work will continue under the sponsorship of Lockheed Aircraft Corporation.

Project 6764: OPTICAL INPUTS TO COMPUTERS

Army Contract DA04(200) AMC-57(Z)
Project Leader: B. Widrow
Staff: K. Belser

The purpose of this project is the construction of a flying spot scanner and digital oscilloscope display to be run by the IBM 1620 computer. It will be used as a research tool to generate binary patterns from A-scope data or other patterns that may be samples from film.

The flying spot scanner equipment is now operational and information from film transparencies is being read into the IBM 1620 computer, and experiments in using such information are commencing.

Project 6766: CONDUCTION EFFECTS SUITABLE FOR ADAPTIVE DEVICES

Army Contract DA04(200) AMC-57(Z)
Project Leaders: B. Widrow and H. Heffner
Staff: G. Rosenberg

The purpose of this project is to examine the possibility of ionic conductivity in thin films of Al_2O_3 , having in mind an adaptive memory device.

This project will be closing with the issuance of a final report.

Project 6767: TWO-LAYER ADAPTION STUDIES

Army Contract DA04(200) AMC-57(Z)
Project Leader: B. Widrow
Staff: F. Glanz

The purpose of this project is to find and investigate the properties of procedures for training a network of Adalines and to study the generalizing properties of such networks.

During the past quarter a final report was started and the analysis of the Madaline generalization experiments described last quarter was carried further. A bound on the error curve for OR output logic has been obtained and comparison with the experimental data is being made. The analysis makes use of the hypersphere area approximation and several theorems from geometrical probability.

During the next month, the analysis will be worked on from two approaches, experiments will be conducted, and work on the final report will be continued.

Project 6772: PATTERN RECOGNIZING CONTROL SYSTEMS

Air Force Contract AF33(657)-11586
Project Leader: B. Widrow
Staff: E. Fraser

The objective of this project is the investigation of the feasibility and properties of a threshold logic controller for a dynamic system of given order. Specifically, the question is whether such a controller may be trained to a configuration that will yield stable over-all system operation regardless of the initial state of either the controller or the dynamic system. This is to be accomplished by the simplest means possible.

A final report for the project is in preparation.

Project 6773: CONVERGENT AUTOMATIC SYNTHESIS PROCEDURES FOR SEQUENTIAL SAMPLED-DATA NETWORKS WITH FEEDBACK

Army Contract DA04(200) AMC-57(Z)
Project Leader: B. Widrow
Staff: P. Mantey

The purpose of this research is to develop convergent automatic synthesis procedures for sequential sampled-data networks with feedback. Conditions are obtained for insuring the stability of these networks, and their optimality according to some performance criterion. The uses of such procedures are two fold: first, for the automatic synthesis of sampled-data networks with feedback; and second, to make possible self-optimization (self-adaption) of adaptive sampled-data feedback networks

in real time, utilizing performance feedback, and therefore capable of following non-stationary inputs. In this context, an adaptive network is defined as one whose variable parameters are to be adjusted in order to minimize some chosen performance criterion. The investigation is concerned both with the techniques for adaptation, and with the performance measures used in the automatic synthesis.

A final thesis report on this project is in publication.

Project 6950: THRESHOLD LOGIC ELEMENTS AND ADAPTIVE SYSTEMS

Tri-Service Contract Nonr-225(24)

Project Leader: R. Mattson

Staff: G. Masters

This project investigates the area of sequential switching circuits which use adaptive threshold logic as the basic building block.

This quarter's efforts have been directed toward a possible use of sequential machines as buffers to provide a better match between slow-speed computer auxiliary equipment and high-speed computers. The redundancy and finite length of data to be operated on is used to recode and compress the actual amount of data to be stored. A sequential machine can then be used to decode and regenerate the original sequence.

Project 6952: A STUDY OF ADAPTIVE INPUT-CODING TECHNIQUES

Tri-Service Contract Nonr-225(24)

Project Leader: R. L. Mattson

Staff: J. D. Chang

This project is concerned with a study of quantizing the analog inputs of a threshold logic unit so that some nonlinearly separable functions of analog variables can be realized.

Work during the last quarter was mainly devoted to the investigation on parallel quantization. It has been found that there always exists a weight vector which maps a given finite set of vectors into a line distinctly or unambiguously. Therefore parallel quantization is always possible for any nonlinear function defined on a finite set of vectors.

A transformation which has some desirable properties has been found also. This transformation is a linear 1-1 (or unambiguous) mapping for the given set of vectors. It can keep the order of images on a line generally in agreement with the order of images mapped by a given weight

vector. Therefore, if a rough idea about where the locations of the images should be is known, this transformation will enable us to find a weight vector which maps the given set of vectors distinctively (or unambiguously) yet the order of the images will follow approximately a preassigned manner.

By using this transformation, it can be shown that the problem of finding a desirable weight vector can be decomposed into a problem of finding a set of weight vectors. The resulting weight vector is equal to a decimally weighted sum of all these weight vectors.

A desirable manner of distribution of the images on a line is the distribution which has minimum number of transitions (i.e., a change from the image of a 1-vector to the image of a 0-vector or vice versa) on that line. This is because the number of transitions relates proportionally to the number of thresholds needed in the parallel quantization. The number of transitions depends upon the particular weight vector used. A method of minimizing the number of transitions has been developed. This method maximizes the distance between the two images of the two centers of gravity of input vectors subject to the constraint that the maximum deviation among the images from the center of gravity is minimum. Although it does not guarantee the minimum number of transitions* always, experimental results show that it does so for most of the times.

In order to make the mapping unambiguous and to further reduce the number of transitions, those images of a different kind that fall on the same point must be pushed in a desired manner by additional weight vectors. For some cases, this cannot be done so ideally. A method of determining the second best manner is necessary. So far, there is no effective method of doing this. An investigation on this matter will be the work for the following quarter.

* Those images of vectors of different kinds that fall on the same point on the line will not be considered during a count of the number of transitions.

Project 7050: COMMUNICATION THEORY

Tri-Service Contract Nonr-225(24)

Project Leader: T. Kailath

Staff: J. Omura, M. Gyi, D. Cogswell,
J. Blumenthal

The purpose of this project is to study basic problems in detection theory, with particular reference to time-variant channels.

A. SINGULAR DETECTION

In a previous summary we described some results on the singular detection of a known signal in gaussian noise. We have been studying similar problems for the detection of gaussian signals in gaussian noise. We have obtained some simple tests for singular detection and also closed-form expressions for the likelihood ratio in several cases.

B. MODULATION TECHNIQUES

To evaluate the SNR-improvement properties of a particular signal processing scheme, it has been necessary to study the transformation of a combination of sine waves by a limiter. M. Gyi has obtained a simple general formula which specializes to the results of Middleton and Jones (Trans. IRE PGIT, Jan 1963) in special cases.

C. HELLINGER DISTANCE

T. L. Grettenberg (SU TR-2004-4) has examined the use of the divergence $[J(1,2) = E_1[\ell(x)] - E_2[\ell(x)]]$, where $\ell(x)^1$ is the logarithm of the likelihood ratio and E_i denote expectations under the two hypothesis $h^{(i)}$ as a tool for signal design. We have recently examined the Hellinger distance as a similar tool.

The Hellinger distance is defined by

$$h(p_1, p_2) = \int_{-\infty}^{\infty} \sqrt{p_1(x)p_2(x)} dx$$

The Hellinger distance has many properties in common with the divergence. For example, Bradt and Karlin [Ann. Math. Stat., 1956] showed that if for two signal sets, α and β say, $J\alpha > J\beta$, then for some choice of prior probabilities $P_{e\alpha} < P_{e\beta}$, where $P_{e\alpha}$ is the probability of error for signal set α . A similar theorem holds for the Hellinger distance.

However, the Hellinger distance appears to be superior to the divergence in many respects. Thus in an example of random signal selection [Grettenberg SU-2004-2, also Trans. IRE-PGIT, Oct 1963] the divergence criterion yields a nonoptimum signal set, while use of the Hellinger distance yields an almost optimum set (cf. Pierce Trans. IRE-PGCS, June 1961). For high SNR or low P_e , we get the optimum set (cf. Pierce, op. cit.). The probability of error can be bounded in terms of h ,

$$1 - \sqrt{1 - h^2} \leq P_e \leq h.$$

The upper bound appears to be exponentially good for low P_e . In fact, it is interesting to note that Gallager's expurgated error exponent, $E_{\text{exp}}^{(0)}$, (cf. Trans. IRE-PGIT, Jan 1965) is just the average Hellinger distance for a signal set. The lower bound is not very tight, except when $h = 0$, which corresponds to singular detection.

We are studying applications of the Hellinger distance to a variety of signal selection problems.

Project 3550: METEOR ECHO PROPERTIES

Tri-Service Contract Nonr-225(24)
Project Leader: L. A. Manning
Staff: ----

The purpose of this project is to elucidate the mechanism of radio reflections from meteor ionization trails, and to use meteoric echoes to investigate physical processes in the lower ionosphere.

Active research on this project ceased with the preparation of a report entitled "The Relation of Wind Profile Statistics to Meteoric Echo Properties." The report has not yet completed the publication process.

Project 3606: IONOSPHERIC WINDS AND IRREGULARITIES IN ELECTRON DENSITY IN THE IONOSPHERE

Tri-Service Contract Nonr-225(24)
Project Leaders: A. M. Peterson and V. R. Eshleman
Staff: R. Nowak, A. A. Burns, and D. D. J. Fang

It appears possible that the winds may provide the driving force for generation of some large-scale irregularities such as sporadic-E patches, and the small-scale magnetic-field-aligned irregularities which cause auroral and "northscatter" radio echoes. Some years ago at Stanford, a relationship was found between sporadic-E patches and E-layer-height field-aligned irregularities. It also appears possible that localized ionospheric current systems may be generated by winds blowing ionization patches across the magnetic field. The recent theoretical work of Buneman and others has shown that streaming electrons in ionospheric current systems can, under certain conditions, cause growing acoustic waves to develop. The acoustic waves in turn cause the equivalent to field-aligned irregularities which can be observed by radar means. Data are available at Stanford from past and presently operating experiments, which provide most of the inputs required for this study.

A technique has been investigated during this period for measuring wind shears in the E region of the ionosphere by the observation of drifting meteor trails. This study indicates that considerable accuracy can be obtained in the shear measurements by the installation of a displaced receiver working in conjunction with the central radar.

For such a measurement, use would be made of the fact that the signal reflected to the receiver at the radar site and the signal reflected to the remote receiver are specularly reflected from the long straight meteor ionization trail. The distance between the two specular reflection points is fixed by geometry and the time to traverse this distance is a function of the velocity of the meteorite. This displaced receiver only needs to measure the time at which the meteor passes the specular reflection point and the wind doppler produced at that height. This information must be returned to the radar site in order that it may be compared with the corresponding information at the radar. Using this information the difference in time (Δt) for the passage of the specular reflection points can be determined as well as the wind doppler at the two sites.

Additional information which must be measured at the radar site include the azimuth angle, range, and velocity of the meteor. As an example of the use of this method for measurement of shears, it has been found that the height difference measurement of the two reflection points can be found to an accuracy of about one kilometer.

If measurements of this type prove feasible in practice, they may permit the checking of the hypothesis that wind shears are responsible for the growth of sporadic-E ionization patches. In this model horizontal wind shear leads to vertical movement of ions and electrons which give rise to the formation of thin layers of ionization.

As noted above, echoes from field aligned irregularities have been observed to occur simultaneously with the sporadic-E patch formation (R. D. Egan and A. M. Peterson, "Backscatter Observations of Sporadic E," Ionospheric Sporadic E, ed. by Smith and Matsushita, Pergamon Press, 1962). Thus wind shear measurements might help to indicate the generation mechanism for both sporadic E and field-aligned irregularities.

QUARTERLY RESEARCH REVIEW
DISTRIBUTION LIST
February 1965

GOVERNMENT

<u>U.S. Army</u>	Director	Office Chief of R and D
Commanding Officer	U.S. Army Combat Dev. Command	Dept. of the Army
USAEI	Communications Electronics Agency	3045 Columbia Pike
	Bldg. 410	Arlington 4, Va.
	1 Ft. Monmouth, N.J.	1 Attn: Mr. L.H. Geiger, Res. Planning Div.
Ft. Monmouth, N.J.	Tech. Library	
1 Attn: Director of Research	OASD (R and E)	U.S. Army Engineer R and D Labs
3 Attn: Chief, Tech. Info. Div.	Rm. 3E1065, The Pentagon	1 Ft. Belvoir, Va.
1 Attn: Chief, Physical Elec. Br., SS and Freq. Cont. Div.	1 Washington 25, D.C.	1 Attn: Tech. Doc. Center
1 Attn: Chf., Circuit Functions Br., SS and Freq. Cont. Div.	Office of Chief of Ordnance	Comm. General
1 Attn: W. Matthei, Solid State and Freq. Cont. Div.	Dept. of the Army	U.S. Army R and D Activity
1 Attn: Rpt. Dist. Unit, SS and Freq. Cont. Div.	Washington 25, D.C.	1 Ft. Huachuca, Arizona 85613
1 Attn: Dir., SS and Freq. Cont. Div.	1 Attn: ORDTX-AR	
4 Attn: A.P. LaRocque, SS and Freq. Cont. Div.	Deputy President	Signal Corps Liaison Office, MIT
	U.S. Army Security Agency Board	77 Mass. Ave., Bldg. 26-131
	Arlington Hall Station	Cambridge, Mass.
	1 Arlington 12, Va.	1 Attn: A.D. Bedrosian
1 Attn: AMSEL-RD-DR	Commanding General	CO, U.S.A. Ordnance Missile Comm.
1 Attn: AMSEL-RD-X	U.S. Army Combat Dev. Command	1 Redstone Arsenal, Ala.
1 Attn: AMSEL-RD-XE	Ft. Belvoir, Va.	1 Attn: Tech. Library
1 Attn: AMSEL-RD-XC	1 Attn: CDCMR-E	
1 Attn: AMSEL-RD-XS	CO, U.S.A. Comm. and Electronics	Commander, Army Ord. Missile Command
1 Attn: AMSEL-RD-N	Combat Dev. Agency	Redstone Arsenal, Ala.
1 Attn: AMSEL-RD-NR	1 Ft. Huachuca, Arizona	1 Attn: ORDKM-RFE, Mr. Lindberg
1 Attn: AMSEL-RD-NE		
1 Attn: AMSEL-RD-ND	Director, Ft. Monmouth Office	CO, Frankford Arsenal
1 Attn: AMSEL-RD-NP	U.S.A. Comm. and Electronics	Philadelphia 37, Pa.
1 Attn: AMSEL-RD-S	Combat Dev. Agency	1 Attn: ORDBA-1520
1 Attn: AMSEL-RD-SA	1 Ft. Monmouth, N.J.	
1 Attn: AMSEL-RD-SE	CO, U.S.A. Elec. Materiel Sup. Agcy.	CO, Frankford Arsenal Library Br.
1 Attn: AMSEL-RD-SR	Ft. Monmouth, N.J.	0270, Bldg. 40
1 Attn: AMSEL-RD-SS	1 Attn: SELMS-ADJ	Bridge and Tacony Streets
1 Attn: AMSEL-RD-P		1 Philadelphia 37, Pa.
1 Attn: AMSEL-RD-PE	CO, U.S.A. Missile Command	CO, Watertown Arsenal
1 Attn: AMSEL-RD-G	Redstone Arsenal, Ala.	Watertown, Mass.
1 Attn: AMSEL-RD-GF	1 Attn: Tech. Library	1 Attn: OMRO
1 Attn: AMSEL-RD-GD		1 Attn: U.S.A. Mat. Res. Agency
1 Attn: AMSEL-RD-FU-1	CO, U.S.A. Materiel Command	
1 Attn: AMSEL-RD/PR (Mr. Garoff)	Washington 25, D.C.	Director
1 Attn: AMSEL-RD/PRG (Mr. Zinn)	1 Attn: R and D Directorate	Ballistics Res. Lab
1 Attn: AMSEL-RD/PRT (Mr. Kaplan)	1 Attn: AMCRD-RS-PE-E	1 Aberdeen Proving Ground, Md.
1 Attn: AMSEL-RD/PRM, Rec. File Cy.		1 Attn: V.W. Richard, BML
5 Attn: AMSEL-RD/SL-SC	Commander, Frankford Arsenal	CO, U.S.A. Sig. Missile Sup. Agcy.
1 Attn: AMSEL-RD/SL-PRM	Philadelphia, Pa. 19137	White Sands Missile Range, N.M.
1 Attn: AMSEL-RD/SL-PA	1 Attn: Dr. Sidney Ross, 1310-64-4	1 Attn: SIGWS-MEW
1 Attn: Dir. of Res. (H.A. Zahl)		
1 Attn: ASRNE	CO, U.S.A. Sig. Mat. Sup. Agency	Commanding Officer
1 Attn: Tech. Doc. Center	Ft. Monmouth, N.J.	U.S. Army Electronics R and D Activity
1 Attn: AMSEL-RD/SL-ADT-E	1 Attn: SIGMS-ADJ	1 White Sands, N.M.
1 Attn: AMSEL-RD/SL-ADT		
2 Attn: Communications Dept.	U.S.A. Materiel Command Proj. Off.	CO, U.S.A. Elec. Proving Ground
1 Attn: AMSEL-RD/SL-PEP	Redstone Arsenal, Ala.	Ft. Huachuca, Ariz.
1 Attn: AMSEL-RD/SL-TNR	1 Attn: AMCPM-ZER-R	1 Attn: Tech. Library
1 Attn: Data Equip. Br.		
1 Attn: AMSEL-RD/SL-PF (Dr. Jacobs)	Engineering Procedures Br.	Dept. of the Army
1 Attn: AFSC Scientific/Tech. Liaison Office	U.S.A. Sig. Mat. Sup. Agency	Office, Chf. of R and D
1 Attn: Marine Corps Liaison Office	Ft. Monmouth, N.J.	Rm. 3D442, The Pentagon
AMSEL-RD/LNR	1 Attn: Millard Rosenfeld	Washington 25, D.C.
1 Attn: Corps of Engrs. Liaison Off.		1 Attn: Res. Support Div.
1 Attn: Logistics Div., AMSEL-RD/PRM	DST, USASCS	
1 Attn: AMSEL-RD/PSM (Mr. Katzman)	Ft. Monmouth, N.J.	CO, U.S.A. Res. Office (Durham)
	1 Attn: Mr. H. Allem	Box CM, Duke Station
CO. U.S. Army Signal Equip. Sup. Agcy.		Durham, N.C.
1 Ft. Monmouth, N.J.	U.S. Army Research Office	15 Attn: CRD-AA-IP
	3045 Columbia Pike	1 Attn: Dr. H. Robl
Chief Signal Officer	Arlington, Va.	
Dept. of the Army	1 Attn: Physical Sciences Div.	Commanding Officer
Washington 25, D.C.		Limited Warfare Lab.
1 Attn: SIGRD		Aberdeen Proving Ground
		Aberdeen, Md. 21005
		1 Attn: Tech. Dir.

CO, U.S.A. Electronics Command
Ft. Monmouth, N.J.
3 Attn: AMSEL-RD

Chief, Library Br.
Office of Chief of Engineers
Dept. of the Army
1 Washington 25, D.C.

OASD (R and E)
Rm. 3C-128, The Pentagon
Washington 25, D.C.
1 Attn: Tech. Library

Commanding Officer
Harry Diamond Labs.
Connecticut Ave. and Van Ness St., N.W.
1 Washington, D.C.

Director
Advanced Res. Projects Agency
1 Washington 25, D.C.

Commanding Officer
U.S. Army Security Agency
1 Washington 25, D.C.

U.S. Navy

Chief of Naval Research
Dept. of the Navy
Washington 25, D.C.
2 Attn: Code 437, Info. Syst. Br.
2 Attn: Code 427
1 Attn: Code 420

CO, ONR Branch Office
495 Summer St.
1 Boston 10, Mass.

CO, ONR Branch Office
1000 Geary St.
1 San Francisco 9, Calif.

Chief Scientist, ONR Br. Office
1030 E. Green St.
1 Pasadena, Calif.

ONR Branch Office
219 S. Dearborn St.
1 Chicago, Ill. 60604

CO, ONR Branch Office
207 W. 24th St.
1 New York 11, N.Y.

Officer-in-Charge
Office of Naval Research
Navy 100, Box 39
Fleet P.O.
16 New York, N.Y.

U.S. Naval Applied Science Lab.
Bldg. 291, Naval Base
Brooklyn, N.Y. 11251
1 Attn: Tech. Library, Code 9832

Director, Naval Research Lab.
1 Washington 25, D.C.
1 Attn: Code 5204 (G. Abraham)
1 Attn: Code 6430
6 Attn: Code 2000
1 Attn: Code 2027
1 Attn: Code 5200
1 Attn: Code 5266-GA
1 Attn: Code 5240
1 Attn: Code 5260
1 Attn: Code 5300
1 Attn: Code 5400
1 Attn: Code 5430

Chief. Bureau of Ships
Dept. of the Navy
2 Washington 25, D.C.
1 Attn: Code 732, A.E. Smith
1 Attn: Code 335
1 Attn: Code 684A, R.H. Jones
1 Attn: Code 681A
1 Attn: Code 686
1 Attn: Code 687E
1 Attn: Code 687D
1 Attn: Code 681A1D
1 Attn: Code 607 NTDS
1 Attn: Code 607A, Cdr. E.B. Mahinske
1 Attn: Code 681A1A, A.H. Young
1 Attn: Code 681A-1
3 Attn: Code 670B
1 Attn: Code 691A1

Chief. Bur. of Naval Weapons
Dept. of the Navy
Washington 25, D.C.
1 Attn: RREN-3
1 Attn: RAAV-44
1 Attn: RAAV-6
1 Attn: ASM Detection and Cont. Div.
1 Attn: RUDC-1
1 Attn: RMWC Missile Weapons Cont. Div.
1 Attn: DIS-31
1 Attn: RAAV, Avionics Div.

Chief of Naval Operations
Dept. of the Navy
Washington 25, D.C.
1 Attn: Op-07T-12
1 Attn: Code Op 94T
1 Attn: Code Op-352
1 Attn: Op-945Y

U.S. Naval Weapons Lab.
Dahlgren, Va.
1 Attn: Tech. Library
1 Attn: G.H. Gleissner, Hd., Comp. Div.
1 Attn: Comp. and Analysis Lab.

U.S. Naval Ordnance Lab
Corona, Calif.
1 Attn: R. Conger, 423
1 Attn: H.H. Wieder, 423
1 Attn: Library

AFSC Scientific-Tech. Liaison Off.
U.S. Naval Air Dev. Center
1 Johnsville, Pa.

CO, U.S. Naval Ordnance Lab
Silver Spring, Md.
1 Attn: Library

Ballistic Res. Labs
Aberdeen Proving Ground, Md.
1 Attn: K.A. Pullen
1 Attn: Chief, Computer Res. Br.

Commander
U.S. Naval Missile Center
Pt. Mugu, Calif.
1 Attn: Code N3232
1 Attn: Code N03022

Navy Dept.
U.S. Naval Avionics Facility
Indianapolis 18, Ind.
1 Attn: Station Library

CO and Director
U.S. Naval Electronics Lab
San Diego 52, Calif.
1 Attn: Library

U.S. Naval Post Grad. School
Monterey, Calif.
1 Attn: Tech. Repts. Librarian
1 Attn: Prof. Gray, Elec. Dept.
1 Attn: Dr. Harold Titus

Weapons System Test Div.
Naval Air Test Center
Patuxent River, Md.
1 Attn: Library

CO (ADL)
U.S. Naval Air Dev. Center
1 Johnsville, Pa. 18974

U.S. Air Force

Chief of Staff
U.S. Air Force
Washington 25, D.C.
1 Attn: AFDR-ER

U.S. Army Signal Liaison Off.
Aeronautical Systems Div.
Wright-Patterson AFB, Ohio
1 Attn: ASDL-9

Commander, ASD
Wright-Patterson AFB, Ohio
1 Attn: SEQSS
1 Attn: ASRNC-21
1 Attn: ASRNC-23
1 Attn: ASRNC-3
1 Attn: ASRNRD
6 Attn: ASRNE-32
1 Attn: Electronic Res. Lab (ASRNEA)
1 Attn: ASRNE-2 (Lt. Col. L.M. Butsch)
1 Attn: ASRNR-32
2 Attn: ASRNEM
2 Attn: ASRNET
1 Attn: ASNPRS-5
1 Attn: ASRNC-23
1 Attn: ASRNC-1

Air Force Avionics Lab, ASD
Wright-Patterson AFB, Ohio
1 Attn: D.R. Moore, Bionics Br. AVTB

Systems Engr. Group (RTD)
Wright-Patterson AFB, Ohio 45433
1 Attn: SEPIR
1 Attn: SEPI

Commandant
AF Inst. of Technology
Wright-Patterson AFB, Ohio
1 Attn: AFIT (Library)

Executive Director
AF Office of Scientific Res.
1 Washington 25, D.C.

School of Aerospace Medicine Div.
(AFSC)
USAF Aerospace Medical Center, ATC
Brooks AFB, Texas
1 Attn: SMAP

AFWL (WLL)
1 Kirtland AFB, N.M.

Commander
Air Proving Ground Command
Eglin AFB, Fla.
1 Attn: APGTRI (Tech. Library)

Commander
AF Missile Dev. Center
Holloman AFB, N.M.
1 Attn: MDR

Director, Air University Lib.
Maxwell AFB, Ala.
1 Attn: CR 4582

Commanding General
Rome Air Dev. Center
Griffiss AFB, Rome, N.Y.
1 Attn: RAALD
1 Attn: RAWCL
1 Attn: Doc. Lib (EMLAL-1)
1 Attn: EMAS/J. Fallik
1 Attn: (EMICE) T.J. Domurat
1 Attn: L. Sues (EMIAD)
1 Attn: Haywood Webb(RAWE)
1 Attn: RCLMA, J. Dove
1 Attn: RAOL
1 Attn: RAWED

Commanding General
AF Cambridge Res. Labs
Air Res. and Dev. Command
L.G. Hanscom Field
Bedford, Mass.
1 Attn: CRB
1 Attn: CROTLR-2
1 Attn: CCRR
1 Attn: CCSD
1 Attn: CRZC
1 Attn: CRXL-R, Res. Library
1 Attn: CRXL, Scientific Library
1 Attn: CRTOTI-2, Electronics
1 Attn: Dr. L.M. Hollingsworth,
Dir., Elec. Res. Directorate
1 Attn: CRW
1 Attn: Mr. Lawrence C. Mansur (CRW)

Data Sciences Lab (CRB)
AFCRL
L.G. Hanscom Field
Bedford, Mass.
1 Attn: Dr. Zschirnt, Sr. Scientist

Commander
AF Ballistic Missile Div.
Hq., Air Res. and Dev. Command
USAF, AF Unit P.O.
Los Angeles, Calif.
1 Attn: WDLPM-1-TDC

Hq., AFSC
Andrews AFB
Washington 25, D.C.
1 Attn: SCSEI
1 Attn: SCTAE

Hq., USAF, (AFRSTB)
1 Washington, D.C. 20330

Electronic Systems Div. (AFSC)
Scientif and Tech. Info. Div.
L.G. Hanscom Field
Bedford, Mass.
1 Attn: ESTI

AFSC Scientific and Tech. Liaison Off.
111 E. 16th St.
1 New York 3, N.Y.

AF Office of Scientific Res.
Washington 25, D.C.
1 Attn: Code SRPP
1 Attn: Code SREE

Foreign Technology Div.
Wright-Patterson AFB, Ohio
1 Attn: TD-C1 (T.M. Hay, Jr.)
1 Attn: TD-CIB
1 Attn: TD-E1

Commerce and Miscellaneous

U.S. Atomic Energy Commission
Division of Research
Washington 25, D.C. 20545
1 Attn: Mr. William C. Gaugh

Atomic Energy Commission
Project Matterhorn
1 Princeton, N.J.

San Francisco Ordnance Dist.
Basic Res. and Special Proj. Br.
P.O. Box 1829, 1515 Clay St.
Oakland 12, Calif.
1 Attn: Mr. M.B. Sundstrom, Chief

NASA
Lewis Research Center
21000 Brook Park Rd.
Cleveland, Ohio 44135
1 Attn: Clifford K. Swartz,
Solar and Chemical Power Br.

NASA
G.C. Marshall Space Flight Center
Huntsville, Ala.
1 Attn: M-G and C-R

NASA
Langley Research Center
Langley Station
Hampton, Va.
2 Attn: Technical Library

NASA
Goddard Space Flight Center
Greenbelt, Md.
1 Attn: C.H. Ehrmann, Code 611.5
1 Attn: Chief, Data Systems Div.

NASA
Washington, D.C. 20546
1 Attn: Dr. H. Harrison

Asst. Secy. of Def. for Res. and Eng.
Information Office Library Br.
The Pentagon
2 Washington 25, D.C.

David Taylor Model Basin
Washington 7, D.C.
1 Attn: Technical Library

Census Bureau
Washington 25, D.C. 20233
Rm. 3183
FOB No. 3
1 Attn: Mr. J.L. McPherson

Program Director
Engineering Section
National Science Foundation
1 Washington 25, D.C.

U.S. AF Security Service
San Antonio, Texas
1 Attn: ODC-R

National Bureau of Standards
Washington 25, D.C.
1 Attn: R.D. Elbourn
1 Attn: S.N. Alexander, Info. Tech. Div.
1 Attn: Librarian

National Security Agency
Ft. George G. Meade, Md.
1 Attn: Howard Campaigne

Diamond Ordnance Fuze Lab
Washington 25, D.C.
1 Attn: Library
2 Attn: Dr. R.T. Young, ORDTL-930
1 Attn: T.M. Liimatainen

Asst. Secy. of Def. (R and D)
Research and Dev. Board
Dept. of Defense
Washington 25, D.C.
1 Attn: Tech. Library

Office of Dir. of Def. (R and E)
Dept. of Defense
Washington 25, D.C.
1 Attn: Office of Electronics

Department of Defense
Defense Communications Agency
Washington 25, D.C.
1 Attn: Code 121A, Tech. Library

Institute for Defense Analyses
400 Army-Navy Dr.
Arlington, Va. 22202
1 Attn: W.E. Bradley

Director
Weapons System Evaluation Group
Rm. 1E875, The Pentagon
1 Washington 25, D.C.

Central Intelligence Agency
Washington 25, D.C.
1 Attn: OCR Standard Dist.

Advisory Group on Electron Devices
346 Broadway, 8th Floor East
New York 13, N.Y.
2 Attn: Harry Sullivan

Advisory Grp. on Reliability of
Electronic Equipment
Office, Asst. Secy. of Defense
The Pentagon
2 Washington 25, D.C.

U.S. Dept. of Commerce
National Bureau of Standards
Boulder, Colorado
1 Attn: Library
2 Attn: Miss J. Lincoln, Chief,
Radio Warning Services Sec.
1 Attn: Central Radio Prop. Lab

The Director
U.S. National Bur. of Standards
Washington 25, D.C.
1 Attn: Sec. 425.01, Mr. G. Shapiro

Director
National Security Agency
Ft. George G. Meade, Md.
1 Attn: R-31
1 Attn: C-15
1 Attn: R-42, Mr. Bartlett
2 Attn: R-304
2 Attn: C3/TDL, Rm. 2C087

Chief, U.S. Army Security Agency
Arlington Hall Station
2 Arlington 12, Va.

Co, Harry Diamond Labs
Conn. Ave. and Van Ness St., N.W.
Washington 25, D.C.
1 Attn: Library, Rm. 211, Bldg. 92

Marine Corps Liaison Office
Bay 4D119, Hexagon
1 Ft. Monmouth, N.J.

Army Liaison Office
Lincoln Lab., P.O. Box 73
1 Lexington, Mass.

U.S. Coast Guard
1300 E St., N.W.
Washington 25, D.C.
1 Attn: EEE, Sta 5-5

Chief, Input Section
Clearinghouse for Federal Scientific
and Technical Information, CFSTI
SILLS Building
5285 Port Royal Rd.
1 Springfield, Va. 22151

Advanced Res. Projects Agency
Office of Secy. of Defense
Washington 25, D.C.
1 Attn: Lt. Col. Wm. B. Lindsay

U.S. Army Electronics Labs
Mt. View Office
P.O. Box 205
1 Mt. View, Calif.

CO, 9560 TSU
U.S. Army Signal Elec. Res. Unit
P.O. Box 205
1 Mt. View, Calif.

AF Systems Comm. Sci. and Tech.
Liaison Office
Los Angeles Air Force Station
Air Force Unit Post Office
1 Los Angeles, Calif. 90045

DDC
Cameron Station
Alexandria, Va.
20 Attn: TISIA

Aerospace Res. Labs
Office of Aerospace Research, USAF
Wright-Patterson AFB, Ohio 45433
1 Attn: ARH

Scientific and Tech. Info. Facility
P.O. Box 5700
Bethesda, Md. 20014
1 Attn: NASA Rep. (SAK/DL)

Universities

School of Engr. Sciences
Arizona State Univ.
Tempe, Arizona
1 Attn: Prof. Spragins

Univ. of Arizona
EE Dept.
Tucson 25, Arizona
1 Attn: Robert L. Walker
1 Attn: Dr. Douglas J. Hamilton
1 Attn: F.A. Lindholm, Assoc. Prof.

U. of Calif. at Los Angeles
Dept. of Engr.
Los Angeles, Calif.
1 Attn: Prof. Gerald Estrin

Calif. Inst. of Technology
Dept. of EE
Pasadena, Calif.
1 Attn: Prof. R.W. Gould
1 Attn: David Braverman
1 Attn: P.C. Samazan

Calif. Inst. of Technology
Jet Propulsion Lab
4800 Oak Grove Dr.
Pasadena 3, Calif.
1 Attn: Documents Library
1 Attn: A.I. Bryan, Sr. Dev. Engr.

U. of California
Dept. of EE
Berkeley 4, Calif.
1 Attn: Prof. J.R. Singer
1 Attn: Prof. R.M. Saunders

U. of California
Electronics Res. Lab
Berkeley 4, Calif.
1 Attn: D.J. Angelakos
1 Attn: T. Van Duzer, Asst. Prof.

U. of California
Lawrence Rad. Lab, Tech. Info. Div.
Bldg. 30, Rm. 101
Berkeley, Calif. 94720
1 Attn: Dr. R.K. Wakerling

U. of California
Lawrence Radiation Lab
Engr. Lib., Bldg. 90/Rm. 2056
Berkeley, Calif. 94720
1 Attn: L.D. Stephens

U. of California
Tech. Info. Div.
Lawrence Radiation Lab
P.O. Box 808
1 Livermore, Calif.
1 Attn: Radiation Lab

Univ. of California
EE Dept.
Santa Barbara, Calif.
1 Attn: Prof. M. Cowley

Univ. of California
Dept. of Engineering
Los Angeles 24, Calif.
1 Attn: C.T. Leondes, Prof. of Engr.

Univ. of California
College of Engineering
Electromagnetics Division
Los Angeles 24, Calif.
1 Attn: R.S. Elliott

Univ. of California, San Diego
Dept. of Aerospace Engr.
La Jolla, Calif.
1 Attn: Dr. S.S. Penner

Carnegie Inst. of Technology
EE Dept.
Schenley Park
Pittsburgh 13, Pa.
1 Attn: Dr. E.M. Williams

Case Institute of Technology
Engineering Design Center
Cleveland 6, Ohio
1 Attn: Dr. J.B. Neswick, Dir.

The University of Chicago
Institute for Computer Research
Chicago 37, Ill.
1 Attn: N.C. Metropolis, Dir.

Univ. of Chicago
Lab for Applied Sciences
Museum of Science and Industry
Chicago 37, Ill.
1 Attn: Library

Columbia University
Dept. of Physics
New York 27, N.Y.
1 Attn: Prof. L. Brillouin
1 Attn: Columbia Radiation Lib.

Columbia University
Columbia Radiation Lab
538 W. 120th St.
New York, N.Y.
1 Attn: D.L. Harrow

Cornell University
Cognitive Sys. Res. Program
Hollister Hall
Ithaca, N.Y.
1 Attn: Dr. E.F. Rosenblatt

Cornell University
Aerospace Engineering
Grumman Hall
1 Ithaca, N.Y.

DePaul University
1215 W. Fullerton Ave.
Chicago, Ill. 60614
1 Attn: Dr. Julius J. Huppert,
Prof. of Physics

Drexel Institute of Technology
Dept. of Elec. Engr.
Philadelphia 4, Pa.
1 Attn: Mr. F.B. Haynes

University of Florida
Dept. of Elec. Engr.
1 Gainesville, Fla.
1 Attn: Prof. W.E. Lear
1 Attn: M.J. Wiggins

George Washington University
School of Engineering and Appl. Sci.
Washington, D.C. 20006
1 Attn: Nelson T. Grisamore,
Asst. Dean (Research)

Georgia Institute of Tech.
Atlanta, Ga. 30332
1 Attn: Library
1 Attn: F. Dixon, Engr. Exper. Sta.

Harvard University
Gordon McKay Library, Tech. Rpts.
Pierce Hall
2 Cambridge, Mass.

Harvard University
Pierce Hall 217
Cambridge 38, Mass.
1 Attn: Div. of Eng. and Appl. Phys.,
Dean Harvey Brooks

University of Hawaii
Honolulu 14, Hawaii
1 Attn: Mr. Kazutoshi Najita, Asst.
Prof. Elec. Engr. Dept.
1 Attn: Dr. Paul C. Yuen, Asst. Prof.
Elec. Engr. Dept.

Univ. of Illinois
Gaseous Electronic Lab
607 E. Healy
Champaign, Ill.
1 Attn: Dr. L. Goldstein

Univ. of Illinois
Dept. of Elec. Engr.
Urbana, Ill.
1 Attn: Antenna Lab
1 Attn: William Perkins
1 Attn: Paul D. Coleman, Rm. 218

Univ. of Illinois
Dept. of Physics
Urbana, Ill.
1 Attn: Dr. John Bardeen

Univ. of Illinois
Digital Computer Lab
Urbana, Ill.
1 Attn: Dr. J.E. Robertson

Univ. of Illinois
Coordinated Sci. Lab
Urbana, Ill.
1 Attn: Prof. Daniel Alpert

University of Illinois
Urbana, Ill.
1 Attn: Documents Div.

State Univ. of Iowa
Dept. of Elec. Engr.
Iowa City, Iowa
1 Attn: Prof. Donald L. Epley

Johns Hopkins University
Applied Physics Lab
8621 Georgia Ave.
Silver Spring, Md.
1 Attn: Mr. A.W. Nagy
1 Attn: Doc. Library
1 Attn: N.H. Choksy
1 Attn: Mr. E.E. Green

Johns Hopkins University
Carlyle Barton Lab
Charles and 34th St.
Baltimore 18, Md.
1 Attn: Librarian
1 Attn: J.M. Minkowski

Linfield Research Institute
McMinnville, Oregon
1 Attn: Guy N. Hickok, Dir.

Marquette University
College of Engr.
1515 W. Wisconsin Ave.
Milwaukee 3, Wis.
1 Attn: Arthur C. Moeller

Mass. Institute of Technology
Cambridge, Mass. 02139
1 Attn: J.B. Weisner, Rm. 6-215
1 Attn: Mr. J.E. Ward, Asst. Dir.,
Elec. Syst. Lab, Bldg. 32-105
1 Attn: Res. Lab of Elec., Doc. Rm.
1 Attn: Miss Aina Sils, Librn. LIR,
Rm. 4-242, Lab for Insul. Res.
1 Attn: D.M. Baumann, Rm. 3-457, Dynam.
Anal. and Control Lab

Mass. Institute of Tech.
Lincoln Laboratory
P.O. Box 73
1 Lexington 73, Mass.
1 Attn: Library
1 Attn: Dr. Walter I. Wells
1 Attn: Library A-082
1 Attn: Kenneth L. Jordan, Jr.

Univ. of Maryland
Inst. for Fluid Dynam. and Appl. Math.
1 College Park, Md. 20742

Univ. of Michigan
Ann Arbor, Mich.
1 Attn: Electron Phys. Lab
1 Attn: Prof. Joseph E. Rowe, Elec.
Engr. Dept.

1 Attn: Dir., Cooley Elec. Lab
1 Attn: Tech. Doc. Service, Inst.
of Sci. and Tech.
1 Attn: Dr. G.E. Peterson, Dir.
Communication Sci. Lab
1 Attn: W. Wolfe, IRIA, Inst. of Sci.
and Tech.
1 Attn: Communication Sci. Lab

University of Minnesota
Dept. of Elec. Engr.
Institute of Tech.
Minneapolis 14, Minn.
1 Attn: Prof. A. Van Der Ziel

Missouri Schl. of Mines and Metallurgy
Elec. Engr. Dept.
1 Rolla, Missouri

Univ. of Nevada
College of Engr.
Reno, Nevada
1 Attn: Dr. R.A. Manhart, Chm. Elec.
Engr. Dept.

New York Univ.
College of Engr.
New York 53, N.Y.
1 Attn: R.F. Cotelllessa
1 Attn: Dr. Morris Kline
1 Attn: Dr. J.H. Mulligan, Chm. EE Dept.
1 Attn: Dr. H. Kallman, Solid State Lab

Northeastern Univ.
The Dodge Library
Boston 15, Mass.
1 Attn: Joyce E. Lunde, Ref. Librn.

Northwestern Univ.
Aerial Measurements Lab
2422 Oakton St.
Evanston, Ill.
1 Attn: Walter S. Toth

North Carolina State College
Dept. of Elec. Engr.
Raleigh, N.C.
1 Attn: Prof. R.W. Lade

Univ. of Notre Dame
Elec. Engr. Dept.
South Bend, Ind.
1 Attn: Eugene Henry

Ohio State Univ.
1314 Kinnear Rd.
Columbus 12, Ohio
1 Attn: Research Foundation
1 Attn: Dr. M.O. Thurston

Ohio State Univ.
2024 Neil Ave.
Columbus 10, Ohio
1 Attn: Prof. E.M. Boone, Dept. of
Elec. Engr.

Ohio State Univ.
Dept. of Physics
174 W. 18th St.
Columbus, Ohio
1 Attn: Dr. M.L. Pool

Ohio University
College of Appl. Sci.
Athens, Ohio
1 Attn: R.C. Quisenberry

The Univ. Library
Oklahoma State Univ.
1 Stillwater, Oklahoma

Oregon State Univ.
Elec. Engr. Dept.
Corvallis, Oregon
1 Attn: H.J. Oorthuys

Polytechnic Inst. of Brooklyn
Brooklyn, N.Y.
1 Attn: Leonard Shaw, Elec. Engr. Dept.
1 Attn: Dr. R.A. Mareus
1 Attn: Dr. N. Marcuvitz, V.P. for Res.

Polytechnic Inst. of Brooklyn
Graduate Center, Rt. 110
Farmingdale, N.Y.
1 Attn: Librarian

University of Pennsylvania
Moore School of Elec. Engr.
200 South 33rd Street
Philadelphia 4, Pa.
1 Attn: Miss Anna Louis Campion

Princeton University
Elec. Engr. Dept.
1 Princeton, N.J.
1 Attn: Prof. F.S. Acton, Engr. Lib.,
Engr. Quadrangle

Purdue University
Electrical Engr. Dept.
LaFayette, Ind.
1 Attn: Library

Rensselaer Polytechnic Inst.
Troy, N.Y. 12189
1 Attn: Library-Serials Dept.
1 Attn: Plasma Res. Lab. Mr. E.H. Holt,
Dir.
1 Attn: Prof. Kenneth E. Mortensen

Res. Inst. of Adv. Studies
7212 Bellona Ave.
Baltimore 12, Md.
1 Attn: Dr. R.E. Kalman

Univ. of Rochester
206 Hopeman
Rochester 20, N.Y.
1 Attn: Dr. G.H. Cohen, Engr. Bldg.

Rose Polytechnic Institute
Dept of Elec. Engr.
Terre Haute, Ind.
1 Attn: Dr. C.C. Rogers

Rutgers University
Physics Dept.
Newark 2, N.J.
1 Attn: Dr. Charles Pine

Stanford Research Institute
Menlo Park, Calif.
4 Attn: External Repts., G-037
1 Attn: Dr. C. Cook

Stevens Institute of Tech.
Hoboken, N.J.
1 Attn: Dr. Bostick

Syracuse University
Syracuse 10, N.Y.
1 Attn: Dept. of Elec. Engr.
1 Attn: Dr. Stanford Goldman

Temple University
Philadelphia, Pa.
1 Attn: Dr. J.L. Bohn

University of Tennessee
Dept. of Elec. Engr., Ferris Hall
1 Knoxville, Tenn.

Texas Technological College Lubbock, Texas 1 Attn: Dir., Inst. of Sci. Engr., Off. of Dean of Engr. 1 Attn: Prof. Harold Spuhler	Aero Chem Research Lab P.O. Box 12 Princeton, N.J. 1 Attn: Dr. Calcote	Dr. Ervin J. Nalos The Boeing Co. Seattle 24, Wash. 1 Attn: MS-1331, ORG. 1-8000
University of Texas Box 8029 Univ. Station Austin, Texas 1 Attn: Def. Res. Lab	Airborne Instruments Lab Comac Rd. Deerpark, L.I., N.Y. 1 Attn: John Dyer, V.P. and Tech. Dir.	The Bunker Ramo Corp. 8433 Fallbrook Ave. 1 Canoga Park, Calif. 91304
The Univ. of Texas Serials Acquisitions Austin, Texas 1 Attn: Mr. J. Womack, Serials Librn.	Amperex Corp. 230 Duffy Ave. Hicksville, L.I., N.Y. 1 Attn: S. Barbasso, Proj. Engr.	Chrysler Corp., Space Div. P.O. Box 29200 New Orleans, La. 70129 1 Attn: Tech. Info. Center
EERL The Univ. of Texas Rt. 4, Box 189 Austin, Texas 78952 1 Attn: Librarian, BFW	Argonne National Lab 9700 So. Cass Ave. Argonne, Ill. 1 Attn: Dr. O.C. Simpson, Dir. Solid State Sci. Div.	Columbia Radiation Lab 538 W. 120th St. 1 New York 27, N.Y.
Tulane University Elec. Engr. Dept. New Orleans, La. 70118 1 Attn: Dr. Nunn	Auerback Corp. 1634 Arch St. 1 Philadelphia 3, Pa.	Convair/General Dynamics P.O. Box 1950 San Diego, Calif. 92112 1 Attn: Engr. Lib. Mail Zone 6-157 VIA: Air Force Plant Rep. San Antonio Air Mat. Area Convair-Astronautics San Diego 12, Calif.
University of Utah Elec. Engr. Dept. Salt Lake City, Utah 1 Attn: Richard W. Grow	Autonetics Div. of No. Amer. Aviation 3370 Miraloma Ave. Anaheim, Calif. 1 Attn: Tech. Lib., Dept. 502-41, Bldg. 202	Cook Research Labs 6401 W. Oakton St. 1 Morton Grove, Ill.
Utah State University Electro Dynamics Labs Logan, Utah 1 Attn: Fon Brown	Avco Corp. Research Lab 2385 Revere Beach Parkway Everett 49, Mass. 1 Attn: A. Kantrowitz 1 Attn: Mr. Gurdon Abell	Cornell Aeronautical Labs, Inc. 4455 Genesee St. Buffalo 21, N.Y. 1 Attn: D.K. Plummer 2 Attn: Library
Utah State University Solid State Elec. Lab Logan, Utah 1 Attn: Mr. C.M. Rushforth, Asst. Prof., Elec. Engr. Dept.	Baird Atomic 33 University Rd. Cambridge 38, Mass. 1 Attn: Dr. Hornig	Eitel-McCullough, Inc. 301 Industrial Way San Carlos, Calif. 1 Attn: Tech. Library 1 Attn: W.R. Luebke
Santa Clara University 1 Santa Clara, Calif. 1 Attn: ORRADRE Library	Bell Telephone Laboratories Murray Hill Labs Murray Hill, N.J. 1 Attn: Dr. J.K. Galt 1 Attn: Dr. J.R. Pierce 1 Attn: Dr. R.M. Ryder 1 Attn: Dr. M. Sparks 1 Attn: D.A. Chisholm 1 Attn: Mr. J.A. Morton 1 Attn: Dr. J.M. Goldey 1 Attn: Dr. S. Darlington 1 Attn: A.J. Grossman	Advanced Technology Corp. 1830 York Rd. Timonium, Md. 1 Attn: Library
The University of Virginia Charlottesville, Va. 1 Attn: J.C. Wyllie, Alderman Lib.	Bell Telephone Labs, Inc. Technical Information Library Whippany Lab Whippany, N.J. 1 Attn: Tech. Repts. Librn.	Electro-Optical Instruments, Inc. 125 N. Vinedo Pasadena, Calif. 1 Attn: I. Weiman
University of Washington Seattle 5, Wash. 1 Attn: A.E. Harrison, Elec. Engr. Dept.	Bendix Corporation Research Laboratories Div. Southfield (Detroit), Mich. 1 Attn: A.G. Peifer 1 Attn: Dr. W.N. Nunn, Jr.	Ewen Knight Corp. Oak and Pine Sts. East Natick, Mass. 1 Attn: Library
University of Wisconsin College of Engineering Dept. of Elec. Engr. Madison, Wis. 1 Attn: Mr. T.C. Gabriel	Bendix Pacific Div. The Bendix Corp. 11600 Sherman Way North Hollywood, Calif. 1 Attn: Engr. Lib.	Fairchild Semiconductor Corp. 313 Fairchild Dr. P.O. Box 880 Mt. View, Calif. 1 Attn: Dr. V.H. Grinich
Worcester Polytechnic Inst. Worcester, Mass 1 Attn: Dr. Glen Richardson	Boeing Scientific Research Labs P.O. Box 3707 Seattle 24, Wash. 1 Attn: G.L. Hollingsworth 1 Attn: E.B. Weinstein	Fairchild Semiconductor Corp. 545 Whisman Rd. Mt. View, Calif. 1 Attn: Dr. R. Noyce
Yale University Yale Station New Haven, Conn. 06520 1 Attn: Dept. of Elec. Engr. 1 Attn: Engr. Lib. 1 Attn: Phys. Lib./Sloane Lab		Federal Scientific Corp. 615 W. 131st St. 1 New York 27, N.Y.
<u>Industries</u>		Geisler Laboratories P.O. Box 252 Menlo Park, Calif. 1 Attn: Librarian
Admiral Corporation 3800 Cortland St. Chicago 47, Ill. 1 Attn: Edith N. Roberson, Librn.		

General Electric Co.
TWT Product Section
601 California Ave.
Palo Alto, Calif.
1 Attn: Micro. Lab, C.G. Lob
1 Attn: Tech. Lib.
1 Attn: D.H. Goodman, Mgr. Mfg. Ops.

General Electric Co.
Defense Electronics Div.-LMED
Cornell University
Ithaca, N.Y.
1 Attn: Library
VIA: Commander, ASD
W-P AFB, Ohio
Attn: ASRNC-5, D.E. Lewis

General Electric Co.
Research Lab
P.O. Box 1088
Schenectady, N.Y.
1 Attn: Dr. Philip M. Lewis
1 Attn: G.E. Feiker, Adv. Tech. Labs,
Bldg. 37-511
1 Attn: R.L. Shuey, Mgr., Info. and
Studies Section

General Electric Co.
Schenectady Tube Operation
1 River Rd.
Schenectady, N.Y. 12305
1 Attn: Mr. E.D. McArthur

General Electric Co.
Electronics Park Bldg. 3, Rm. 143
Syracuse, N.Y.
1 Attn: Doc. Librn., Yolanda Burke

General Electric Co.
Rectifier Components Dept.
Advance Rectifier Engr.
Auburn, N.Y.
1 Attn: Gerald C. Huth

General Electric Co.
Research Laboratory
Appl. Phys. Section
P.O. Box 1088
Schenectady, N.Y.
1 Attn: V.L. Newhouse

General Electric Space Sciences Lab
Space Technology Center
King of Prussia, Pa.
1 Attn: Dr. D.B. Miller

General Precision, Inc.
Link Group
1451 California Ave.
Palo Alto, Calif. 94304
1 Attn: Tech. Lib.

General Tel. and Elec. Lab
Bayside 60, N.Y.
1 Attn: L.R. Bloom

Gilfillan Bros.
1815 Venice Boulevard
Los Angeles, Calif.
1 Attn: Engr. Lib.

Hallicrafters Co.
4401 W. Fifth Ave.
Chicago 24, Ill.
1 Attn: Mr. W.F. Teichmiller
1 Attn: H. Elsenberg, Res. Engr.

Hewlett-Packard Co.
1501 Page Mill Rd.
1 Palo Alto, Calif.

Hoffman Science Center
P.O. Drawer H
1 Santa Barbara, Calif.

Hoffman Electronics Corp.
Military Prod. Div., Sys. Dept.
Hoffman Electronic Park
El Monte, Calif. 91734
1 Attn: L.A. Saggiani

Hughes Aircraft Co.
Florence at Teale St.
Culver City, Calif.
1 Attn: Solid State Group M107
1 Attn: Tech. Doc. Center
1 Attn: Mr. A.S. Jerrens, Aero. Grp.
1 Attn: Dr. N.I. Hall, V.P. Engr.

Hughes Aircraft Co.
Semiconductor Div.
P.O. Box 278
Newport Beach, Calif.
1 Attn: Library
1 Attn: Tech. Librarian

Hughes Aircraft Co.
Bldg. 600, Mail Sta. D-251
P.O. Box 3310
Fullerton, Calif.
1 Attn: Mr. A. Eschner, Jr.
Ground Systems Group

Hughes Aircraft Co.
3011 Malibu Canyon Rd.
Malibu, Calif.
6 Attn: Mr. H.A. Iams, Res. Labs

Huggins Laboratories
999 E. Arques Ave.
1 Sunnyvale, Calif.

International Business Machines
Components Div.
Poughkeepsie, N.Y.
1 Attn: E.M. Davis (Dept. 410)

International Business Machines
Data Systems Division
Box 390 Boardman Rd.
Poughkeepsie, N.Y.
1 Attn: J.C. Logue

International Business Machines
Research Library, Box 218
1 Yorktown Heights, N.Y.

IBM ASD and Res. Lib., Bldg. 078
Monterey and Cottle Roads
San Jose, Calif.
1 Attn: Dr. Mih Yin, Dept. 472

IBM ASD Research Library
P.O. Box 66
Los Gatos, Calif. 95031
1 Attn: Miss Marjorie Griffin

International Business Machines
Tech. Reports Center
Space Guidance Center
Federal Systems Division
1 Oswego, N.Y.

ITT Laboratories
15151 Bledsoe Street
San Fernando, Calif.
1 Attn: F.E. Randle, Librn.
1 Attn: C.V. Stanley

ITT Federal Laboratories
500 Washington Ave.
Nutley 10, N.J.
1 Attn: Mr. R.C. Gremling

Technical Library
ITT Electron Tube Division
P.O. Box 100
Easton, Pa.
1 Attn: A.W. McEwan, Dir.

International Tel. and Tel. Corp.
ITT Laboratories Div.
390 Washington Ave.
Nutley 10, N.J.
1 Attn: J. Le Grand

Jansky and Bailey
Systems Engineering Div.
Atlantic Research Corp.
Shirley Highway and Edsall Rd.
Alexandria, Va. 22314
1 Attn: J.J. Renner

Korad Corp.
2520 Colorado Ave.
Santa Monica, Calif.
1 Attn: Mr. F.P. Burns, Mgr. Ops.

Laboratory for Electronics Inc.
1075 Commonwealth Ave.
Boston 15, Mass. 02215
1 Attn: Lib. (Mrs. A. Cakste, Librn.)

Laboratory for Electronics, Inc.
1079 Commonwealth Ave.
Boston 15, Mass.
1 Attn: Dr. H. Fuller

Lear Siegler, Inc.
Space Systems Center
3171 S. Bundy Dr.
1 Santa Monica, Calif.

LEL, Inc.
75 Akron Street
Copiague, L.I., N.Y.
1 Attn: Mr. Robert S. Mautner

Lenkurt Electric Co.
San Carlos, Calif.
1 Attn: M.L. Waller, Librn.

Librascope Group
General Precision, Inc.
808 Western Ave.
Glendale 1, Calif.
1 Attn: Engr. Lib.

Litton Industries, Inc.
960 Industrial Rd.
San Carlos, Calif.
1 Attn: Tech Library

Lockheed Aircraft Corporation
Georgia Division
Marietta, Ga.
1 Attn: Dept. 72-15

Lockheed Electronics Co.
Military Systems
U.S. Highway 22
Plainfield, N.J.
1 Attn: C.L. Optiz

Lockheed Aircraft Corp.
Missile and Space Div.
P.O. Box 504
Sunnyvale, Calif.
1 Attn: G.W. Price
1 Attn: Tech. Info. Center

Lockheed Missile and Space Div.
Dept. 5240, Bldg. 202
Palo Alto, Calif.
1 Attn: Mr. M.E. Browne

Loral Electronics Corp.
825 Bronx River Rd.
Bronx, N.Y. 10472
1 Attn: Louise Daniels, Librn.

Marquardt Aircraft Co.
16555 Saticoy St.
P.O. Box 2013-South Annex
Van Nuys, Calif.
1 Attn: P.M. Grant

The Martin Co.
Baltimore 3, Md.
1 Attn: Scientific-Tech. Lib.
Mail J398

The Martin Co.
P.O. Box 5837
Orlando, Fla.
1 Attn: Engr. Lib., M.P. 30

Maxson Electronics Corp.
460 West 34th St.
New York 1, N.Y.
1 Attn: M. Simpson

Melpar, Inc.
3000 Arlington Blvd.
Falls Church, Va.
1 Attn: Librn.

Micro State Electronics Corp.
152 Floral Ave.
Murray Hill, N.J.
1 Attn: Saul Lederhandler

Microwave Associates
North West Industrial Park
Burlington, Mass.
1 Attn: Librn.
1 Attn: Dr. Kenneth Mortenson

Microwave Electronics Corp.
3165 Porter Dr.
Palo Alto, Calif.
1 Attn: Stanley F. Kaisal
1 Attn: M.C. Long
1 Attn: J.B. Gaenzle

Minneapolis Honeywell Reg. Co.
Semiconductor Prod. Lib.
1177 Blue Heron Blvd.
1 Riviera Beach, Fla.

Minneapolis Honeywell Reg. Co.
Aeronautical Div. Los Angeles
1915 Armacost Ave.
Los Angeles 25, Calif.
1 Attn: Tech. Library

The MITRE Corp.
Bedford, Mass.
1 Attn: Library

Monsanto Research Corp.
Station B, Box 8
Dayton 7, Ohio
1 Attn: Mrs. D. Crabtree

Monsanto Chemical Co.
800 N. Lindbergh Blvd.
St. Louis 66, Mo.
1 Attn: Mr. E. Orban, Mgr. Inorganic
Dev.

Motorola, Inc.
Western Center
8201 East McDowell Rd.
Scottsdale, Arizona
1 Attn: Library

Motorola, Inc.
P.O. Box 5409
Phoenix 10, Arizona
1 Attn: Dr. H.W. Welch, Jr., Gen.
Mgr. Solid State Sys. Div.

Motorola, Inc.
Solid State Devices Lab
Scottsdale, Arizona
1 Attn: John Cacheris, Mgr.

Motorola Semiconductor Prod. Div.
5005 East McDowell Rd.
Phoenix, Arizona
1 Attn: Dr. A. Lesk
2 Attn: Dr. R.M. Warner, Jr.

Motorola, Inc.
Chicago Military Elec. Center
1450 North Cicero Ave.
Chicago, Ill. 60651
1 Attn: George Anagnos
VIA: Motorola, Inc.
Chicago 51, Ill.
Attn: Sec. Officer

National Biomedical Res. Inst.
8600 16th St.
Silver Spring, Md.
1 Attn: Dr. R.S. Ledley

Norden Division
United Aircraft Corp.
Norwalk, Conn.
1 Attn: Alice Ward, Librn.

Nortronics
Palos Verdes Research Park
6101 Crest Rd.
Palos Verdes Estates, Calif.
1 Attn: Tech. Info. Center

North American Aviation, Inc.
Columbus Division
Engineering Data Services
4300 E. Fifth Ave.
1 Columbus 16, Ohio

Philco Tech. Rep. Div.
P.O. Box 10
Ft. Washington, Pa.
1 Attn: F.R. Sherman

Philco Corp.
Jolly and Union Meeting Roads
Blue Bell, Pa.
1 Attn: Mr. J.P. Spratt
1 Attn: Dr. M.E. Lasser, Dir.
1 Attn: C.V. Bocciairelli

Philco Corp.
Lansdale Div.
Lansdale, Pa.
1 Attn: Dr. C.G. Thornton, Gen. Mgr.,
Spec. Prod. Op.

Philco Corp., Lansdale Div.
Church Rd.
Lansdale, Pa.
1 Attn: J.R. Gordon

Polorad Electronics Corp.
43-20 Thirty-Fourth St.
Long Island City 1, N.Y.
1 Attn: A.H. Sonnenschein, Asst. to
the Pres.

Radiation, Inc.
Melbourne, Fla.
1 Attn: Librarian

Radio Corp. of America
RCA Labs
David Sarnoff Res. Center
Princeton, N.J.
1 Attn: Dr. Jack Sklansky
1 Attn: Harwick Johnson

Radio Corp. of America
Defense Electronic Products
Missile and Surface Radar Engr.
Moorestown Engr. Lib. 127-221
1 Moorestown, N.J.

Radio Corp. of America, ASD
P.O. Box 588
Burlington, Mass.
1 Attn: Lib.

The Rand Corp.
1700 Main St.
Santa Monica, Calif.
1 Attn: Helen J. Waldron, Librn.
1 Attn: Library

Raytheon Manufacturing Co.
Research Division
Waltham, Mass. 02154
1 Attn: Dr. Herman Statz
1 Attn: Res. Div. Library
1 Attn: J.M. Lavine

Raytheon Manufacturing Co.
Spencer Laboratory
Burlington, Mass.
1 Attn: Librn., Microwave and Pwr.
Tube Div.
1 Attn: Dr. H. Scharfman

Raytheon Co.
P.O. Box 1542
Goleta, Calif.
1 Attn: Librarian

Raytheon Co.
Bedford, Mass.
1 Attn: Mrs. I. Britton, Librn.

Raytheon Co.
Semiconductor Lib.
350 Ellis St.
Mt. View, Calif.
2 Attn: L.M. Johnson

Raytheon Manufacturing Co.
1415 Boston-Providence Turnpike
Norwood, Mass.
1 Attn: Mr. L. Edwards

RCA Laboratories
Princeton, N.J.
1 Attn: Dr. W.M. Webster

Radio Corp. of America
Bldg. 108-110
Moorestown, N.J.
1 Attn: H.J. Schrader

Radio Corp. of America
Surface Communications Div.
Front and Market Sts., Bldg. 17-C-6
Camden, N.J.
1 Attn: K.K. Miller, Mgr. Minuteman
Proj. Office

Revere Copper and Brass, Inc.
Foil Division
196 Diamond Street
Brooklyn 22, N.Y.
1 Attn: Vincent B. Lane

Rocketdyne
6633 Canoga Ave.
Canoga Park, Calif.
1 Attn: Dr. Boden, Dept. 093

Sandia Corp., Sandia Base
Albuquerque, N.M.
1 Attn: Mrs. B.R. Allen, Librn.

Sigmatron, Inc.
Santa Barbara Airport
Goleta, Calif. 93017
1 Attn: Dr. David Heinz

S.F.D. Laboratories, Inc.
800 Rahway Ave.
1 Union, N.J.
1 Attn: Dr. J. Saloom
1 Attn: Dr. S.K. Farney

The STL Tech. Library
Doc. Acquisitions
Space Tech. Labs, Inc.
One Space Park
1 Redondo Beach, Calif.

Sperry Rand Res. Center
North Road
Sudbury, Mass.
1 Attn: Alan Steeves, Librn.

Sperry Electron Tube Div.
Sperry Rand Corp.
Gainesville, Fla.
1 Attn: Librn.

Sperry Gyroscope Co.
Div. of Sperry Rand Corp.
Great Neck, L.I., N.Y.
1 Attn: Leonard Swern (M.S. 3T105)
1 Attn: Mr. R.L. Wathen
1 Attn: K. Barney, Engr. Dept. Head
Mail Station F7

Socony Mobil Oil Co.
Field Research Laboratory
P.O. Box 900
Dallas 21, Texas
1 Attn: Librn.

Sylvania Electric Products, Inc.
500 Evelyn Ave.
Mt. View, Calif.
1 Attn: Tech. Library

Sylvania Electric Products, Inc.
Tech. Info. Services
1 Mt. View, Calif.

Sylvania Electronic Systems
P.O. Box 205
1 Mt. View, Calif.
1 Attn: Donlan Jones
1 Attn: Optics Dept., Bldg. 4
1 Attn: Mr. E.O. Ammann, Bldg. 4

Sylvania Electric Products, Inc.
Waltham Laboratories
100 First Ave.
Waltham 54, Mass.
1 Attn: Librn., Sylvania Elec. Sys.
1 Attn: Mr. E.E. Hollis

Sylvania Electric Products, Inc.
Applied Res. Lab
40 Sylvan Rd.
Waltham 54, Mass.
1 Attn: Mr. C. E. Arnold

Technical Research Group
Rt. No. 10
1 Melville, N.Y. 11749

Texas Instruments, Inc.
P.O. Box 5012
Dallas 22, Texas
2 Attn: Semiconductor Comp. Lib.
1 Attn: Tech. Repts. Service, MS-65

Tektronix, Inc.
P.O. Box 500
Beaverton, Oregon
4 Attn: Dr. J.F. DeLord, Dir. of Res.

TRW Space Technology Labs
One Space Park
Redondo Beach, Calif.
1 Attn: Dr. J.W. Peterson

Tucor, Inc.
59 Danbury Rd.
Wilton, Conn.
1 Attn: Mrs. M.E. Osband

Varian Associates
611 Hansen Way
Palo Alto, Calif.
1 Attn: Tech. Lib.

Varian Associates
BOMAC Div.
Salam Rd.
Beverly, Mass. 01915
1 Attn: Res. Lib.

Vitro Laboratories
200 Pleasant Valley Way
West Orange, N.J.
1 Attn: Miss B.R. Meade, Librn.

Warnecke Electron Tubes, Inc.
175 W. Oakton St.
Des Plaines, Ill.
1 Attn: F. Voltaggio, Jr., Dir. of
Marketing

Watkins-Johnson Co.
3333 Hillview Ave.
Palo Alto, Calif.
1 Attn: Dr. H.R. Johnson

Weitermann Electronics
4549 North 38th St.
1 Milwaukee 9, Wis.

Westinghouse Electric Corp.
P.O. Box 284
Elmira, N.Y.
1 Attn: Sheldon S. King
1 Attn: Carl Miller, Elec. Tube Div.

Melbourne J. Hellstrom, Supv. Engr.
Westinghouse Electronics Corp.
Molecular Electronics Div.
Box 1836
1 Baltimore, Md. 21203

Westinghouse Electric Corp.
Westinghouse Air Arm Div.
Box 746
Baltimore 3, Md.
1 Attn: H.B. Smith, Mgr. Engr. Dept.
1 Attn: G.R. Kilgore

Westinghouse Elec. Res. Labs
Beulah Rd., Churchill Boro
Pittsburgh, Pa. 15235
1 Attn: R. Heikes, Dir. of Solid
State Sci., R and D

Westinghouse Electric Corp.
R and D Center, Bldg. 501
Beulah Rd.
Pittsburgh 35, Pa.
1 Attn: Dr. G.C. Sziklai
1 Attn: J.G. Castle, Jr., 401-1B5

Westinghouse Electric Corp.
Semiconductor Div.
Youngwood, Pa.
1 Attn: R.E. Davis

Zenith Radio Corp.
6001 Dickens Ave.
Chicago 39, Ill.
1 Attn: J. Markin

Laboratory of Automatic Control Sys.
Tech. Univ. of Denmark, Lundtofte
1 Lyngby, DENMARK

The University of Adelaide
Adelaide, SOUTH AUSTRALIA
1 Attn: BARR Smith Library

University of Western Australia
Nedlands, WEST AUSTRALIA
1 Attn: Prof. A.R. Billings
Hd. of Elec. Engr.